Burning Behaviour of Heavy Gas Oil from the Canadian Oil Sands

by

Patrick Mulherin

A thesis
presented to the University of Waterloo
in fulfillment of the
thesis requirement for the degree of
Master of Science
in
Mechanical Engineering

Waterloo, Ontario, Canada, 2014

I hereby declare that I am the sole author of this thesis. This is a true copy of the thesis, including any required final revisions, as accepted by my examiners.

I understand that my thesis may be made electronically available to the public.

Abstract

This work presents the first systematic investigation and characterisation of the burning behaviour of *untreated heavy gas oil* from the Canadian oil sands, an intermediate product in the upgrading process of forming synthetic crude oil from bitumen. As this oil is an intermediate product and has little commercial value, there has been little characterisation of the burning behaviour or propensity for boilover of the fuel. The objective of this study was to investigate the global burning behaviour of untreated heavy gas oil in the effort to document key fire parameters and unique burning characteristics of the fuel, and compare with those presented in literature. This experimental series consisted of measurements of the heat release rate, rate of fuel consumption, and flame spread rate, as well as observations of overall pool fire behaviour, using heavy gas oil as well as kerosene as a reference. Further experiments investigated the effects of water suppression spray on the pool fire behaviour, and the propensity for boilover during small-scale fires.

It was found that the fire properties of heavy gas oil were consistent with those of other heavy oils, most notably those of heavy fuel oil. The burning behaviour of the heavy gas oil was well represented by the traditional correlations for fire behaviour of heavy hydrocarbon fuels. Some of the measured properties for the heavy gas oil included an infinite diameter fuel regression rate of 3.0 mm/min, heat of combustion of 43.5 MJ/kg, and flame spread rate of 0.8 cm/s. Temperatures measured through the depth of the fuel layer indicated that a hot-zone did not form, and the observation was confirmed based on mass burning rates and fuel boiling temperatures that did not vary over the burning duration.

At low initial fuel temperatures, the burning of the heavy gas oil was intensified by water emulsified within the oil, which led to an increase in each of the measured fire characteristics, especially that of flame spread rate. In this case, small volumes of flaming oil were projected out of the test pans, as well as into the flame column. Furthermore, the heavy gas oil was found to 'weather' over time, resulting in an oil with higher density and lower volatility, which caused each of the measured fire properties to decrease during the six month weathering period considered here.

The heavy gas oil in the present experiments was found to have a significant propensity to mix with steam, forming a froth-like substance that expanded in volume across the surface of the fuel. This phenomenon was observed when suppression water was sprayed on the heated fuel surface, as well as in fires established over deep pools of fuel with a water sublayer. The expansion of the froth resulted in overflow of burning fuel from the experimental test pans, and thus caused fire spread beyond the pan walls. Finally, thin layer boilover was observed in heavy gas oil pool fires with a water sublayer, leading to both an increase in fire intensity and fire spread beyond the test pans.

Acknowledgements

First and foremost, I would like to thank my supervisor, Dr. Elizabeth Weckman, for her unwavering guidance throughout the duration of this project. It was she who convinced me to complete a Masters of Applied Science degree, and her support and teachings have made this a positive learning experience for me. Her expertise in all areas of fire safety, especially pool fire dynamics, was invaluable in understanding the burning behaviour of this heavy gas oil. Her comments and constructive criticisms have allowed me to develop personally and professionally throughout this degree, and I am honoured to have had the chance to work with her.

Many people assisted me throughout this degree, and I would like to begin with thanking Mr. Gord Hitchman for his support and discussions during this project. His guidance in instrumentation and experimental design helped to greatly shorten the learning curve in fire performance testing and increased my confidence in the measured results.

I would like to thank Dr. Grunde Jomaas and Dr. Roydon Fraser for their contributions in the review process. Their comments and criticisms were extremely helpful in forming a conclusive thesis.

I would also like to thank the various co-op students who helped with the instrumentation and experimental set-up for the various experiments. Dorian Bouchet, Adithia Gopi, and Kevin Gordon were all hugely helpful in preparing for experiments as well as in the significant task of cleaning the apparatus afterwards.

Finally, I would like to acknowledge all of my colleagues at the University of Waterloo Live Fire Research Facility for their friendship, support, and, especially, their good humour. I sincerely hope to have the chance to work with them again in the future.

Table of Contents

List of Tables

List of Figures

Chapter 1

Introduction

The number and severity of industrial fires has been in decline over the past century; however, the possibility of large scale pool fires cannot be neglected. From 1950 to the present, over 500 large pool fire accidents have occurred worldwide [1], with over 133 severe storage tank fires causing catastrophic damage [2]. The potential for large scale fires is significant as well; it is estimated that there are more than 650,000 aboveground oil storage facilities, comprising more than 3 million individual storage tanks in the U.S. alone [3]. Spill and pool fires from such facilities have caused enormous damage to infrastructure and often consume valuable product; however, it is difficult to quantify the exact economic cost of these industrial fires. Nonetheless, due to incidents that have taken place, the potential social and environmental impacts are well understood [4–6].

Pool fires occur as a result of spills of flammable liquids, or on flammable liquid materials stored in tanks, given the presence of an ignition source. Ignition of many storage tank fires occurs as a result of lightning strikes, human error, or failure of automated systems [2]. After initiation, spill and tank fires can quickly grow to diameters exceeding 100 m [3], presenting a challenge to fixed fire suppression systems as well as first responders.

The primary hazards associated with large scale pool fires include the rate of flame spread across the fluid surface and consequent rate of fire growth, as well as the radiative flux from the flame column to the surroundings. However, perhaps the most significant hazard in the case of atmospheric storage tank fires is that of boilover. Boilover results in the rapid and often violent ejection of the burning tank contents, causing an increase in fire intensity and significant spread of fire outside the tank walls. Notable storage tank boilovers have occurred in Venezuela, the United Kingdom, Poland, and the United States within the past 60 years [2], having caused significant property damage and loss of life.

A thorough characterization of the burning behaviour of individual fuels is required to properly assess fire hazards in the case of a spill, storage tank, or other type of large area pool fire. Such information can help to predict and model the consequences of these fires, as well as to design suppression systems, coordinate fire department activities, and ensure adequate separation of industrial facilities. Material properties and thermophysical data for the fuel, coupled with theoretical calculation methods, are typically used to provide order of magnitude estimates of the expected burning behaviour of liquid-fuelled fires [7,8]. However, well-targeted experimental studies conducted at both large and small scale are still required to improve the accuracy of the data and reliability of the calculations and thereby increase confidence in the predictions.

There has been a significant volume of research into the behaviour of pool fires [9–19], and the properties and empirical calculations of many fuels have been well documented [20–23]. Furthermore, the phenomenon of boilover has been studied since the early 20^{th} century, and has been documented for many types of fuels [23–32]. However, there exists a variety of fuels for which the burning behaviour is not adequately understood, and the potential for boilover has not been established. To date, research on boilover has been primarily limited to crude oils; however, boilover has occurred in storage tanks containing fuels not previously known to be susceptible to boilover – including heavy oils. The ejection of burning fuel during boilover in these cases has killed and injured first responders and caused significant damage to the surrounding areas [33, 34].

An example of a fuel for which there has been little research into the burning behaviour is *heavy gas oil*. Heavy gas oil is an intermediate product that is produced during the process of upgrading bituminous oil, mined from the Canadian Oil Sands, to synthetic heavy crude oil. It is believed that 30% of discovered oil deposits worldwide are contained in bituminous form throughout Western Canada [35]. With recently discovered oil deposits and new extraction technology, the extraction and production of raw and refined hydrocarbons from bituminous oil is a major contributor to the Canadian economy and has seen rapid growth in recent years [35]. As such, there is a significant quantity of untreated heavy gas oil held in large volume storage tanks throughout Western Canada.

The extraction of oil from oil sands is a complex procedure, and is described in brief here. The Canadian oil sand deposits are typically located near the surface and surface mining techniques are used to expose the bitumen. The clay-infused bitumen is excavated from the ground in large pieces and is crushed to reduce the size and allow the sands to mix with water. The crushed ore is then mixed with heated water and stored in large separating tanks, where the oil is recovered from the water and sand when it floats on top of the water. This recovered bitumen is comprised of approximately 60% bitumen, 30% water, and 10% solids by weight [35]. The bitumen is then processed to remove the additional water and

solids, where untreated heavy gas oil is the oil that is recovered during separation. It is designated as 'untreated heavy gas oil' before it has been treated to remove nitrogen and sulphur contained in the base material. Following the separation process, a significant volume of water remains in the oil, and as a result part of the further upgrading process includes storing the heavy gas oil at elevated temperatures. The elevated temperature lowers the viscosity of the oil, and aids in the migration of water downward to the bottom of the storage tank. A layer of water therefore forms at the bottom of the storage tank and accumulates over time with continued feed of oil into and out of the tank; and is periodically drained.

Heavy gas oil is a dense, viscous oil containing a range of hydrocarbons, considered to be from C_{10} to C_{60}, and is characterized by a wide range of boiling temperatures [36]. Some of the general material properties of the heavy gas oil are presented in Table 1.1. As the density of the oil is only slightly lower than that of water, separation of the oil and the water occurs slowly. At the same time, the oil is highly viscous, leading to emulsification of micro-scale water particles within the oil. The volume of water emulsified in the oil is not insignificant, and has been measured to be up to 1100 ppm upon entry to the settling tanks.

Table 1.1: General properties of untreated heavy gas oil [36].

Colour	**Smell**	**Viscosity**	**Flashpoint**	**Class**
Brown/green	Strong hydrocarbon	High	150 °C	IIIB Combustible

Heavy gas oil is an intermediate product in the upgrading process and consequently has little commercial value. For this reason, detailed thermophysical and material property data for heavy gas oil are scarce, and there is little known about its burning behaviour. As the burning properties of heavy gas oil have not been fully characterized, when required, they have been assumed equivalent to other better characterized surrogate fuels. As an example, kerosene is a common fuel – referenced in various forms as lantern kerosene, tractor fuel oil, JP-8, and aviation fuel – and its burning characteristics have been systematically studied throughout the past century. Referenced data for the fire properties and burning behaviour of kerosene includes data collected during experiments on pool fires of diameters ranging from 0.01 m to some of the largest experiments ever conducted, at over 80 m in diameter [37]. Finally, many correlations and empirical formulations used in fire hazard and consequence assessment have been based on experimental results for kerosene pool fires.

Several parameters can be used as inputs to semi-empirical models to estimate the consequences of large-scale hydrocarbon pool fires [8]. For example, the fuel regression rate is a parameter that relates to the burning duration of pool fires, the rate of heat release, as well as the time available before boilover. The rate of flame propagation of a fuel affects the rate of fire growth, the time available for fixed suppression systems to activate, and the expected difficulty in suppressing the fire. Other relevant parameters can include the propensity for boilover, and the effects of suppression spray to the fuel surface. These parameters must be measured experimentally, and a range of experimental conditions must be considered to assess the effects of experimental design and increase the confidence in the results.

This research is focused on determining the behaviour of heavy gas oil pool fires under conditions approximating those that might be encountered in a storage tank fire. The initial assessment of the burning behaviour will include direct measurements of the fuel regression rate, heat release rate, and flame spread rate in small-scale, constrained pool fires with relatively thick fuel layers. Complementary experiments will be conducted to better understand the risks associated with heavy gas oil pool fires, including the propensity for boilover and the potential effectiveness of water suppression sprays on the fire. The objectives of this study, then, are threefold:

- to investigate and document the burning characteristics of untreated heavy gas oil, including fuel regression rate, heat release rate, flame spread rate, and effectiveness of water suppression, and compare with results presented in literature for similar fuels,
- to identify fuels having well documented fire properties that are consistent with heavy gas oil, and
- to gain insight into the boilover propensity of untreated heavy gas oil and further the pool of experimental data on boilover of heavy oils.

In particular, this study compares small scale experimental results with empirical correlations found in literature, with the intent to provide fundamental information to model fires in heavy gas oil pools. Comparable experiments were conducted with kerosene to validate the experimental methods and compare the heavy gas oil to a well referenced fuel. The measured experimental parameters are compared with other values presented in the literature, and fuels with comparable fire performance properties are identified. These small and mid-scale experiments provide insight into the unique fire properties of heavy gas oil, and can be used to validate existing experimental correlations that are useful for engineering design.

This work includes a review of literature relevant to the present objectives, a description of the experimental methods, and a discussion of the experimental measurements. The literature review, found in Chapter 2, provides background relevant to pool fire behaviour, experimental measurement methods, as well as a review of literature on the storage tank boilover phenomenon. A comprehensive description of the experimental methods is presented in Chapter 3, detailing the apparatus used for measurement of the heat release rate, flame spread rate, water spray suppression, and burning behaviour. The experimental measurements and discussion is presented in Chapter 4, including fuel regression rate, heat release rate, flame spread rate, and an analysis of boilover of heavy gas oil is shown in Section 4.8. Lastly, final conclusions and recommendations from the experimental results are presented in Chapter 5.

The scope of this study is confined to providing initial insight into the basic burning properties of untreated heavy gas oil. It has been well established that the burning properties of liquid fuels can vary widely for fires of small to large diameter [22, 37–40]; therefore, the results and discussion provided within this work are only valid for the range of fire sizes and experimental conditions for which the present experiments were conducted. It is not intended for these results to be directly scaled to estimate the consequence of real fires. Finally, the present results are not applicable for any hydrocarbon fuel other than the heavy gas oil as presented in this work.

Chapter 2

Background

Pool fires have been an area of research for many years and there exists a significant volume of literature on the subject. This section details a review of literature relevant to the behaviour of pool fires, in particular with respect to the rate of fire growth, and the rate of energy release. This is followed by a brief perspective on theory and experiments related to the boilover phenomenon which has been observed during fires in storage tanks containing oils. Finally, a review of the experimental methods that have been successfully used to measure the various fire properties is discussed.

2.1 Pool Fires

There has been considerable research conducted into the behaviour of medium and large-scale liquid fuelled 'pool' fires. The resulting database of experimental results and empirical correlations are a valid source of information on the general burning characteristics of such fires and can serve as validation for comparison with new experimental measurements. However, variations in the experimental conditions under which various aspects for pool fire behaviour have been measured can have a significant effect on the measured results. This section investigates pool fire theory and the various effects of key experimental parameters on the burning behaviour of liquid fuels.

The liquid fuel in a pool must vapourize, and form a sufficient volume of flammable gas above its surface for the fuel to ignite and burn as a pool fire. For fuels with a vapour pressure lower than ambient pressure, a cloud of flammable vapour will readily form above the pool surface. Conversely, fuels with high vapour pressure, such as the heavy gas oil

being studied in the present work, must be heated to the flashpoint temperature before they vapourise sufficiently to form a flammable vapour concentration above the liquid [41]. In both cases, once the cloud of flammable gases has formed, ignition will occur given an ignition source of sufficient energy [42–44].

The localized ignition of sub-flashpoint fuels has been found to cause a convective current in the liquid beneath the fuel surface. This convective current promotes mixing of the heated fuel near the ignition source with cooler fuel, resulting in more of the bulk fuel being heated by the ignition source. In small-scale experiments by Murad et al. [43], a constant power incandescent wire igniter was used to test the ignition delay of alcohol pool fires under various conditions. In these experiments, a strong correlation between ignition delay and both the pool depth and pan diameter was found. The ignition delay was found to increase with pool diameter up to diameters of 5 cm, and with pool depth up to depths of 1.5 cm. Once the pool was larger than these dimensions, no further dependence of ignition delay on diameter or depth was found. It has also been shown by several authors that the significance of the convection currents may be limited by the fuel viscosity and surface tension [43, 44].

Once a small area of flame is established on a pool surface, that flame will spread radially from the point of ignition. Much research has been done to investigate flame propagation across liquid fuels, primarily to study the rate of fire growth in aviation fuel spills [45–48]. Other studies have been conducted towards investigating and developing models for the physical phenomena involved in the spread of flame across liquids [49–53].

The flame spread on liquid fuels is well known to be a function of initial fuel temperature [45,47,54] and again depends upon the bulk fuel temperature relative to the fuel flashpoint temperature. When the fuel is above the flashpoint temperature, a vapour rich zone exists above the fuel surface, and flame spread is governed by rates of vapour formation and mixing with air above the fuel surface. Flame spread across liquid fuels below the flashpoint temperature, on the other hand, is governed by rates of mixing, heating and vapourization of the fuel in the liquid phase [45].

Flame spread in high flashpoint fuels, therefore, is controlled primarily by surface tension-induced convection currents feeding heated fuel into the region ahead of the flame front [54]. In this case, convection within the fuel dominates the rate of flame spread and the effect of radiative heating from the flame to fuel ahead of the flame front is minimal. This was confirmed in experiments by Mackinven et al. [54], where the radiative flux to the fuel ahead of flames established on n-decane pools was shielded by a blocking object. Only a small difference in flame spread rate was seen between the shielded and unshielded experiments. Two types of flame spread are possible in liquid fuels below the flashpoint,

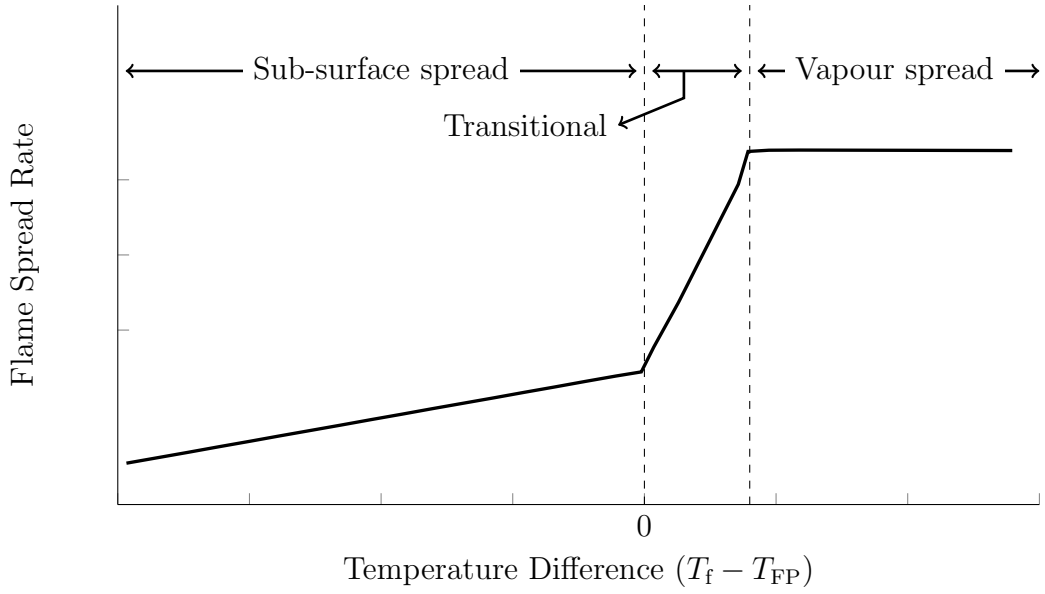

Figure 2.1: Effect of difference between fuel temperature and fuel flashpoint on the rate of flame propagation (Adapted from [41]).

namely pulsating and uniform flame spread [55]. The mechanism for the pulsating flame spread is relatively disputed, but is believed to occur when the fuel is significantly below the flashpoint and requires a period of mixing to generate sufficient vapours for the flame to propagate. The flame therefore propagates and retracts while the fuel ahead of the flame front is heated. A uniform flame spread is seen when the liquid is close to the flashpoint temperature, and requires little heating to vapourize the fuel ahead of the flame front.

A commonly referenced profile of the effect of fuel temperature on flame spread rate for a range of hydrocarbon fuels is shown in Figure 2.1, as reported by Glassman and Hansel [56]. It can be seen that the flame spread rate increases with fuel temperature (T_f) to the flashpoint temperature (T_{FP}), which is the temperature at which the vapour zone above the fuel surface reaches the lower flammability limit. Past this point, the flame spread rate increases more quickly with increased temperature until the temperature at which the vapour zone reaches a stoichiometric mixture. At temperatures greater than this, the flame spread becomes independent of fuel temperature because any additional flammable gases that form have to mix with air to produce a concentration within the flammability limits, and will not contribute directly to increased flame spread.

Mackinven et al. [54] performed one of the most thorough investigations of experimental influences on measurements of flame spread rate over liquid fuels. This study used a horizontal, narrow tray to investigate various parameters on the flame spread of n-decane. Parameters included the effect of test pan width and material, fuel thickness and initial bulk fuel temperature. Lastly, a thickening agent was used to vary the viscosity of n-decane to study the effect of fuel viscosity on flame spread. These experiments helped to confirm the temperature dependence findings of Glassman and Hansel, and the liquid surface tension and viscosity were found to affect the sub surface mixing during flame spread of high flashpoint fuels.

In comparison to quiescent conditions, the radiative flux to the liquid surface becomes dominant in wind-blown conditions [57], where the flame tilts further towards the surface and flame spread rate increases with increasing wind speed. Airflow above the surface of the fuel is also known to affect the rate of flame propagation, as air movement promotes mixing and also alters the structure of the buoyant fire plume. In experiments by Ross and Miller [57], amongst others, it was found that airflow in a direction concurrent with the direction of flame spread tilted the flame towards the fuel surface. This flame tilt increases the radiative flux to the surface and enhances fuel vapourisation ahead of the flame, which in turn decreases pulsations in the flame spread and increases the rate of flame propagation. Conversely, countercurrent airflow was found to slow the rate of flame propagation, likely due to the flammable gases produced ahead of the flame front being blown back into the flame column, thereby reducing the forward movement. Interestingly, Ross and Miller also determined that there was a limiting value countercurrent airflow, at which the spread of flame on the fuel surface was actually arrested by the opposed airflow.

The flame will spread along the surface of a liquid pool until it reaches the limits of the pool area, at which point the fire enters a steady burning period. This period of steady burning is often of the most interest, as it represents the most typical fire hazard and is the longest duration burning period in thick layer pool fires. The rate at which fuel in a liquid pool fire is consumed is typically expressed in one of two methods. The first – often used in small scale measurements – is mass loss rate (MLR), typically reported in kg/m^2s. The second – used in large scale experiments and in reports of actual fires – is liquid fuel regression rate (FRR), reported in units of mm/min. As large scale experiments and real fires are typically beyond the capacity of load cells, fuel surface regression is measured and, as necessary, converted back to mass loss rate. Similarly, many small-scale experiments are conducted with a small fuel layer thickness, making direct measurements of regression rate difficult; therefore, mass loss rate measurements are often taken.

Regardless of the value measured, mass loss rate and fuel regression rate are taken to be interchangeable based on an average value of the fuel density and the burning surface area of the pool, as:

$$R = \dot{m}\frac{1}{\rho A} \quad \text{and} \quad \dot{m} = R\rho A \tag{2.1}$$

where $\dot{m}$ is the mass burning rate, R is the fuel surface regression rate, A is the surface area of the pan, and ρ is the fuel density.

One of the first, and most frequently cited, experimental analysis of liquid burning rates was presented by Blinov and Khudyakov in 1961 [38]. This work included an extensive analysis of the burning behaviour various hydrocarbon fuels – from light to heavy oils – at a wide range of pool diameters, and was presented as a characteristic plot of various materials. This characteristic curve of regression rate versus pan diameter is shown in Figure 2.2. In their work, the regression rate was first found to decrease as a function of increasing diameters for small diameters, stayed approximately constant for a small range of medium diameters and then increased again, to an approximately constant value of 4 mm/min for pan diameters greater than 1 m in most of the fuels tested.

From this analysis, it was determined that there are three dominant fluid flow regimes affecting the fuel regression rate of pool fires. Laminar flow predominates the fire plume for small pool sizes, and conduction to the pan walls increases with pan diameter, therefore lowering the regression rate as diameter increases. For pan diameters in the middle range ($0.03 < d < 1$ m), the fire transitions from laminar to turbulent flow with increasing diameter, and flame radiation gradually becomes the dominant mode of heat transfer. Finally, the fire becomes fully turbulent at diameters greater than 1 m, where the regression rate is driven by radiation from the flame to the fuel surface, and is therefore independent of pan diameter [23].

The characteristic regression rate curve is seen in most fuels, and a limiting regression rate of 4 mm/min is considered to be accurate for most hydrocarbon fuels. Overall, the results of Blinov and Khudakov are consistent with most of the experimental results presented in the literature [22, 58, 59]. This curve is therefore presented for use in fire hazard calculations by the SFPE [20] and Drysdale [21], among others.

Small scale pool fires are of little interest outside of academic research; therefore, much of the work on regression rate has been done to characterize the burning behaviour of medium and large scale pool fires, mostly greater then 0.05 m in diameter [22, 23, 59–62]. Further work has been done to determine an empirical fit for the diameter dependence

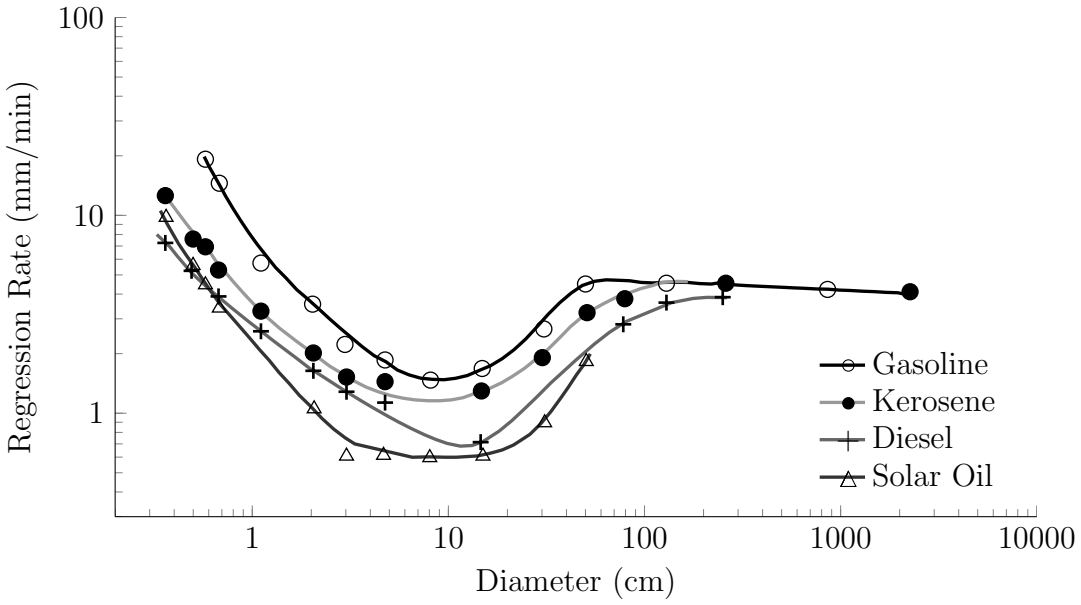

Figure 2.2: Effect of pan diameter on liquid fuel regression rate for various fuels as measured by Blinov and Khudyakov (Reproduced from [41]).

on the regression rate for hydrocarbon fuels [22, 63], among others. As a result, the fuel regression rate can also be reported as an empirical fit to a negative exponential of the pan diameter [22], such as

$$\dot{m}'' = \dot{m}''_{\infty} \left(1 - e^{-k\beta d}\right) \tag{2.2}$$

where $k\beta$ is an empirical fit parameter, and $\dot{m}''_{\infty}$ is an area normalized mass burning rate for pools of 'infinite' – or greater than 1 m – diameter [22]. This type of exponential growth is limited to pan diameters greater than 0.2 m, as it does not consider the effects of conduction to the pan burner for small diameter fires. As the fuel regression rate is linearly derived from the mass burning rate as a function of the fuel density, a more useful form of the fuel consumption rate is provided in equation 2.2.b.

$$R = R_{\infty} \left(1 - e^{-k\beta d}\right) \tag{2.2.b}$$

This is the form proposed by Burgess [59], where R is the fuel surface regression rate at a given diameter and R_{∞} is the predicted regression rate for pools of 'infinite' diameter.

Values of both R_∞ and $\dot{m}''_\infty$, as well as $k\beta$ have been measured by various researchers and comprehensive lists for various fuels have been tabulated by Babrauskas [22], Drysdale [21], Burgess [59], the SFPE [20], among others. For heavy hydrocarbon fuels such as that of interest here, the infinite mass burning rate is in the range of 0.039 kg/m^{2}s for kerosene to 0.022 kg/m^{2}s for some crude oils. Similarly, the empirical coefficient ranges from 3.5 m^{-1} to 1.7 m^{-1} for kerosene and heavy fuel oil respectively [22].

There has been significant research into defining empirical relations for the effect of pool diameter on burning rate; however, these are affected by the measurement method, and can vary significantly based on the composition of the fuel as well. Therefore, some work has been done to develop fuel consumption rate formulas that incorporate the material properties of the fuel. An infinite diameter fuel regression rate was proposed by Grumer et al. [64], that incorporated the material properties of a blended fuel and is based on several heat transfer simplifications. This relation is shown in equation 2.3.

$$R_\infty = 1.27(10^{-6}) \left[\frac{\sum_{i=1}^{N} n_i \Delta h_{c_i}}{\sum_{i=1}^{N} n_i \Delta h_{v_i} + \sum_{i=1}^{N} m_i \int_{T_o}^{T_b} C_p(T) dt} \right] \tag{2.3}$$

However, this relation requires detailed information about each component in the fuel – such as the heat of combustion Δh_C, heat of vapourisation Δh_v, and specific heat capacity C_P – and therefore cannot reasonably be applied to complex mixtures of hydrocarbons, where the exact composition is often poorly specified. Furthermore, it has been found that a complex fuel blend with components of widely varying volatility will not burn at a uniform rate. Rather, the highly volatile components will burn at a higher fuel consumption rate initially, then the burning rate will decrease as the heavy components are consumed [65]. This method has therefore not gained widespread adoption, and the experimental measurement methods are typically employed instead.

While the constant fuel regression rate at diameters past 1 m as presented by Blinov and Khudayov is commonly quoted, there is debate about the effect of fuel type on the diameter dependence of regression rate, as well as the physical processes that dominate burning in large diameter pans. Chatris et al. [63] measured an increase in fuel burning rates for diesel and gasoline pool fires with diameters from 1.5 to 3.0 m, yet no change for fire diameters between 3.0 and 4.0 m. Koseki [66], conversely, found a decrease in fuel regression rate from a pan diameter of 1 m to 20 m using crude oil. The amount of data at very large scale pan diameters is limited, and the quality of these results is likely to be largely affected by experimental conditions, including wind and ambient temperatures. It is difficult to control the experimental conditions at this scale, and it is expected that

the exact conditions varied between researchers – as well as between tests by the same researchers – during these measurements, possibly explaining these discrepancies.

While the effect of pan diameter on fuel regression rate is well researched and extensively documented, there are several other factors that affect the fuel regression rate as well. For example, as the burning rate is directly impacted by the availability of oxygen to the flame, the distance from the fuel surface to the rim of the pan has been found to have an impact on the rate of mass loss. The effect of lip height has not been investigated as extensively as the effect of diameter; however, correlations to account for this affect have been proposed. The most applicable model to estimate the effect of lip height on rate of mass loss has been proposed by Dlugogorski [67] based on the non-dimensionalized lip height, $H^* = H_{\text{lip}}/d$ where H_{lip} is the height between the fuel surface and the pan lip. For most hydrocarbons, this correlation takes the general form of the diameter dependent mass loss rate weighted by an exponential decay empirical fit, in the form of equation 2.4, where η is a fitted parameter found from experimental results.

$$\dot{m} = \dot{m} \exp\left(-\eta H^*\right) \tag{2.4}$$

The burning of liquid fuels is greatly dependent on the pool depth, with the burning of thin layer spill fires having different characteristics from the burning of deep storage tanks. When the fuel layer is thin, heat from the flame column is transferred through the fuel layer and into the bottom boundary; thereby acting as a heat sink, and reducing the energy available to vapourise the fuel. A reduction in fuel regression rate is therefore found with decreased fuel layer thickness [63, 68–70]. The dependence of the rate of fuel consumption on the fuel thickness has been found to decrease for initial fuel thickness greater than 5 mm for pan diameters of 0.15 to 0.5 m [68]. Furthermore, experiments by Mealy et al. [71] have determined that the surface onto which the fuel is spilled affects the rate of fuel consumption. Porous surfaces and surfaces with high heat capacity are shown to decrease the fuel regression rate in thin fuel layer spill fires due to the large heat sink effect.

The temperature of the liquid fuel also affects the burning rate, as the net heat radiated from the flame column to the fuel surface must bring the temperature of the fuel to the vapourisation temperature before fuel can vapourise. In fuels at elevated initial temperatures, less energy is required for heating the fuel, leaving more energy to vapourise the fuel. While the mechanisms are well defined, there has been little systematic study of the effects of initial fuel temperature on the burning rate of liquid fuels. Randsalu [72] performed a rudimentary investigation on the effects of fuel temperature on the regression

rate of 2.0 m diameter Jet-A pool fires. He found a mild increase in the measured regression rate over a 13 °C increase in initial fuel temperature. These results are not conclusive, as the ambient air temperature also increased incrementally with the fuel temperature in these experiments. Chen et al. [73] performed an extensive analysis of the effects of fuel temperature on regression rate in pools of n-heptane, using a temperature controlled test pan. In this experiment they found the burning rate during the steady burning period to be effectively constant; regardless of the initial fuel temperature. This is counter to the expected behaviour, especially since they considered a range of temperatures from ambient, 20 °C, to the boiling point of the fuel, at 120 °C. However, these experiments used a small initial fuel thickness of 13 mm, and it is expected that heat feedback from the pan bottom would have become significant as the fuel layer decreased below 5 mm.

In addition to the conditions effecting the burning characteristics of pool fires mentioned previously, there are a number of environmental factors which can influence fire behaviour. These factors are important when attempting to model the burning of pool fires, as well as to compare data from other researchers where large scale experiments could not be performed in tightly controlled laboratory conditions. One of the primary atmospheric conditions is that of prevailing winds. It is well understood that wind affects the flame shape, and therefore the heat transfer processes from the flame to the pan and fuel. However, there is disagreement throughout the literature on the overall effects of wind on the liquid fuel regression rate.

Blinov and Khudyakov [38] initially found that the fuel regression rate increased by $30 - 40\%$ in pools of diesel, kerosene, and gasoline at diameter greater than 1.3 m when the wind speed increased from 0 to 3 m/s. This was thought to be a result of better mixing of oxygen and fuel vapours throughout the flame column, therefore increasing the combustion efficiency. More complete combustion caused increased radiative feedback to the fuel surface, thereby increasing the regression rate. These experiments also found that the effect of increased wind speed on regression rate became negligible past a wind speed of 25 m/s. Best [74] also found an increase in regression rate with wind speed in 2.0 m diameter JP-8 pool fires, and documented an increase in regression rate of 36% for an increase in wind speed from 3 to 10 m/s. The results of Best, Lam, and Randsalu presented some of the most highly controlled experimental evaluations of the effect of wind on fire behaviour, having been done in a large wind test facility [72, 74, 75]. The results of other researchers are often presented as measured fuel regression rates as functions of average ambient wind conditions, and thus the data are subject to large variability.

It is well understood that the fire intensity grows with increasing fire diameter. The most meaningful measure of fire intensity is heat release rate (HRR), which is a measure of

the rate of total energy output of a fire per unit time – measured in watts. The definition of the rate of heat release is as follows:

$$HRR = \chi \dot{m} \Delta H_{\mathrm{C}} \tag{2.5}$$

where χ is the combustion efficiency, and ΔH_{C} is the theoretical heat of combustion of the sample. As the heat release rate is directly proportional to the mass burning rate, it is clear that the heat release rate is largely impacted by diameter of the fire. Furthermore, when the mass loss rate for liquid fuels is defined as in equation 2.2, the basic heat release rate relation (equation 2.5) can be equated as:

$$HRR = \chi \Delta H_{\mathrm{C}} \left[\pi \left(\frac{d}{2} \right)^2 \dot{m}''_{\infty} \left(1 - e^{-k\beta d} \right) \right] \tag{2.5.b}$$

While a strong dependence on diameter is evident, the heat release rate is largely affected by the regression rate of the liquid fuel, therefore the conditions such as initial fuel temperature, wind speed, lip height, and the other factors discussed previously all have an effect on the heat release rate of pool fires.

The combustion efficiency, χ, is an important factor in the determination of the heat release rate. The combustion efficiency is measured as a fraction of the maximum possible energy that can be released at a given time, with 1 representing the theoretical condition of 'complete combustion'. The combustion efficiency is typically determined from experimental heat release rate measurements, as compared to the theoretical heat of combustion. For example, equation 2.5 can be isolated for the combustion efficiency; where the total energy released is found from the integral of the measured heat release rate, and the maximum possible energy release is found by the total mass multiplied by the heat of combustion, as shown:

$$\chi = \frac{\int (HRR)\, dt}{m_{\mathrm{i}} \Delta H_C} \tag{2.6}$$

where HRR is the measured heat release rate curve and m_{i} is the initial sample mass. As the combustion efficiency is derived from experimental results, it too, is dependent on the experimental conditions, much the same as heat release rate and fuel regression rate.

In reality, combustion processes taking place in liquid fuelled fires are not ideal, and the combustion efficiency is found to decrease with increased fuel complexity [8], due to the

increased energy requirements to vapourise the fuel at the surface. Pool fires in alcohols and simple hydrocarbons have a combustion efficiency nearing 1, and produce a nearly invisible flame and little smoke. Fires fuelled by heavy oils, by comparison, have a much lower efficiency and produce a luminous flame and thick, black smoke. The combustion efficiency is also found to decrease with increased pool diameters, and is hypothesized to be a result of the decreased availability of oxygen to the center of the flame column as the pan diameter increases [62].

As the heat release rate is a measure of the rate of energy release of a fire and increases with pan diameter, so too does the flame height. The fire plume is comprised of three regions: the persistent flame zone, intermittent flame zone, and the buoyant plume [76]. These regions are shown graphically in Figure 2.3. In quiescent wind conditions, a visible flame is continually present in the persistent flame zone, where a vapour rich region exists directly above the fuel surface. Vapours that are not consumed within this region are elevated by the buoyancy of the heated gases, and are combusted in the intermittent flame zone as oxygen is mixed with the vapours. Finally, the buoyant plume contains heated combustion products and any remaining unburnt fuel vapours. While all three of these phases make up the fire plume, there is a large variation in the position of the flame tip at any given time. Due to the inherent variation of the flame height with time, the flame height – or flame length – is often defined at the location along the centreline where flame is present 50% of the time [77]. The frequency at which flame is present at a given height from the base of the fire is termed the flame intermittency, and is a measure of the probability that flame is present at a location at a given time. The intermittency therefore has a value of 1 in the persistent zone, where flame is continually present, and approaches 0 with increasing distance from the fuel surface. An example of the intermittency as a function of height above the fuel surface is shown on the left side of Figure 2.3.

Similar to fuel regression rate, Blinov and Khudyakov performed a series of experiments to investigate the effect of fire diameter on the fire plume height [38]. This study resulted in a graphical representation of the flame height as a function of pan diameter for a range of hydrocarbon fuels where the flame height normalized by pan diameter was seen to decrease with increasing diameter. This plot is shown in Figure 2.4 for a number of hydrocarbon fuels. As well, they observed a nearly consistent diameter normalized flame height for pan diameters greater than 2 m for most hydrocarbon fuels.

Analytical models and correlations for the flame height have been proposed by various researchers. A strong correlation between the heat release rate and flame height was found by Heskestad [78]. His semi-empirical relation for flame height as a function of heat release rate is shown in equation 2.7, where L_{f} is the 50% frequency intermittent flame height, and Q is the expected heat release rate at pan diameter d.

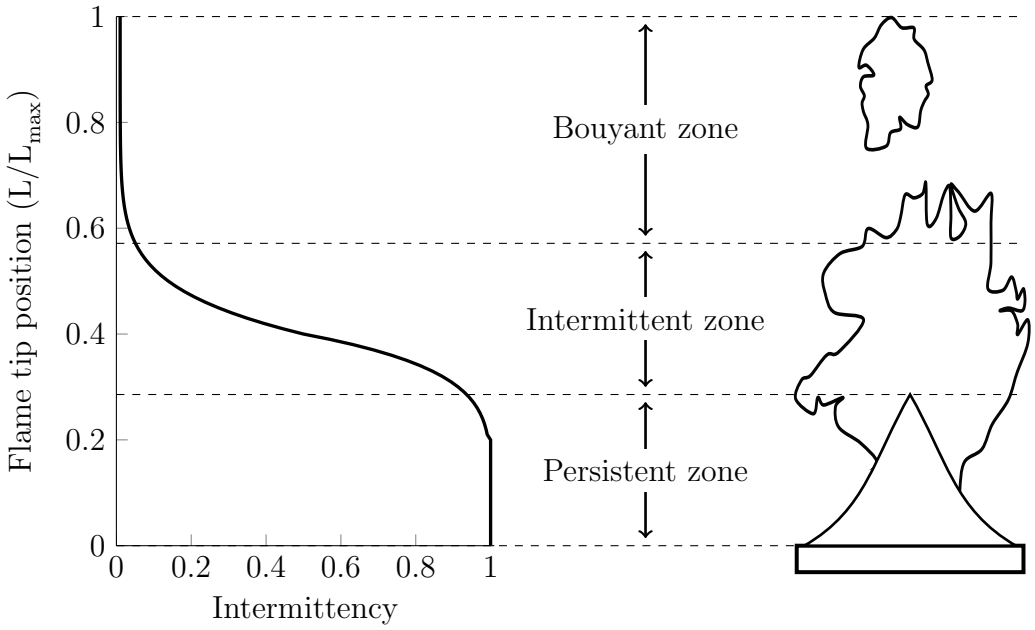

Figure 2.3: Flame intermittency as a function of flame height, showing flame zones.

$$L_{\mathrm{f}} = 0.23Q^{2/5} - 1.02d \tag{2.7}$$

Again, the heat release rate model shown in equation 2.5.b can be used to estimate the flame length as a function of pan diameter and material properties, such as

$$L_{\mathrm{f}} = 0.23\left[\chi \dot{m}''_{\infty} \Delta H_{\mathrm{C}} A \left(1 - e^{-k\beta d}\right)\right]^{2/5} - 1.02d \tag{2.7.b}$$

This relation is consistent with the experimental results of Blinov and Khudyakov shown in Figure 2.4, where fuels with a higher heat of combustion are found to have a greater flame length. Overall this expression has been found to be highly durable for many liquid hydrocarbon fuels, regardless of the thermophysical properties. This correlation is therefore used for fire hazard estimations by the United States Nuclear Regulatory Commission [79] and the SFPE Handbook of Fire Protection Engineering [20], among others, for heavy hydrocarbon pool fires.

Pool fires are characterized by a complex energy exchange between the flame column and the fuel. Radiation from the flame column is incident on the pool surface, and the energy is then conducted through the depth of the fuel. The energy impinging on the fuel

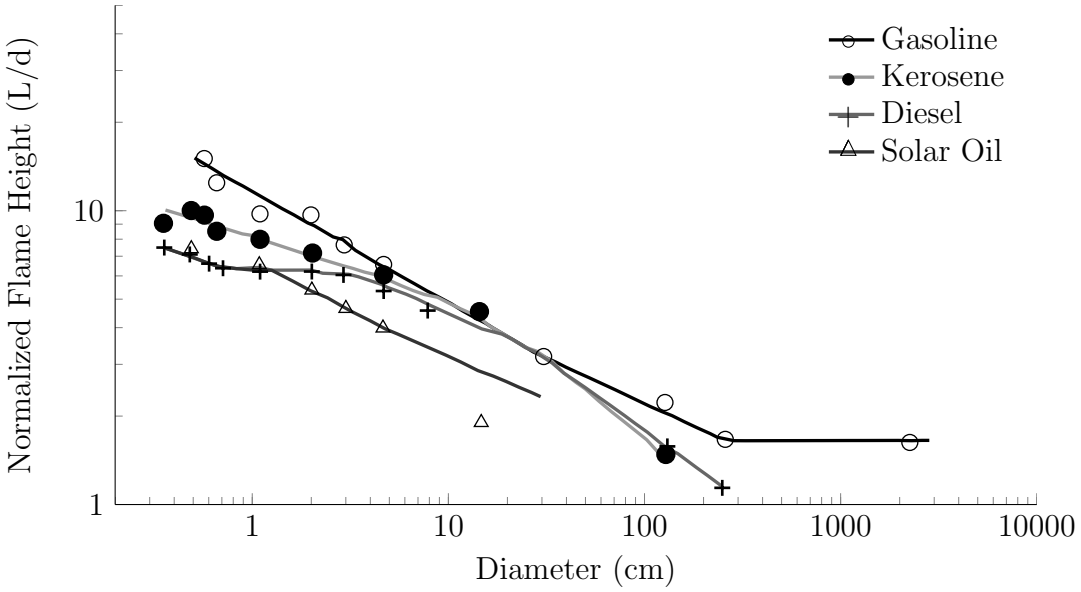

Figure 2.4: Effect of pan diameter on flame height for various fuels as measured by Blinov and Khudyakov (Reproduced from [41]).

surface heats the liquid below the surface through conduction and convection. Part of this energy is lost to vapourisation of the fuel at the surface - which then combusts and releases more energy to the fire column. Energy supplemental to that required to vapourize the liquid is conducted through the fuel, heating the bulk liquid below the surface.

How energy is transferred into the bulk liquid, and the resulting temperature distribution into the depth of a liquid pool fire, is of significant academic interest, and has been extensively studied [80–83]. Many studies have measured the temperature distribution through the depth of a fuel, as well as attempted to characterize the radiation feedback to the fuel surface. Fuels can be subdivided into two primary categories based on the details of heat transfer into the bulk liquid fuel. These are the traditional fuels – such as gasoline, kerosene, diesel – which burn as relatively stable pool fires, and those fuels that form a hot-zone – such as crude oil which, under certain conditions, can result in boilover.

Figure 2.5 shows a schematic of temperature profiles into the depth of a liquid pool fire, representing the two heat transfer conditions. These profiles show the location of the fuel surface in red, and demonstrate the regression of the fuel surface and corresponding temperature profile at three separate times, $t_{1\rightarrow3}$, during the burning period. Figure 2.5a shows the temperature distribution through the depth of a traditional fuel, where the tem-

perature decays exponentially from the boiling temperature at the surface to the initial temperature near the bottom of the pool. Figure 2.5b shows the same plot of temperature through the depth of hot-zone forming fuel. The hot-zone is characterised by a growing band of fuel at a temperature approximately that of the boiling point. A more comprehensive discussion of the considerable literature on the formation of hot-zones and the theory of boilover is provided in Section 2.2.

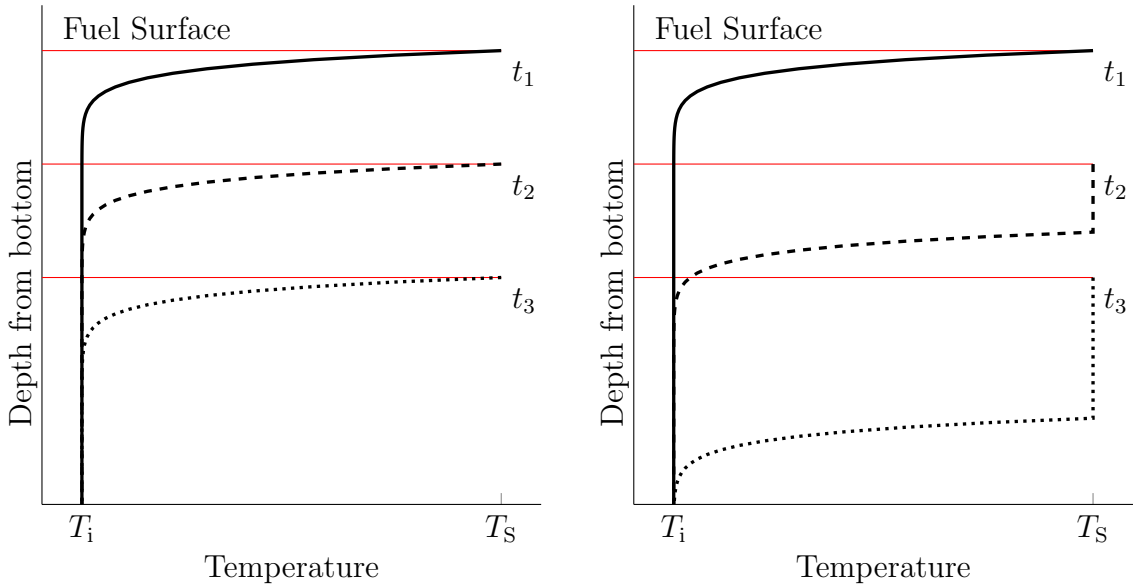

(a) Traditional fuel.

(b) Hot-zone forming fuel.

Figure 2.5: Temperature distribution through fuel depth at different times (t_{1-3}) for a traditional fuel (2.5a) and a hot-zone forming fuel (2.5b), showing fuel regression and temperature decay from fuel surface (T_S) to initial fuel temperature (T_i).

A one dimensional model has been proposed by Torero et al. [84] to describe the temperature distribution in the fuel for large diameter, thin fuel layer oil spills on the ocean. The one dimensional model was assumed to be valid in this situation, where the surface area is much greater than the area of the edges of the pool (having negligible edge height), thereby negating any pool edge effects. This model is therefore also applicable for large diameter storage tanks, where the heat loss from the tank walls is minor compared to the heat input to the fuel surface. This model is derived from the basic heat equation as solved in the form of transient heat conduction into an infinite solid, and is shown in equation 2.8.

$$\frac{T(y) - T_\infty}{T_\mathrm{s} - T_\infty} = \exp\left(-\frac{R}{\alpha}\left(y - y_\mathrm{s}(t)\right)\right) \tag{2.8}$$

In this model, $T(y)$ is the temperature at depth y from the surface, R is the assumed steady state fuel regression rate, and α is the thermal diffusivity of the fuel. It is important to note that this model is independent of time, as the liquid assumes a constant temperature profile into the depth of the fuel during the steady burning period. Moreover, the model shows that there is little dependence of the temperature distribution on pan diameter, most notably past 1 m in diameter, when the regression rate becomes constant with increased diameter. This model predicts the temperature through a homogeneous fuel layer; however, the effect of the water layer becomes significant as the fuel layer thickness decreases [84]. Several two-layer models have been proposed to account for the effects of the water sublayer [84, 85]; however, they will not be discussed in this work as this level of complexity may only be necessary in situations having a small fuel layer thickness.

Of further interest is the temperature distribution into the depth of fuels forming a hot-zone, and significant research has been devoted to modelling this. It is understood that the temperature decay under the hot-zone is well represented by the thermal decay of a traditional fuel; however, the growth of the hot-zone is not well predicted. Nakakuki [86] performed an intensive analysis of the heat transfer mechanisms in medium-scale fuel oil and gasoline pool fires, and compared a multi-dimensional model with experimental measurements. This model predicted the formation and spread rate of a hot-zone for the fuel oil; however, the model was not validated for other hot-zone forming fuels.

Alnasser [85] constructed a finite element model of a crude oil storage tank and compared the effects of various levels of model complexity on predictions of hot-zone formation and growth. The important phenomena considered included temperature dependent material properties, convection currents, and reservoir wall heat transfer. When compared with experimental results presented in literature (for example, from [87]), the model was used to compute results with varying degrees of success. The observed differences were attributed to the lack of information on experimental parameters presented in the literature. It is unclear how the model would perform if compared to experimental results with well-defined parameters. Of note from this study was that a change in fuel density as a function of temperature was required for the computational model to predict the formation and growth of a hot-zone.

Should a fire continue to grow and become well established, the primary objective in mitigating the consequences is often to suppress the fire. In storage tanks, pool fires may burn valuable products in which case attempts are made to suppress the fire without

corrupting the bulk liquid fuel, such that the product can be reclaimed. Despite the importance of fire control and extinguishment, suppression of pool fires – especially with water as the suppression agent – has not been widely studied. Due to the limited number of large-scale experimental results, there is little evidence to suggest a suppression water volume flow rate for a given fire heat release rate or tank diameter; and recommended fire suppression practices are often based on historical evidence [2, 88].

Water has a high heat capacity and is well known to be effective at suppressing fires in combustible solids. Water spray is often not used on liquid tank fires; however, since violent interactions between the water and heated fuel can sometimes occur. Also, the high flame spread rates of liquid fuels might allow the flame to quickly propagate back across previously suppressed areas, thus reducing the effectiveness of the water spray. Instead, Aqueous Film Forming Foams (AFFF) are often mixed with water and used to suppress hydrocarbon pool fires [88]. This agent forms a viscous film that spreads across the fuel surface and acts to separate oxygen from the fuel vapours without mixing into the fuel, thus suffocating the flames while also cooling the fuel at the surface. However, procurement of sufficient quantities of AFFF foam for suppression of large diameter storage tanks can be prohibitively expensive. Therefore, there is increased interest in using high volume water spray suppression systems for the control of storage tank and other large area pool fires.

Water sprays act to suppress pool fires through various mechanisms, most notably through heat absorption from the flames and surrounding environment, reduction of heat feedback to the fuel surface, generation of steam with consequent oxygen displacement, and dilution of the fuel vapour-air mixture near the flame core [89]. Several studies have been completed to analyse the effectiveness of water suppression on small and large scale hydrocarbon pool fires. Ho [90] investigated the effect of mean water droplet size in water mist suppression systems for high flashpoint hydrocarbons. He found that application of water sprays to heated oil systems enhanced mixing of the heated layer near the surface with the bulk oil, rapidly reducing the fuel temperature at the surface. The effect of the water interaction with the flame as well as the cooling effects in the bulk oil were found to quickly reduce the fire intensity, and eventually extinguish the fire. Jianghong et al. [91] analysed the effect of water mist suppression systems on the heat release rate of small scale ethanol pool fires using the cone calorimeter. They found a strong correlation between increased nozzle pressure in the water mist system (hence more and finer droplets) and decreased heat release rate in the fires. The energy from the flame required to vapourise the water droplets is therefore assumed to detract from the energy directed back to the fuel surface, thus lowering the energy available to produce flammable vapours.

Many hydrocarbon fuels, most notably oils, have densities close to, but lower than that of water, allowing water droplets from suppression sprays to sink into the fuel layer.

This can potentially cause the tank to overflow during suppression or, in some situations, increase the risk of phenomena such as *frothover* or *boilover*.Frothover occurs when suppression water is applied to oil pool fires and the water begins to sink into the hot fuel layer. Heat transfer from the hot oil at the surface brings the water to the boiling temperature, forming steam. The steam then mixes with the heated oil, resulting in the formation of a froth-type substance with a volume nearly 1100 times greater than the original oil. This rapid volume expansion overfills the tank in many cases, and can result in the heated oil and steam mixture spilling over the tank walls and spreading the flaming oil beyond the tank walls. In all cases such phenomena are unexpected and can certainly pose a significant risk to first responders and infrastructure. Boilover in storage tanks occurs as a result of a mechanism similar to slopover and frothover, and is described in detail in Section 2.2.

Pool fire behaviour has been of academic interest for many years, and there has been a significant volume of research devoted to better understanding the physics as well as the consequences of liquid fuelled fires. There is a clear disagreement between experimental results from various researchers about the effects of the various parameters on pool fire burning characteristics. Many correlations exist for the burning characteristics of liquid fuels; however, reliable data on the exact experimental conditions under which the experiments were performed are often not presented and many aspects of the behaviour have not been researched for all fuels. These limitations make comparison of experimental and predicted parameters difficult, where much of the error in the documented results is due to the difficulties in maintaining consistent experimental conditions for large-scale experiments. Furthermore, while there are empirical models to describe the burning behaviour of liquid fuels, there is little evidence to support the validity of these models beyond the experimental pan dimensions used in their development. Some physical and semi-empirical models have been well vetted for the prediction of small scale fire behaviour, but are not considered valid for predicting the behaviour or large scale real fires, or in cases of fires involving fuels with complex compositions. Nonetheless, the various empirical relations listed in the sections above are currently the best methods for modelling and predicting the burning behaviour of liquid fuels. For this reason, this study presents a comparison of the burning behaviour of heavy gas oil with the behaviour predicted by different models in an effort to ensure that the burning behaviour this novel fuel is adequately captured by these correlations.

2.2 Boilover

Boilover is one of several phenomena in which heated or flaming fuel is ejected from storage tanks during control and suppression of a pool fire. Boilovers can result in significant damage and often injure first responders, as evidenced by the 17 meter diameter storage tank boilover in Venezuela which caused over 150 casualties, and well over 20 million dollars in damages [33]. A fire in the United Kingdom in a 78 meter diameter tank containing crude oil resulted in a series of three boilovers, injuring six fire fighters and igniting two adjacent tanks, and had a total cost of 10 million pounds [2,34]. Because of the potentially devastating consequences of boilover, it has been the subject of a considerable amount of research.

Boilover is defined as the sudden expulsion and projection of tank contents during a surface fire, thought to be caused by water explosively vapourising into steam from under the contents [29]. Prior to 'boilover', heat is transferred through a thick fuel layer, resulting in the rapid vapourisation of a water sublayer and the ejection of a volume of flaming oil. It is characterized by a significant increase in flame column height, fire spread beyond the tank, and possible rupture of the tank walls. While the definition and consequences of boilover are well understood, the physical processes contributing to boilover remain largely undefined and are widely debated among experts [92].

There are two distinct types of boilover documented in literature, and these are often erroneously referred to interchangeably as boilover. The first case, most often referred to as *boilover* [27,28,87,92–94], involves the formation of a layer of heated oil that grows with time into the depth of the fuel at a rate greater than that of the regression rate of the liquid fuel. The layer of heated oil eventually interacts with a water sublayer near the bottom of the tank. In this case, a thick layer of fuel exists at the time of boilover (as exemplified in Figure 2.5b) and a significant volume of burning oil is ejected from the container. Thick layer boilover can therefore cause significant damage due to the projection of oil beyond the tank walls, and is thought to be the cause of the fatalities and destruction in historical boilovers such as Milford Haven [34].

The second type of boilover, *thin layer boilover* [25, 27, 31, 68, 92, 95], occurs mainly in fires fuelled by single component hydrocarbons. It occurs when the depth of the fuel layer decreases sufficiently that heat conducted through the fuel is able to initiate the boiling process at the fuel-water interface. In this case, there is only a thin layer of fuel in the tank at the time of boilover (as shown in Figure 2.5a). Thin layer boilover is therefore characterized by splashing of the fuel layer as the water layer boils violently, however with little ejection of fuel from the pan. It is clear, then, that thick layer boilover presents the

most severe scenario and will therefore be the focus of this section. In the effort to reduce ambiguity, 'thick layer boilover' will hereafter be referred to as boilover, while 'thin layer boilover' will be referenced by the full name for the remainder of this work.

In many cases, traces of water are added to crude oil during the extraction process, during cleaning of storage tanks, or from leaks in the tank roof [92]. Since it is impossible to remove all the water from crude oils while they are being stored, and since the density of oil is generally lower than that of water, the formation of a water sublayer in the storage tanks is generally unavoidable. Refineries attempt to remove the excess water from the tanks on a regular basis; however, it is believed that a water sublayer less then ten millimeters thick is sufficient to cause boilover during a tank fire [29]. For this reason, boilover is a primary concern in most facilities containing atmospheric hydrocarbon storage tanks, and facilities are often designed to mitigate the affects of boilover in the case of one.

The fuel characteristics and storage tank conditions necessary for boilover were originally defined by Hall in 1925 [58], and have since been elaborated by other researchers. The properties of fuels that are considered to pose the potential for boilover are that (1) the fuel must have a wide range of boiling temperatures [92], (2) the fuel must be highly viscous [92], and (3) the mean boiling temperature of the fuel must be greater than that of water, or 100 °C [96]. In addition, there must be a water sublayer beneath the fuel [92]. As highly complex fuel mixtures, crude oils are considered to be the most susceptible to boilover, though boilovers have also occurred in other fuels [2]. For example, the catastrophic boilover in Venezuela occurred in a tank containing high-flashpoint heating oil which had previously been thought to not present the risk of boilover [33].

A simplistic criterion has been established to estimate the probability of boilover based solely on material properties. This semi-empirical relation considers the mean fuel boiling temperature T_b, viscosity ν, and range of fuel boiling temperatures T_b. The boilover probability, F_boil, as calculated in equation 2.9, must be greater than 0.6 for the fuel to pose the possibility of boilover [23].

$$F_\mathrm{boil} = \left[\left(1 - \frac{393}{T_\mathrm{b}}\right)\left(\frac{\Delta T_\mathrm{b}}{60}\right)\left(\frac{\nu}{0.73}\right)\right]^{1/3} > 0.6 \tag{2.9}$$

The stages of boilover can be broken into three sections, namely the quasi-steady period, the premonitory period, and the boilover period [23, 26, 94, 97]. The quasi-steady period starts with ignition of the fuel and is a period of steady burning. During this period the flame structure, fuel burning rate, heat release rate, and other quantifiable measurements resemble those of traditional pool fires as were discussed previously. The duration of this period depends on the initial fuel thickness, with duration increasing proportionally with

increase in fuel thickness. At some point, the premonitory period starts as heat transferred through the fuel layer begins to heat the water beneath the fuel, bringing the water surface to the boiling temperature. At this point, water bubbles begin to break free from the surface and travel through the fuel layer. Once heated by high temperatures near the fuel surface, the bubbles rapidly expand and burst, resulting in crackling sounds and the ejection of oil particles. Finally, rapid boiling of the water sublayer results in the formation of steam which leads to ejection of much of the tank contents in the ensuing boilover period.

It is well established that boilover requires the initiation of boiling in the water sublayer at the fuel-water interface, while a thick fuel layer remains over top of the water. However, the path of heat transfer from the heated fuel surface to the water layer has not been established despite continued research. It was initially proposed by Hall [58] that heat is transferred by a layer of heated oil that grows in thickness with time. This heated layer is often referred to as a 'hot-zone', an 'isothermal layer', or a 'thermal band', and has been measured in numerous studies (for example [28, 32, 92, 98]). Hall proposed that the high temperature of the bottom boundary of the hot-zone causes the surface of the water layer to superheat, thus creating steam. Due to the high expansion ratio of water vaporizing into steam – as high as 1700:1 – an explosive force is generated beneath the contents, forcing the ejection of the tank contents. Figure 2.5b shows an example of the zone of heated oil growing with time at a rate greater than the fuel regression rate.

There have been several studies focussed toward defining the mechanisms for the formation and growth of the hot zone. Initial experiments by Blinov and Khudyakov [38] showed evidence that the formation of a hot-zone was driven largely by heat transfer through the pan walls, and into the fluid at a distance from the surface. This has since been refuted; however, by experiments that found that the bottom boundary of the hot zone was at a temperature exceeding the temperatures measured on the pan walls at the corresponding locations, indicating that there was a net heat loss from the fluid in the hot-zone to the pan walls [92].

It has also been proposed that the vapourisation of lighter hydrocarbons within the fuel layer results in bubbles of fuel vapour that migrate to the surface of the fluid prior to burning at the surface. The flow of vapour bubbles and heat transfer with the fuel layer results in a mixing of the heated fuel layer, and homogenizes the temperature of the hot zone. This has been supported by experiments conducted by Hasegawa [99], where the formation of vapour bubbles and violent oscillations of the fuel water interface were visually observed. It was thought that the interface oscillation was caused by the rapid formation of vapour bubbles near the interface. The movement of the vapour bubbles from the interface towards the surface was therefore considered to be evidence of convective currents through the fuel layer, and a possible cause of the hot-zone formation.

The most common theory of boilover, supported by Koseki [29, 40, 66, 87, 93, 98], Garo [95, 100], the LASTFIRE group [28], and others, is that a hot-zone forms in the bulk liquid as a result of a distillation process in the heated fuel near the surface. This theory considers that heating of the fuel near the surface causes the migration of lower boiling point hydrocarbons toward the surface which vaporize and burn there. The distillation of the low density hydrocarbon fractions results in the formation of a layer of heavier product with density greater than that of the original oil. The layer of heated, high density oil gradually thickens with time and – coupled with regression of the fuel surface – eventually reaches the water sublayer at the bottom of the tank. Comparable to the physical process of boilover, this layer of heated oil causes the water layer to boil, resulting in thick layer boilover.

The distillation theory has been supported by experiments in which the fuel burning characteristics change over the course of the burning duration. For example, the surface temperature has been found to decrease over the burning duration in hot-zone forming fuels, indicating that light hydrocarbons are consumed initially, leaving an increasingly dense residual [28, 87, 101]. The mass loss rate has also been found to decrease during the burning period, which helps to support that the light fractions are consumed at a greater rate initially [65]. Conversely, measurements of the fuel density at various locations within the hot zone have shown that the density of the heated oil did not differ significantly from the original oil at ambient temperatures [99], suggesting that the distillation of the fuel is not responsible for the hot-zone formation. These experiments do not represent a conclusive analysis; however, as only a small difference in densities is required for one liquid to sink into another.

Regardless of the specific mechanisms of hot-zone formation, there have been numerous attempts to characterize the growth and properties of hot-zones in crude oils. The layer of constant temperature has been found to grow at a rate of approximately $5 - 30$ mm/min for various types of crude oil [29, 92, 98]. The temperature of the hot-zone has been found to be approximately the same as that of the burning fuel surface [87], and varies by less than 1 °C/mm from the fuel surface to the bottom boundary of the hot-zone [98], indicating the uniformity of temperature in that region. It has also been determined that the bottom boundary of the hot-zone is at a higher temperature than the pan wall at the same position [92], indicating that heat transfer from the flame through the pan wall is likely not the cause of hot-zone growth. The rate of hot-zone growth is greater than the regression rate of crude oils, (for example, a regression rate of 2 mm/min is expected for 20 m diameter pans of crude oil [93]); therefore, the hot-zone can expand through the depth of the fuel and contact the water sublayer even when a thick layer of fuel remains. Furthermore,

studies have found that the severity of boilover is proportional to the fuel depth at the time of boilover [92, 93], and is therefore proportional to the initial fuel depth as well.

The time to boilover is an important parameter in the case of storage tank fires, as it is often used to estimate the length of time first responders have to control the fire before commencing evacuation. Figure 2.6 shows measurements of time to boilover for a hot-zone forming fuel as measured by Koseki [29] and for a non hot-zone forming fuel as measured by Garo et al. [100].

For a hot-zone forming fuel, the time to boilover is roughly calculated as the initial fuel depth times the sum of the rate of hot-zone growth rate and fuel regression rate, or

$$t_{\mathrm{BO,thick}} \approx \frac{h_{\mathrm{i}}}{R + u_{\mathrm{HZ}}} \tag{2.10}$$

An example of time to boilover as a function of initial fuel depth for a hot-zone forming fuel is shown in Figure 2.6a. The time to boilover in hot-zone forming fuels can been seen to be largely independent of pan diameter, as the increase in fuel regression rate with increased diameter is small compared to the magnitude of the hot-zone growth. Therefore, there is a strongly linear correlation between the time to boilover and the initial fuel thickness – irrespective of pan diameter.

In comparison to the above correlation for time to boilover in hot-zone forming fuels of various fuel depths, thin layer boilover occurs when the fuel layer is reduced in depth sufficiently for the heated fuel near the surface of the fuel to boil the water sublayer. The time to boilover in this case is the thickness of the 100 °C isotherm subtracted from the initial fuel height divided by the regression rate, or

$$t_{\mathrm{BO,thin}} = \frac{h_{\mathrm{i}} - h_{T=100\ ^{\circ}\mathrm{C}}}{R(d)} \tag{2.11}$$

Figure 2.6b shows measurements of time to boilover at different fuel depths for a non hot-zone forming fuel. In this case, there is a strong relation between the pan diameter and time to boilover, as well as the initial fuel thickness and time to boilover. As the depth of the 100 °C isotherm is relatively constant for these pan diameters, the trend lines in this plot have a slope equal to the regression rate at that pan diameter.

Also of interest in characterizing the overall hazard in the event of a boilover is the intensity of boilover, a parameter relating to observed changes in fire behaviour during boilover. Parameters such as volume of fuel ejected, growth of flame column, and increase

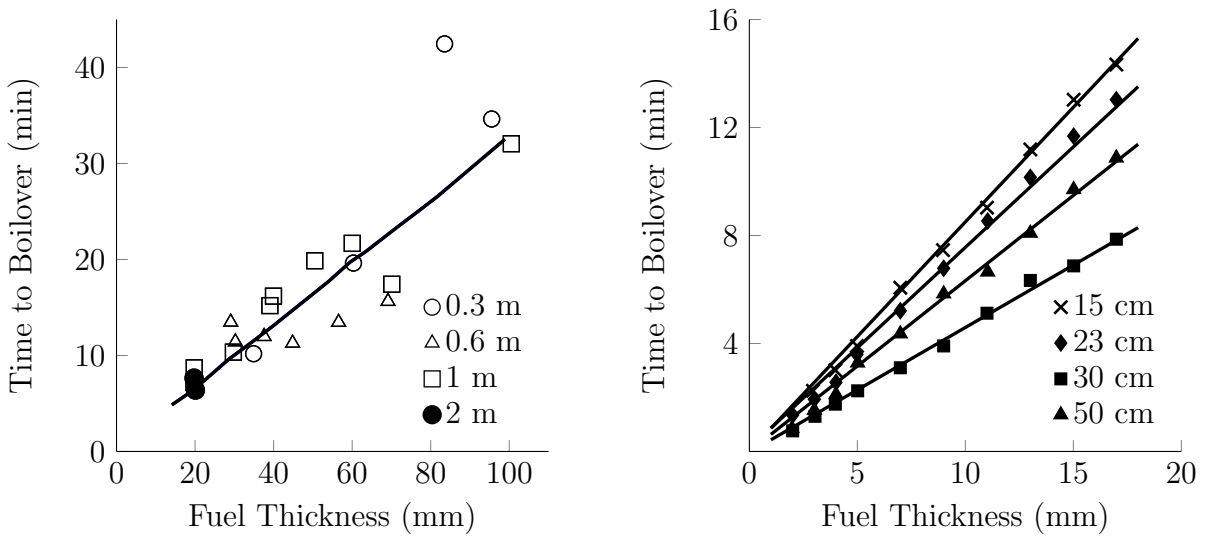

(a) Hot-zone forming fuel.

(b) Non hot-zone forming fuel.

Figure 2.6: Time to boilover as measured for a hot-zone forming fuel (2.6a) (Reproduced from [98]), and non hot-zone forming fuel (2.6b) (Reproduced from [100]).

in burning rate can be derived from the boilover intensity. A common definition of the boilover intensity is taken as

$$I_{\mathrm{BO},\dot{m}} = 100\frac{\dot{m}_{\mathrm{BO}} - \dot{m}}{\dot{m}} \tag{2.12}$$

where I_{BO} is the boilover intensity, and can be calculated with both peak and average values of mass loss rate during boilover, $\dot{m}_{\mathrm{BO}}$ [25]. The boilover intensity has also been represented from the change in fuel consumption rate as the ratio of the steady state regression rate to the maximum regression rate during boilover [98], or

$$I_{\mathrm{BO},R} = \frac{R}{R_{\mathrm{BO}}} \tag{2.13}$$

Alternatively, the intensity of boilover has also been related to the increase in measured heat flux from the flame column from a constant distance [98], as

$$I_{\mathrm{BO},q} = \frac{q_{\mathrm{BO}}}{q} \tag{2.14}$$

where q is the measured steady state heat flux and q_{BO} is the maximum measured heat flux during the boilover period. Generally, these two boilover intensity ratio calculation methods are within a very good margin of each other, and the mass burning rate method is consistently slightly larger [98]. These measurements of boilover intensity give a reasonable estimate for the increase in fuel consumption rate during boilover, therefore can provide insight into the increase in the heat release rate and other fire parameters discussed in Section 2.1 previously.

As boilover results in the ejection of flaming fuel and spread of fire beyond the container walls, it is a challenge to apply standard measurement methods to boilover intensity, and as such, it is not often measured. Realizing that both of the classic definitions of boilover intensity – change in mass loss, and change in radiative flux – are parameters directly related to the heat release rate, Laboureur [23] made an estimate of boilover intensity based on measurements of the increase in flame height during boilover since flame height is also directly related to heat release rate. This flame enlargement study was presented as an empirical correlation for boilover experiments using diesel oil, as shown in equation 2.15.

$$\frac{L_{\mathrm{bo,max}}}{L_{\mathrm{mean}}} = 15\left(1 - exp\left(-9\left(10^{-4}\right)\frac{h_{\mathrm{i}}}{d}\right)\right) \tag{2.15}$$

Boilover in storage tanks is a primary concern for the spacing requirements of storage tanks, as well as in the design of fire suppression systems. Regardless of the extensive research conducted on boilover in oils, the fundamental processes causing the formation of a hot-zone and subsequent boiling of the water layer remains unknown. Much research has been conducted to understand the boilover behaviour of crude oils; however, there is little information on the propensity of boilover in many heavy oils. Further study is required, then, to identify the possibility of boilover in heavy oils to ensure that first responders are adequately prepared in the event of a fire in a storage tank containing these fuels.

2.3 Experimental Measurement Methods

As is evident from the brief literature review above, a great volume of literature exists on the measurement and documentation of various key parameters that relate to the burning behaviour of pool fires. Throughout the past century, many techniques have been employed to measure the various characteristics that form input into the empirical correlations outlined above. This section details the measurement methods that have been successfully employed to measure these key parameters, as well as the relative errors encountered with use of these methods.

2.3.1 Rate of Fuel Consumption

Systematic measurement of the rate of fuel surface regression during pool fires has been performed extensively by various researchers since one of the first systematic studies by Hall in 1925 [58]. Due to the inherent issues in directly measuring the regression rate of a pool fire, these studies employed a range of different measurement methods. This section examines some of the methods used to measure the fuel regression rate of medium and large scale pool fires.

Randsalu [72] performed an exhaustive study on many of the techniques that had been used for measuring the fuel regression rate of pool fires. Some of the most notable and commonly used techniques include: a load cell [59], a thermocouple array through the fuel depth [102, 103], differential pressure transducers [103, 104], or a sight glass [38, 74]. Many experimentalists have also used a volumetric consumption method for estimation of an average fuel burning rate. In reality, this latter method is often the only tractable measurement method in very large experiments.

In the analysis by Randsalu [72], it was found that each of the first four methods was adequate for measuring the regression rate of large scale Jet-A pool fires. In fact, a maximum difference of 9% in measured values of fuel regression rate was found between the methods. Of those, the load cell, thermocouple rake and volumetric consumption methods merit further discussion here. These methods were found to have excellent test-to-test consistency, ease of implementation, and did not impact the fire behaviour.

Fuel regression rate has been derived from measurements of mass loss rate for a variety of pan diameters, ranging from 0.03 to 2.0 m (for example, in [23, 59, 65, 72]). In the method, the pan is placed on a load cell and the instantaneous mass is measured as a function of burning time. The regression rate is then determined from equation 2.1, based on fuel density and pan area. While highly accurate load cells are available, this method is subject to experimental errors. Firstly, load cells have been shown to record changes in ambient wind speed or direction as a change in mass [72]. Secondly, the method requires accurate measurements of the fuel density, which can change with variations in fuel temperature, and therefore may not remain consistent throughout the burning period, particularly for complex hydrocarbon fuels [65].

Linearly arranged thermocouples at a defined spacing, or thermocouple rakes, have been used in several pool fire experiments and are well vetted for measurement of fuel regression rate in large scale fires. Randsalu [72] used a thermocouple rake for regression rate measurements in 0.3 and 2.0 m diameter Jet-A pool fires. Ditch et al. [105] used a thermocouple rake in a much smaller, 0.1 m diameter, pan and derived the fuel regression

rate from recorded temperature data. In both cases, some error was introduced from establishing a characteristic temperature to indicate that the flame front had passed over the thermocouple bead. Randsalu [72] found that the error in the thermocouple regression rate measurement, as compared to the volumetric method, increased as the characteristic temperature approached and surpassed the boiling temperature of the fuel.

In the volumetric method, the fuel regression rate is determined via measurement of the volume of fuel placed into the container before ignition and again after the burning period. In addition the total burn time is measured so that an average fuel regression rate can be determined for the fire. The volumetric regression rate has been found to be accurate for long duration burning periods, where the steady burning period is significantly longer than the initial fire spread following ignition and the period of fire decay as the fuel level decreases.

2.3.2 Rate of Heat Release

Accurate measurements of the heat release rate from a burning fuel are typically achieved either via direct measurement method based on the principal of oxygen depletion calorimetry, indirectly from measurements of the radiative heat flux to a target, or calculation methods such as from measurements of fuel regression rate and equation 2.5.b. These methods are reviewed in turn below.

Inherent in the method of oxygen depletion calorimetry is the assumption that a constant amount of energy is released per unit mass of oxygen consumed by the fire. This constant amount of energy has been found to be 13.1 MJ/kg per kilogram of oxygen consumed, and is known to vary by less than $\pm 5\%$ for hydrocarbon based materials [106]. Several devices have been developed to utilize the concept of oxygen consumption calorimetry to determine the rate of heat release, for example the cone calorimeter.

The cone calorimeter is the most common heat release rate calorimeter currently in use, and is widely considered to be the standard testing apparatus for heat release measurements [107]. It was originally developed in 1982 at the National Bureau of Standards (now National Institute of Standards and Technology) [108].

The cone calorimeter uses a conical radiant heater to heat the surface of a sample until it forms sufficient vapour to ignite, with or without a pilot igniter positioned just above the sample surface. As the sample burns, the hot exhaust gases are drawn through a series of gas analysers. Measurements of the decrease in oxygen in the combustion products are used to calculate the heat release rate. A correction factor can be applied to the calculated

heat release rate when measurements of the carbon monoxide and carbon dioxide are simultaneously made [107, 108].

In general, the technique for oxygen consumption calorimetry testing is stipulated in the ASTM E 1354: *Standard Test Method for Heat and Visible Smoke Release Rates for Materials and Products Using an Oxygen Consumption Calorimeter* standard [109]; however, neither this standard test method, nor any other current standard referencing the cone calorimeter, has a provision for use in measurement of heat release from liquid fuels [109–112]. In actuality, the apparatus configuration and testing standard protocols are designed and optimized for use in testing solid fuels.

Regardless of this limitation, the cone calorimeter has been successfully used to measure the heat release rate and smoke development of liquid fuels in research applications [42, 65, 71, 91, 113, 114]. Much work is being done using the cone calorimeter to determine the necessary conditions for ignition in weathered fuels in the effort to examine the ignition of oil spills on the ocean [115, 116]. Finally, some work is being done to estimate the hazard from large diameter pool fires based on the results of small scale cone calorimeter measurements [117].

The heating element of the cone calorimeter has been used in various studies on ignition and heat release rate of liquid fuels [42, 91, 116]; however, the uniform incident radiant flux from this element to the surface of the fuel is not representative of a realistic pool fire scenario and is therefore not often used in studies on liquid fuels. Instead, the cone element is often bypassed and the spark igniter removed, in which case the fuel is ignited with an external ignition source such as a propane torch [65]. In this manner, a comparative ranking of the heat release rate, radiative fraction, heat of combustion, and smoke production from different crude oil samples was performed using the cone calorimeter [65]. In this study, no attempt was made to extrapolate the small scale data to the fire hazard at larger diameters or to estimate the effect of different initial conditions on key parameters of fire behaviour. Jianghong et al. [91] investigated the effects of water suppression on small pans of kerosene, and used the cone calorimeter to quantify the effect of the water spray on heat release rate.

In most cases, a pan of 0.05 to 0.15 m diameter is used for liquid fuel measurements under the cone calorimeter, mainly due to the dimensions of the test chamber, and the limitations of the load cell. Pans made of quartz, stainless steel, or Pyrex glass are typically used. In this small scale configuration, the lip height has a negligible impact on the fuel burning rate[1]; therefore, the fuel in the pan is often not automatically replenished during small scale cone calorimeter tests.

[1] In a 0.10 m diameter pan, a change in lip height from 0 to 10 mm will cause approximately 2% decrease in fuel burning rate [67].

The premise of oxygen consumption calorimetry has also been applied to large scale calorimeters, and an intermediate scale known as the furniture calorimeter has been developed by Fire Testing Technology as well. There has been little published work on heat release rate measurements of liquid fuels using an intermediate scale calorimeter, and almost no literature on the use of a furniture calorimeter to investigate the burning behaviour of pool fires. However, other large scale oxygen consumption calorimeters have been used to measure the heat release rate of large pool fires, including the use of well ventilated compartments [117, 118], and industrial scale calorimeters [119].

Due to the scarcity of comparative experimental measurements from the cone calorimeter and these large scale apparati, at the present time, there has been no systematic investigation into scaling results from the cone calorimeter to those from the furniture calorimeter using identical samples. Ezinwa et al. [120] compared fire scaling models with data from the cone calorimeter and furniture calorimeter for polyurethane foam. In these tests, they found a strong correlation between the heat release rate of large samples under the furniture calorimeter and the area normalized heat release rate of small samples under the cone calorimeter. In other research, Soderbom et al. [121] investigated the effects of ignition on the heat release measurements under the furniture calorimeter. In these tests, the location and intensity of the ignition source was found to have a significant effect on the ignition period in upholstered furniture, most notably in the time to peak heat release rate. However, once a fully developed fire was initiated, there was no quantifiable difference in the measured heat release rate. This trend has also been found for small scale pool fire heat release rate measurements under the cone calorimeter [65].

While the method of oxygen consumption calorimetry and the cone calorimeter apparatus is the most common method of measuring the heat release rate in fires, there exists some variability in the measured values. The accuracy of the cone calorimeter, representing the difference between the known and the measured heat release rate of a given sample, is well defined and has been measured to be approximately $\pm 5\%$ [122] for carefully executed tests. Similarly, the accuracy of large-scale furniture and industrial calorimeters have been found to be within $\pm 7\%$. However, regardless of the accuracy of the apparatus, there can be a significant variation in measured values of heat release rate of the same sample when testing is done at different test labs and sometimes even by different operators within the same lab. A round robin series of cone calorimeter experiments resulted in estimates for the peak heat release rate repeatability and reproducibility of 17 percent and 23 percent, respectively [122]. The difference between cone calorimeter measurements worldwide has been attributed to operator error, apparatus calibration, and sample preparation; and is found to be minimal within inter-laboratory experiments.

Other attempts to characterize the heat release rate of liquid pool fires have been made, albeit with limited success. A frequent estimation of the heat release rate is done using a bomb calorimeter, a lab scale apparatus used to measure the theoretical heat of combustion using thermodynamic principals [7,82]. Given the theoretical heat of combustion, the heat release rate can be estimated using equation 2.5, coupled with an assumed mass loss rate and combustion efficiency values. Inherent in this method is the error associated with assuming or measuring values for mass loss and estimating combustion efficiency, as these parameters are highly dependent on the physical configuration of an individual test system.

Estimations of the heat release rate from large diameter pool fires has been also been attempted through the measurement of flame height and use of correlations, such as given in equation 2.7, to back calculate the associated value of heat release rate. Others have attempted to measure the radiative flux from the flame column using radiometers at precise distances from the fire [62,65,123,124]. The heat release rate is then calculated using point source or other thermal radiation models to determine the total energy released from the fire. In each case, these methods are extremely sensitive to measurement accuracy, input assumptions for the models used and the environmental conditions, especially wind.

2.3.3 Rate of Flame Propagation

Mackinven et al. [54] performed one of the earliest and most significant flame propagation experiments for liquid fuels. These experiments were conducted to investigate the effects of various experimental conditions on the measured value of flame spread rate for a range of liquid fuels. The parameters investigated included the burner pan materials and dimensions, as well as fuel ignition methods. This study ultimately resulted in the introduction of a proposed standardized flame propagation apparatus, as well as a standard test method for measuring the flame spread rate over liquid fuels.

Extensive measurements were conducted to determine the effect of both pan width, and initial fuel depth, on the flame spread rate [54]. It was found that both dimensions had a significant impact on measured values of flame spread. Figure 2.7 shows the effect of fuel depth (Figure 2.7a) and pan width (Figure 2.7b) on the flame spread rate over aviation kerosene at sub-flashpoint temperature.

The rate of flame spread was found to increase with increased fuel depth, until a fuel depth of approximately 20 mm. At fuel depth greater than this, only small increases in flame spread rate were noted, and the behaviour represented that expected over a fuel layer of infinite depth. At fuel thickness less than 2 mm, the flame would self-extinguish and no flame spread was recorded. The flame spread also increased with increased test pan width.

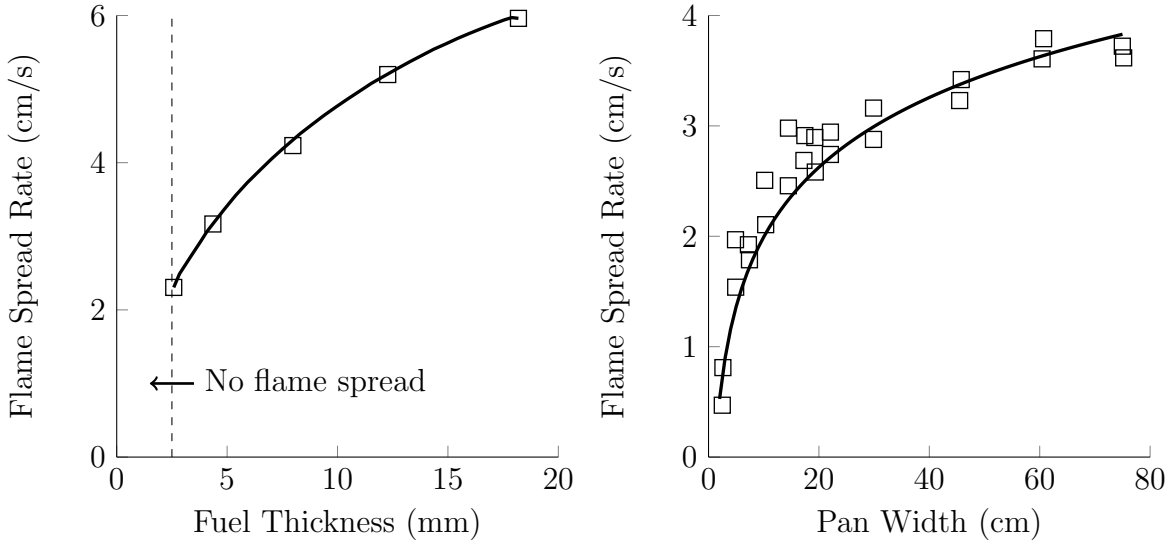

(a) Initial fuel thickness.

(b) Pan width.

Figure 2.7: Effect of fuel layer thickness (a) and test pan width (b) on the flame spread rate of aviation kerosene (Reproduced from [54]).

In this case, a limiting flame spread was noted for pan width of approximately 80 cm; however, a nearly constant flame spread rate was found past 40 cm, with only a small increase in rate between 40 and 80 cm [54]. It should be noted that the square symbols in Figure 2.7b represent experimental measurements with both aluminium and Pyrex glass test pans, indicating a relative independence of flame spread on pan material.

Mackinven et al. [54] also recommended a standard test procedure for measuring the flame propagation rate. This procedure recommended that experiments be conducted in a wind and temperature controlled laboratory equipped with extraction fans for the combustion products. Measurements of initial fuel temperature, air temperature and humidity were to be recorded prior to ignition. The fuel was to be kept in a temperature controlled bath until immediately prior to test start. Ignition of the pan was achieved by igniting a small portion of hexane or alcohol at one end of the pan, and allowing the flame to propagate from there. Once flame spread to the extent of the pan, the fire was to be suppressed with a flame resistant board [54].

Many recent flame spread rate measurements have followed the directions of Mackinven et al. to a large degree. White et al. [45] performed a series of experiments on aviation kerosene, using a stainless steel test pan 1.63 m long by 0.20 m wide. A minimal fuel

thickness of 25 mm was used in these experiments. Gou et al. [46] used a narrower pan than that recommended by Mackinven, at 100 cm long, by 10 cm deep and 4 cm wide, to measure the flame spread rate of kerosene with an obstacle in the spread path. Finally, Zhou et al. [48] performed a number of experiments to investigate the temperature dependence of flame spread rate, using a pan with dimensions of 100 cm long, 12 cm, wide and 4 cm deep.

Flame front location during the flame spread period has been measured by various methods in documented experiments. Mackinven et al. [54] measured the flame front visually and recorded the time at which the flame front passed a set of marked locations, as well as using a series of phototransducers. They concluded that either method produces accurate results and found less than 10% difference between the two methods. Zhou et al. [48] used a combination of digital cameras, infrared cameras, and submerged thermocouples to locate the flame front. In this experiment, each of the three measurement methods produced comparable measurements of flame spread rate. It can be said then, that the visual observation of flame position therefore provides a consistent and low cost measurement of flame propagation rate.

2.3.4 Temperature Profile

Temperature profiles through the depth of the liquid fuel during a surface pool fire are frequently recorded [27, 27, 29, 32, 87, 92–96, 98, 125]. Many of these experiments used a thermocouple array to measure the formation of a hot-zone within the fuel, and the growth of that layer over time [32, 87, 94]. Other experiments have used thermocouples to model the heat transfer into the fuel and predict the temperature profiles [84, 92]. Lastly, infrared cameras are often used to measure the temperature profiles though the flame [37, 126], as well as monitor the pan walls for evidence of formation of a hot-zone [37, 127].

Since the formation and growth of hot-zones has been found to be largely independent of pan diameter [21, 66, 98, 100] various sizes of pans have been used in previous research. Koseki measured a hot zone in crude oil samples using pans ranging from 0.3 to 2.7 m diameter, and using a variety of fuel layer thickness of 35 to 100 mm at each diameter [98]. Other small-scale measurements of a hot-zone have been achieved in pans of diameter between 7 cm [32] and 5 m [93].

In addition to the pan diameter for the pool fire experiments, the pan material has been found to affect the heat transfer modes in pool fires. Hot-zone formation has been investigated in pans of various materials, and a distinct hot-zone has been documented in pans constructed of stainless steel, glass, and steel with insulated walls [32]. There is

little consensus on the effect of pan material on hot-zone formation, as the exact heat transfer mechanisms and magnitudes of each have been found to differ for different pan materials [23]. Furthermore, the pan materials is known to have a larger effect on the burning characteristics at small scales [67].

The measurement of the time evolution of a temperature distribution through the depth of the fuel during a pool fire experiment is typically done using of an array of thermocouples, often named a thermocouple rake. The design and installation of thermocouple rakes to measure temperatures during a fire presents a significant challenge, and numerous designs have been used in recent experiments.

In many experiments by Koseki, a special pan was constructed, allowing for the penetration of the thermocouple leads through the bottom of the test pan [98]. In this case, the thermocouple leads are kept away from the flame column, minimizing the risk of heat conduction along the thermocouples themselves. However, this design also constrains the thermocouple rake to a single position in the fuel, and can only be used for the design pan.

In experiments by Garo, an array of thermocouples was inserted through the pan wall, below the water level [96]. The thermocouple rake then extended towards the fuel surface and pan bottom. This also insured that the thermocouple leads were well insulated from the flames, however shared many of the same issues for a rake inserted from the bottom of the pan. In both the case of wall and bottom penetration, issues arise from sealing the hole as well as protecting the sealing material from the fire. Also, heat transfer though the wall and into the thermocouple lead can affect the measurements in small diameter experiments.

Several researchers have inserted thermocouple rakes into the test pan from the top. This design allows the rake to be quickly removed for maintenance and exchanged between test pans, and does not require penetrations through the sides or bottom of the test pans. Randsalu [72] inserted a stand alone thermocouple rake into 0.3 and 2.0 m test pans to record the fuel regression rate. The thermocouple leads traversed the width of the pan in the cold liquid fuel and then out of the pan near the pan walls, where there was minimal interaction of the leads with the flame. The thermocouple leads travelled sufficient distance in the cold fluid that any effects of heat transfer due to the thermocouple leads was considered negligible. Ditch et al. [105] also measured the fuel regression rate using a thermocouple rake inserted into the pan from the top. This experiment was very similar to that done by Randsalu, however the pan diameter was much smaller, showing that only a small length of thermocouple lead needs to be submerged in the cold fuel to negate the effects on measured temperature of flame attachment along the thermocouple leads.

Finally, Laboureur [23] used a multi-purpose rake inserted into the pan from the top, such that it could be quickly exchanged between different test pans. In this experiment, the thermocouple leads were inserted through a steel tube that was used to protect the thermocouple leads, as well as to maintain the desired thermocouple tip spacing. In initial experiments it was found that the steel tube conducted significant heat from the flame, down the tube, and into the thermocouple beads, thereby affecting the measured temperatures. Iterations of this rake design determined that an extended horizontal lead between the pipe and the bead acted as a heat sink, allowing for more accurate measurements of the fluid.

From the discussions above, it is clear that there are many experimental methods that have been successfully used to gain understanding into the burning behaviour of liquid fuelled pool fires. Some of the most common basic measurements that provide a better understanding of the burning characteristics include that of fuel regression rate, heat release rate, and temperature history. A subset of these experimental techniques was chosen to match the specific objectives of the present study. Further discussion of these, as well as a detailed description of the experimental protocols adopted in this research is provided in the next Chapter.

Chapter 3

Experimental Methods

As reviewed in Section 2, the burning characteristics of liquid fuels can be adequately summarized through measurements of the flame spread rate, heat release rate, and interaction with water. Global measurements of all these properties simultaneously is not practical as it requires a broad range of large scale experiments with significant instrumentation. In this work, therefore, each of these properties was measured in a series of individual experiments. An instrumented pan burner was used as the main experimental apparatus and, where the scale or configurations of this apparatus limited the measurements, additional experiments were designed and used. This chapter outlines the apparatus and methods used to measure and characterize the burning characteristics of the heavy gas oil. Experiments were also conducted with kerosene to compare the heavy gas oil with a well documented fuel, as well as to validate the experimental methods.

3.1 Experimental Parameters

3.1.1 Test Facility

All experiments were conducted at the University of Waterloo Live Fire Research Facility (UWLFRF), a satellite facility of the University of Waterloo (UW), located on the grounds of the Waterloo Region Emergency Services Training and Research Complex (WRESTRC). This facility is comprised of a large, open experimentation area, as well as small-scale laboratory equipment and extensive outdoor areas.

All experiments were conducted in the period of February 2013 through to November 2014, and were performed in weather representative of the given seasons. Atmospheric

temperatures during the experiments varied from -5 °C within the experimental enclosure during the spring to 25 °C during large scale experiments outside in the summer months. Experiments outside were conducted during days with low wind speeds, and on clear days with no rain.

3.1.2 Test Fuels

The primary experiments were conducted to characterize the burning properties of the untreated heavy gas oil. Additional experiments were conducted with kerosene to compare the burning properties of heavy gas oil with those of a well researched fuel. The properties of both fuels are shown in Table 3.1, as quoted from their respective Material Safety Data Sheets [36, 128].

Table 3.1: Material properties of test fuels used in this study [36, 128].

Fuel	**Density** (kg/m^3)	**Viscosity** (cP)	**Boiling Temperature** (°C)	**Flashpoint** (°C)
Heavy Gas Oil	980	10000	460	150
Kerosene	820	1.64	240	42

The untreated heavy gas oil samples were shipped from Alberta in 208 L (55 gal (US)) drums in three separate shipments throughout the duration of the experiments, namely in February, June, and September of 2013. Heat release rate measurements were taken for each barrel to ensure the consistency of the fuel throughout the experiments. The samples were extracted from a storage tank through a port near the bottom of the tank, and are assumed to be representative of the bulk heavy gas oil stored within the tank. The oil was stored at the UWLFRF in a drum that was maintained at a temperature of 40 ± 3 °C, using an electric resistance heating blanket. This was done to aid in the downward migration of any water that had emulsified with the oil during transport. Before testing, the fuel was further heated in an industrial oven to the appropriate initial fuel test temperatures; however, the duration of time each sample of oil spent at elevated temperature was not accounted for in the final results. Heat release rate measurements were taken throughout the testing period to ensure the consistency of energy content and equivalent composition of the fuel. Fuel density measurements were taken throughout the testing period to account for any differences in test fuel density from experiment to experiment.

A significant issue encountered in the initial experiments was the related to pockets of emulsified water that were present in the heavy gas oil. A full discussion on the effects of the emulsified water is presented in Section 4.6, however a summary of the issue is presented here since it directly impacted the experimental method. In the early experiments, it was found that as pockets of water in the bulk oil superheated due to the fire on the fuel surface, the water vapourised into steam, resulting in a series of small explosions. These, in turn, caused expulsion of particles of flaming oil from the test pan, and therefore presented a safety hazard during the testing. From experimental analysis it was determined that the viscosity of the oil lowered sufficiently at temperatures above 40 °C for the emulsified water to migrate toward the bottom of the reservoir. This volume of water at the pan bottom did not constitute sufficient water to generate a water sublayer that would cause a boilover; however, aided to reduce the microexplosions and consequent fuel ejections. For this reason, in all experiments, the heavy gas oil was heated to a temperature of approximately 50 °C prior to ignition in an effort to 'dry' the oil and minimize the risk of microexplosive behaviour.

Low-odour lantern kerosene was chosen as the reference fuel due the availability and low cost. It has a similar density and heat of combustion as the kerosene used in experiments documented in literature, so the present results were expected to be comparable to those reported in the literature. The kerosene was purchased from *Home Hardware* in 19 L (5 gal (US)) pails throughout the experimentation period. The kerosene was purchased in February 2013 and July 2013, and, similar to the heavy gas oil, heat release rate measurements were taken with fuel from each pail.

3.1.3 Test Pans

Due to the variety of experimental measurements required in this research, a number of different test pans were used to measure the different burning characteristics of the heavy gas oil. Various diameters of pan were used to study the effect of diameter on the burning characteristics of the test fuels, and large area pans were used to measure the flame spread rate and suppression characteristics. A summary of the test pans is shown in Table 3.2.

It is known that the pan material has an effect on the burning behaviour of small scale pool fires [67]. Therefore, results from the 0.11 and 0.19 m diameter glass pans are presented with an appropriate level of uncertainty in comparison to results obtained from fires in metal pans.

Table 3.2: Description of test pans used for liquid fuel burning characteristics experiments.

Pan	**Diameter** (m)	**Depth** (m)	**Material**	**Test Series Use**			
				HRR	*FSR*	*Boilover*	*Suppression*
Petri Dish	0.11	0.025	Glass	x			
0.19 m	0.20	0.20	Glass	x		x	
0.26 m	0.26	0.30	Steel	x		x	
0.30 m	0.30	0.10	Steel	x			
0.60 m	0.59	0.30	Steel	x	x	x	
1.12 m [a]	1.12	0.10	Steel	x	x		x
2.00 m	2.02	0.15	Steel			x	x
3.4x2.0 m			Steel		x		

[a] Square pan with 1 m sides and 1.12 m equivalent diameter.

3.2 Pan burner and Instrumentation

Simultaneous measurements of various burning characteristics of heavy oil as well as the kerosene reference fuel were recorded using an instrumented pool burner apparatus. A schematic of the instrumented burner is shown in Figure 3.1 with the relevant components labelled. The apparatus was designed to accommodate pans of various diameters and depths. A load cell was used to measure the instantaneous mass of the test pan and an array of thermocouples was used to measure fire gas temperatures as well as the fuel temperature at set locations into the bulk fuel. Digital video cameras were used to visually record the experiments, and infrared cameras were used to measure thermal profiles along the pans walls and into the flaming regions of the fire.

For the heat release rate, flame spread rate, and water suppression measurements, the experiments were limited in terms of the size and orientation of the pool burner, and therefore specific experimental configurations were used for these tests, and are detailed in Section 3.3 to Section 3.5.

Experiments conducted using the smaller diameter (0.19 to 0.3 m) pan burner were conducted inside the UWLFRF test lab, while the larger scale experiments and boilover experiments were conducted outside. In all experiments the thermocouple rake and test pan were placed within a 2.0 m diameter outer pan for the containment of any spillover during the experiment as well as to contain ejected fuel in the event of boilover. In the

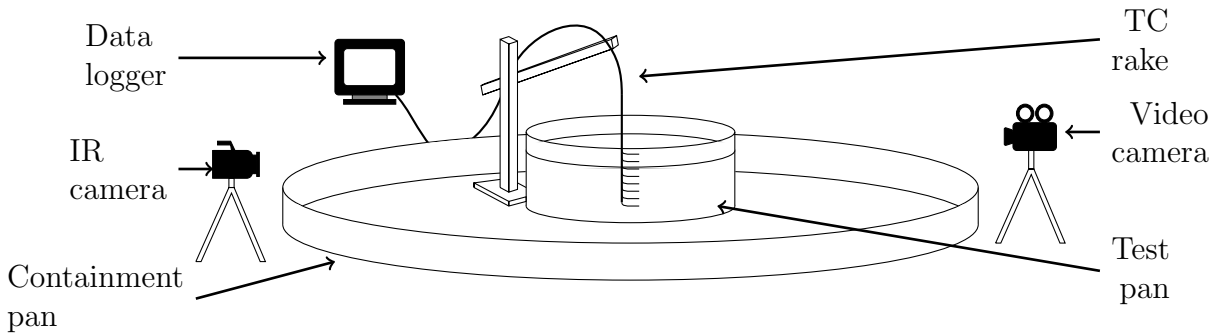

Figure 3.1: Schematic of instrumented pool burner experimental apparatus.

experiments outdoors, large screens were used to block the wind and reduce the effects of ambient wind on the fire characteristics, as well as minimize the heat transfer from the flame through the side of the pan fan due to the flame tilt and direct impingement on the pan wall.

The thermocouple rake was constructed using a series of 12 Omega *K-208F* type 'K', stainless steel sheathed thermocouples with 0.19 mm overall diameter mounted on a 6.4 mm (1/4 in) diameter steel rod for structural support. The thermocouples are known to have high temperature resistance and fast thermal response [129] and were chosen for the present experiment since the thermocouples would be exposed to the cool temperature fluid as well as the flame zone. The thermocouple leads were run along the supporting rod, and held in place with wire. At the designated locations, the thermocouple lead was bent away from the support rod, allowing for 5 ± 0.1 cm of horizontal lead prior to the thermocouple bead. This design allowed for micro-adjustments of the thermocouple bead heights, with a dimensional tolerance of approximately ± 1 mm.

The standard calibration uncertainty of Type-K thermocouples is typically taken as the larger of ± 2.2 °C, or $\pm 0.75\%$ of the measured temperature above 0 °C [129]. For the temperatures measured within the liquid, this represents a measurement error of 3.5 °C at the maximum measured temperature of 460 °C. This measurement error is taken to be negligible in comparison to the measured temperature, and is not expected to affect the trends in the measured temperature profiles.

Two variations of thermocouple rake were used throughout the experiments. A schematic of the two thermocouple rake designs is shown in Figure 3.2. Figure 3.2a shows the linear rake, in which all the thermocouple beads are aligned, that was used to measure the temperatures through the centerline of the test pan. Figure 3.2b shows the second rake

design, in the form of a grid, that was used to measure the temperatures a various heights in the fuel, as well as at radial positions away from the center of the pan.

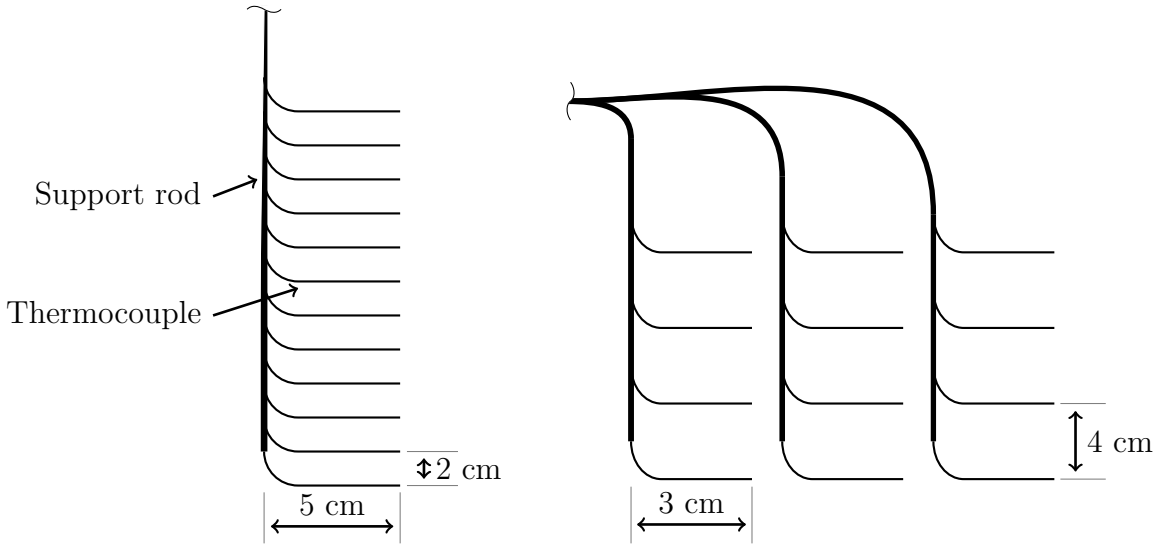

(a) 1-D TC rake. (b) 2-D TC rake.

Figure 3.2: Linear (3.2a) and grid (3.2b) thermocouple rake arrangements used in instrumented pool burner experiments.

In all cases, the thermocouple rake was inserted into the pan from the top as to avoid the necessity for drilling holes into the test pan to accommodate the thermocouple leads. This also allowed the use of the same thermocouple rake for comparable measurements in pans of different dimensions and materials. In all cases, the rake was submerged into the fuel until the bottom thermocouple contacted the pan bottom, therefore a dimensional tolerance of ± 1 mm was assumed for the thermocouple rake relative to the absolute pan location. Unfortunately, with this design the thermocouple leads had to be run out of the pan through the flame column, leading to possible heat conduction through the leads. Initial experiments were therefore performed to ensure that the flame impingement on the thermocouple leads did not impact the measured results within the fluid. With the 5 cm spacing from the spine of the rake to the thermocouple bead, there was found to be sufficient heat transfer away from the thermocouple lead to ensure negligible conduction from the flame through the lead to the bead location.

Temperature data acquisition was conducted using a compact *FieldPoint*, PC-based, distributed system manufactured by *National Instruments*. This system consisted of a

modular backplanes connected via Ethernet cable to a computer running *LabVIEW* acquisition software. Instantaneous temperature recordings were taken at 2 second intervals and logged to a save file for later processing.

In addition to the temperature data, instantaneous measurements of the pan and fuel mass were recorded using strain gauge based load cells beneath the test pan. Two different load cells were used: the cone calorimeter employs a strain gauge load cell with a quoted accuracy of ± 0.1 g [107], while the furniture calorimeter uses a strain gauge load cell with capacity of 500 kg and accuracy of ± 1 g. For the larger scale furniture calorimeter tests, a layer of fire bricks and a layer of cement board was placed between the load cell and the pan to reduce heat transfer to the cell from the pool fire above.

In each experiment, the load cell was calibrated from a lower limit of zero mass to an upper limit of mass greater than the total sample mass. Measured values of mass were then output as calculated from the linear calibration of mass to the output voltage signal and were recorded using the *LSHRcalc* (version 3) software developed by Fire Testing Technology. A sampling frequency of one measurement per 3 seconds was used for recording the sample mass during these experiments.

Visual images of the experiments were recorded using digital cameras. Throughout the different experiments, video recordings were focused to obtain information on various features of the fires. These included overall characterization of the flame geometry and features of the fire plume, visual observation of the fuel regression rate, visualization of the fuel-water interface, and visualization of boilover. The video images were taken in full high definition (1080p) at 30 frames per second.

In addition to the visual recordings, infrared images were recorded for each experiment. In most of the experiments, the infrared images were focused on the pan walls to thermally profile the bulk fuel but other recordings were also taken to monitor the flame shape and fire characteristics. The infrared camera used in these experiments was a *FLIR Systems* 'FLIR T650sc' purchased from FLIR Systems Inc, Wilsonville, Oregon, US. This camera used an uncooled microbolometer detector and measures in the spectral range of 7.5 to 12.0 μm. It records at capture rate of 30 Hz. Temperature measurements between -40 to 2000 °C are possible, and thermal measurements have a quoted accuracy of the greater of ± 2 °C or $\pm 2\%$ of the measured temperature [130], given good knowledge of target emissivity.

A limitation of the thermal imaging camera was the pre-defined temperature ranges set by the manufacturer, of either -40 to 160 °C or 100 to 600 °C. For these experiments, the infrared images were calibrated to the higher temperature range as the measured temperatures near the fuel surface would saturate the image when the camera was set

on the 160 °C range. Temperatures below 100 °C could still be measured at the higher temperature range; however, some accuracy was lost on these measurements. As well, assumptions such as the air temperature and humidity, distance between emitter and receiver, and object emissivity had to be made for each test. It is difficult to quantify the effects of these assumptions on the accuracy of the measured temperatures; therefore, the infrared camera results were used solely to define temperature trends – such as the formation of a hot-zone – and characteristics of the flame column.

Experiments to monitor the burning characteristics of the test fuel were conducted in the following steps. In each experiment, the mass of the test pan was recorded prior to being filled to the top with fuel. After filling, the mass of the pan was again measured. The mass of the added fuel was calculated as the difference in total mass with fuel and pan mass. The pan was then placed in an industrial oven set at the desired fuel test temperature for 3 to 12 hours, and heated until an equilibrium temperature was achieved.

The pan full of preheated fuel was then placed on the load cell, and the thermocouple rake was inserted from the top of the pan. Measurements of initial fuel temperature, ambient temperature, and wind speed were recorded for each test. Three minutes of baseline data was collected for the thermocouples and load cell prior to ignition of the fuel, and the video cameras and infrared cameras were started. The fuel was then ignited using a propane torch, and allowed to burn freely until flameout. The full set of temperature and mass data, and video and infrared traces were recorded throughout the test. Time of ignition, time of full flame cover, and time at flameout were recorded for each test, as were the times of occurrence of any unique events. Video recordings were also later used to verify the timing of the various events.

For experiments focused towards determining the propensity for boilover in the heavy gas oil, some variations of the aforementioned experiment were made. The instrumented pan burner was used as described above; however, the fuel layer was floated on a layer of water in efforts to encourage boilover to occur. Prior to each boilover experiment, a known volume of water was added to the test pan, and a known volume of fuel was floated on top of the water layer. Mass of both water and fuel were determined, the fuel was ignited with a propane torch and the fire allowed to burn freely until boilover. Measurements of initial fuel depth, regression rate, fuel depth at boilover, flame height, and temperatures were taken. Due to the possibility of flame spread beyond the pan walls in the boilover experiments, the load cell was not used. Temperature measurements were acquired using the thermocouple rakes described previously and the computer data logger. Finally, digital and infrared images of the flame shape and pan walls were recorded throughout the experiments.

3.2.1 Fuel Regression Rate Measurements

One of the most important parameters governing the burning behaviour of liquid pool fires is the rate of mass consumption of the fuel because it is related to both the fire heat release rate and the time available before boilover. This is often expressed as the fuel regression rate, as the mass loss rate is not easily measured during large scale experiments, nor is it possible to monitor in real fires. Due to the relative importance of the regression rate data in this work, several measurement techniques were used for each experiment to independently determine an accurate regression rate value. Each of the fuel regression rate measurement methods are described in the following, and where possible, the reported fuel regression rate is taken to be the average value of multiple methods.

The average fuel regression rate of a pool fire is best represented by the rate of liquid fuel regression during the steady burning period. The steady burning period also corresponds to that time in which the highest rate of mass loss occurs and thus, to the period of greatest hazard in the case of real fires. As the burning duration of pool becomes very long, the fuel regression rate during the steady burning period approaches the average fuel regression over the entire burning period. Therefore, the average fuel regression rate of the present short duration pool fires is taken to be that of the regression rate only during the steady state burning period.

Volumetric Regression Rate

The most straightforward method of determining the fuel regression rate was through direct visual measurements of the fuel thickness. Measurements of the fuel thickness at the beginning and at the end of the experiment were taken using a depth gauge and a measuring tape. The average visually measured fuel regression rate, FRR_{vol}, was then calculated from the difference in fuel thickness from start to end of burn, divided by the length of the steady burning period, as shown in equation 3.1.

$$FRR_{\text{vol}} = \frac{\Delta h}{\Delta t} \tag{3.1}$$

where Δh is the change in fuel thickness from ignition to flameout, and Δt is the total burning time. This method incorporates the assumption that the burning rate was constant throughout the burning period, which was confirmed by mass measurements as shown in Figure 3.3. In the experiments using glass pans, this was further assessed by monitoring the fuel level throughout the burning period. In this case, the average regression rate

was found from the average of a number of discrete regression rate computations, as in equation 3.2.

$$FRR_{\text{vol,avg}} = \frac{1}{n}\sum_{i=1}^{n}\left(\frac{\Delta h}{\Delta t}\right) \tag{3.2}$$

where n is the number of discrete fuel surface height measurements. This method was found to produce errors in the regression rate measurements in work conducted by Randsalu [72]; however, the latter experiments were conducted with a very short steady burning period (only five and ten minutes), therefore the growth and decay stages represented a significant portion of the total burn time. In the present experiments the burn time was between 60 and 180 minutes, and the pre-burn and burnout periods were seen to be less than 10% of the total burning period, therefore causing a minor error in the measurements.

Mass Consumption Regression Rate

The second method utilized for determining fuel regression rate in the present research was through mass measurements. The load cell described in Section 3.2 was used to measure the instantaneous mass of the fuel throughout the burning period for small and mid-scale experiments – namely the heat release rate and burning characteristics experiments. By obtaining the instantaneous mass at discrete times throughout the burning period, a curve of sample mass as a function of time can be created. A representative example of a mass loss curve is shown in Figure 3.3.

The mass loss rate can be determined as the slope of the line or the slope of a linear curve fit to the measured mass data. As can be seen in Figure 3.3, the mass loss is fairly consistent throughout the steady burning period in the present experiments, therefore a well-defined value of mass loss rate can be determined using

$$MLR = \frac{\Delta m}{\Delta t}. \tag{3.3}$$

where Δm is the difference in measured mass during the steady burning period. The mass loss rate is related to the rate of regression of the fuel surface through the surface area of the pool and the density of the fuel. By assuming that the fuel density does not change significantly throughout the burning period, a constant factor can be applied to the mass loss rate to estimate the fuel regression rate. This is shown in equation 3.4, where A is the area of the burning pool and ρ is the density of the fuel.

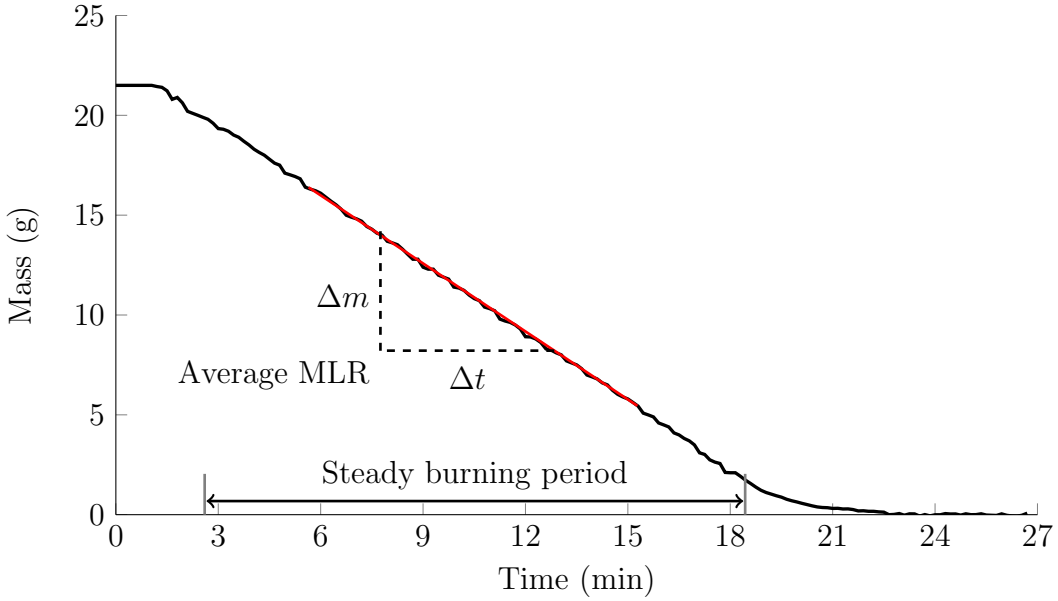

Figure 3.3: Characteristic mass history curve for pool fire experiments in cone calorimeter.

$$FRR_{\text{mass}} = \frac{1}{A\rho} MLR \tag{3.4}$$

With the assumption of a well-behaved pool fire, having a linear curve of mass loss rate, estimates of the liquid fuel regression rates are similarly well-defined. In this case, the value of average fuel regression rate is representative of the regression rate of the entire steady burning period.

Thermocouple Regression Rate

The liquid fuel regression rate was derived, for some experiments, from characteristic temperature readings measured using the thermocouple rake described in Section 3.2. By using a constant spacing for the thermocouples in the thermocouple rake, a linear rate of fuel surface regression was determined based on observations of when a given thermocouple indicated temperatures commensurate with the known boiling temperature of the fuel. A characteristic time-temperature curve for heavy gas oil is shown in Figure 3.4, where a the shape of the temperature trace indicating passage of the thermocouple out of the liquid

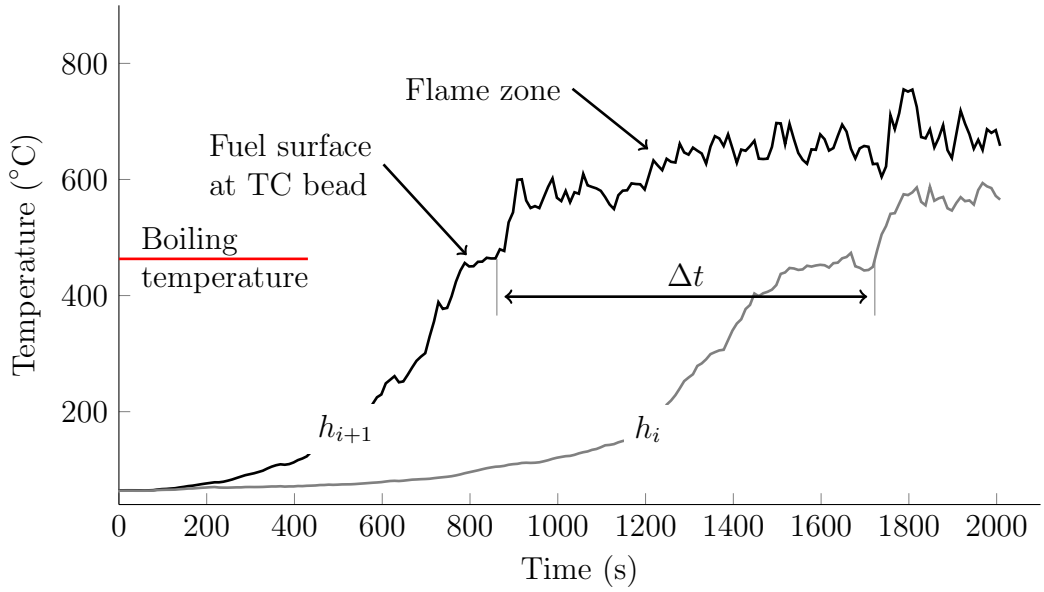

Figure 3.4: Characteristic temperature as a function of time curves at two locations, as measured in heavy gas oil pool fire.

fuel is visible at a temperature of approximately 460 °C. Temperatures measured in the range of 500 to 800 °C indicate that the thermocouple has entered into the flame region.

As can be seen, the temperature at a given thermocouple rises sharply to approximately 460 °C, the boiling temperature of heavy gas oil, and then remains constant for a brief period, before increasing sharply as the thermocouple enters the persistent flame zone of the fire. The period of approximately constant temperature is likely a result of the thermocouple entering into the fuel vapour core above the liquid fuel surface, and therefore the time at which the thermocouple first reads a temperature of 460 °C is taken as the location of the top of the fuel surface for a given thermocouple. The fuel regression rate is then found by taking the thermocouple spacing divided by average of the times for the fuel surface to regress from one thermocouple to the next.

$$FRR_{\text{thermocouple}} = \frac{1}{n}\sum_{i=1}^{n}\left(\frac{h_{(T_{\text{C,TC}})_{\text{i+1}}} - h_{(T_{\text{C,TC}})_{\text{i}}}}{\Delta t}\right) \tag{3.5}$$

Experiments conducted by Randsalu [72] indicated that the thermocouple measurement method yielded very accurate values for fuel regression rate for large Jet-A fires. Further, it was observed through analysis of the characteristic temperature chosen as the indicator

of liquid fuel surface affected the precision of the method. As would be expected, the error in estimated fuel regression rate increased with use of successively increasing temperatures above the boiling point of the liquid, as these temperatures represent locations within the vapour zone of the fire. In contrast, measurements of fuel regression rate were found to be relatively accurate when estimated based on each thermocouple registering the same temperature, using a temperature within the range of temperatures between the boiling temperature and the initial fuel temperature [72]. For this reason, 460 °C was taken as the characteristic temperature by which to determine the fuel regression of the heavy gas oil, because it falls near to, but below, the actual boiling temperature of the oil.

Infrared Camera Regression Rate

The fourth method that was used for measuring the fuel surface regression rate was a method based on following temperature contours measured using the FLIR infrared camera as described in Section 3.2. This method was used in experiments to determine the general burning characteristics of the heavy gas oil, as well as in the suppression experiments. Fuel regression rate was determined using infrared camera images of the thermal profile of the pan wall, interpreted based on tracking a 'characteristic' temperature contour for the fuel surface through the burning period. The rate of change of position of this characteristic temperature was determined to be the rate of fuel surface regression. Similar to the thermocouple regression rate measurement method, this method relied on the assumption of a constant temperature profile into the fuel depth, such as was found for the heavy gas oil and kerosene.

While a temperature close to the known fuel boiling temperature, approximately 460 °C, was used for the thermocouple regression rate measurement, it was not used in the infrared calculations for a number of reasons. First, there is significant flame impingement onto the pan wall which increases heat transfer through the wall near the fuel surface level. This effect would therefore be captured by the infrared camera, thereby introducing error into the measurement of regression rate. Therefore, a temperature that is characteristic of a location further into the depth of the oil reduces the potential for interference from the effects of flame impingement and produces a more repeatable measurement. Furthermore, the temperature as measured by the infrared camera is highly dependent on the input parameters – such as the object emissivity, distance from object, and temperature range calibration. In these experiments, it was not expected that the infrared camera based temperature measurements would accurately capture a characteristic temperature of 460 °C to mark the fuel surface. Instead, a temperature of 200 °C, or a location approximately

1 cm beneath the surface, was used to track the fuel regression rate in the infrared camera based measurements.

For a given experiment, the infrared camera was set to an image capture frequency of 15 seconds, and each image was exported as a *CSV* file. The exported files are shown as a grid of 760 by 380 cells (consistent with the pixel resolution of the camera), with each cell representing the temperature at one pixel as measured by the camera. A calibration image was used to define the dimensions of each pixel as translated back to the actual dimensions of the pan experiment, and a conversion of pixels to millimeters was used to define the actual position of the characteristic temperature in reference to the pan. This image calibration was calculated by

$$C_{\mathrm{x}} = \frac{L_{\mathrm{x}}}{N_{\mathrm{pix}}} \quad \text{and} \quad C_{\mathrm{y}} = \frac{L_{\mathrm{y}}}{N_{\mathrm{pix}}} \tag{3.6}$$

where L represents the dimensions of the calibration object, and N_{pix} is the number of pixels represented by the image as captured by the infrared camera. The coefficient C is therefore the conversion factor in mm/pix for both the horizontal (x) and vertical (y) orientations. The actual location of the 200 °C contour is found from the location of the pixel in the captured image at that temperature, using equation 3.7, where $N_{(T_{\mathrm{C,IR}})}$ is the number of pixels between the bottom of the pool burner and the characteristic temperature.

$$h_{(T_{\mathrm{C,IR}})} = C_{\mathrm{y}} * N_{(T_{\mathrm{C,IR}})} \tag{3.7}$$

The rate of fuel regression was then calculated from the change in actual position of the 200 °C characteristic temperature in each frame divided by the 15 second interval between captured images. The calculation method is shown in equation 3.8.

$$FRR_{\mathrm{infrared}} = \frac{1}{n} \sum_{i=1}^{n} \left(\frac{h_{(T_{\mathrm{C,IR}})_{\mathrm{i+1}}} - h_{(T_{\mathrm{C,IR}})_{\mathrm{i}}}}{15 \text{ s}} \right) \tag{3.8}$$

To reduce uncertainty in the measurements of the fuel regression rate, measurements of regression rate were taken from three separate locations for each time period using the procedure above. An average of the three independent measures of regression rate was then calculated for each time period, and the overall regression rate is presented as an average of the regression rate throughout the entire steady burning period, as shown in equation 3.8.

3.3 Rate of Heat Release

The rate of heat release is a fundamental fire property governing the behaviour of, and hazard from, a fire. The flame height, fire temperature, and radiation from the flame are all directly related to the heat release rate. The rate of heat release from the heavy gas oil fires under study here was measured at the University of Waterloo Live Fire Research Facility using oxygen consumption calorimetry in a small-scale cone calorimeter, as well as in a medium-scale furniture calorimeter. Complementary analysis of the energy density of the fuel was completed by measuring the heat of combustion in oxygen of the fuel in an adiabatic bomb calorimeter. A description of these apparati is provided in the following subsections, along with an explanation of the principle of operation of each instrument and further detail of the procedures used for each measurement in the present research.

3.3.1 Bomb Calorimeter

Adiabatic bomb calorimeters are a standard method which can be applied to measure the total energy released during the complete combustion of a sample in an oxygen rich environment. As a reference to later measurements of heat release rate using the cone and furniture calorimeters, measurements of the heat of combustion of 1 g samples of heavy gas oil and kerosene were conducted using an adiabatic bomb calorimeter at the University of Waterloo. No pre-test sample preparation was required for the kerosene; however, the heavy gas oil was heated at 90 °C for 12 hours and then allowed to cool to ambient temperatures prior to being tested. This was in an attempt to drive off any water emulsified into the oil, as the water would cause an error in the measured values for heat of combustion.

A schematic of an adiabatic bomb calorimeter is shown in Figure 3.5, with the relevant components labelled. The bomb calorimeter is comprised of a constant volume 'bomb', in which the sample and a length of ignition wire are inserted. The bomb is placed in a bucket containing a known volume of water, all of which are contained within an adiabatic jacket.

The full test method is presented in the test standard *ASTM D 240: Standard Test Method for Heat of Combustion of Liquid Hydrocarbon Fuels by Bomb Calorimeter* [131], and is described briefly here. In the apparatus used here, the sample bomb was filled with pure oxygen to a pressure of approximately 30 atm, thereby making the atmosphere within the bomb effectively 100% oxygen. At the start of the test, electrical energy was discharged through the ignition wire, causing heating of the wire and igniting the test sample. The

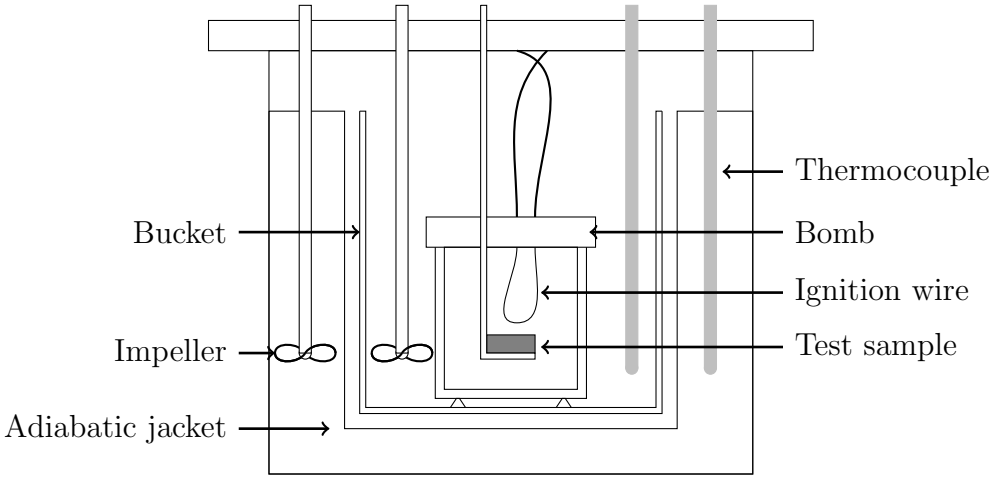

Figure 3.5: Schematic of the bomb calorimeter.

combustion of the test sample increased the temperature within the 'bomb', and therefore the temperature of the water in the bucket. An impeller in the bucket constantly mixed the water so that the bucket thermocouple measured an average temperature of the water. The adiabatic jacket was designed to impart an adiabatic boundary condition on the system by minimizing the temperature difference between the bucket and the surroundings. A proportional-integral-derivative (PID) controller measured the temperature of the water in the bucket and controlled the rate of flow of hot water into the jacket to maintain the temperature of the jacket at approximately the same temperature as that of the water in the bucket. Once there was no further increase in temperature in the bucket, it was assumed that the system has reached steady state, and the test was stopped. The mass of the sample tray was measured before and after the test, and the mass of any residual after the test was subtracted from the mass used in the calculations.

The heat of combustion of the sample was then determined through thermodynamic principles, where the heat energy transferred into the water was assumed to be the total energy produced during combustion and was determined from the temperature increase of the water bath. The higher heating value of the sample was then measured as the difference in temperature of the water bath from start to finish of the test, representing the change in thermal energy of the water. As a length of ignition wire was also combusted, and therefore added to the measured value of overall energy generated within the sample bomb, the net heat of combustion of the sample must be adjusted to account for this energy. As well, energy generated by the formation of nitric acid from the combustion products was corrected for the measured value of the overall energy content of the sample.

The heat of combustion of the sample was computed from the recorded water bucket temperatures as follows:

$$\Delta H_{\mathrm{C}} = \frac{-q_{\mathrm{wire}} m_{\mathrm{wire}} - q_{\mathrm{NO_3}} M + C^* \Delta T}{m_{\mathrm{fuel}}} \tag{3.9}$$

where C^* is a calibration factor for the specific calorimeter. The calibration factor accounts for the heat retained in the sample bomb, as well as the efficiency of heat transfer from the bomb to the surrounding water. In this case, the calibration factor was determined by measuring the temperature rise during combustion of benzoic acid, a calibration substance with a well-defined heat of combustion of 26.44 kJ/g [131].

3.3.2 Oxygen Depletion Calorimetry

Small and large scale heat release rate measurements were conducted using the cone calorimeter and furniture calorimeter test apparatus at the University of Waterloo Live Fire Research Facility. This section describes the experimental methods used for these tests.

The UWLFRF cone calorimeter is manufactured by Fire Testing Technology (FTT) from London, UK [132]. This apparatus is in frequent use and is maintained and calibrated as per recommended guidelines from FTT. The data from the cone calorimeter is recorded on a personal computer running *Windows XP Professional*. All data smoothing algorithms and calculation methods are performed on the raw data within the native Fire Testing Technology *ConeCalc* software, version 5. While UWLFRF is not a certified testing facility, the cone calorimeter at UWLFRF meets the minimum specifications for use in the ASTM E 1354 standard [109].

Real time measurements are made of the sample mass, volume flow, species concentrations and soot production. Mass was measured via a strain gauge load cell with an accuracy of 0.01 g and a maximum range of 2000 g. Volume flow in the exhaust duct was measured from a orifice plate, interfaced to an appropriate pressure transducer and thermocouple arrangement, with a resolution of 0.1 g/s. Oxygen gas analysis was done with a paramagnetic oxygen analyser, with operating range of 0 to 25%, and the concentrations of carbon oxides were determined using a non-dispersive infrared sensor. Finally, smoke production was measured with a 0.5 mW helium neon laser and accompanying photodiodes. A full description of each of the cone calorimeter components can be found in the *Cone Calorimeter User's Guide* [107], and in the original apparatus documentation [108].

As mentioned in Section 2, the most comprehensive test method for measuring the heat release rate of a small sample of solid hydrocarbon-based material is the ASTM E 1354 standard [109]. While not explicitly stated in the standard, the methodology for testing the heat release rate of liquid hydrocarbon-based fuels should not be different than that for solid fuels, as the theory behind oxygen consumption calorimetry is independent of fuel type under test. Therefore, the ASTM E 1354 calibration and testing methodology [109] was used wherever possible for these liquid fuel experiments.

Calibrations of the cone calorimeter system were performed each test day, and followed the standardized calibration method exactly. Due to the burning characteristics and nature of the heavy gas oil and kerosene, the following alterations from the ASTM E 1354 standard were implemented for the present tests:

- a glass petri dish was used as the test pan,
- the cone heater and spark igniter were disabled,
- a propane torch was used to ignite the fuels,
- a glass fibre pad was placed under the test pan to insulate the load cell and platform from heat and splatter from the burning sample, and
- the spacing between the sample and cone heater was made as large as was possible whilst making sure the hot fire gases were collected by the cone hood and exhaust system.

Figure 3.6 shows a schematic of an oxygen depletion calorimeter, with all of the components relevant to this discussion labeled. Of note from this schematic is the differences between the current set-up and a traditional cone calorimeter, such as described by Babrauskas [108]. A Pyrex glass petri dish, having inside dimensions of 0.106 m diameter, and 0.015m pan wall height, was used for a test pan in the cone calorimeter experiments, and a series of larger, metal pans were used for furniture calorimeter experiments.

Both the heavy gas oil and kerosene burned freely without any requirement for heat flux to the fuel surface, and the additional heat flux imparted by the cone heater was not representative of the burning conditions in a real pool fire; therefore, the cone heater was not used for these experiments. Furthermore, insufficient volumes of flammable gases were produced from either of the fuels at ambient temperatures for the spark igniter to ignite the pools so the spark igniter was disabled and a propane torch was used to ignite the fuel instead.

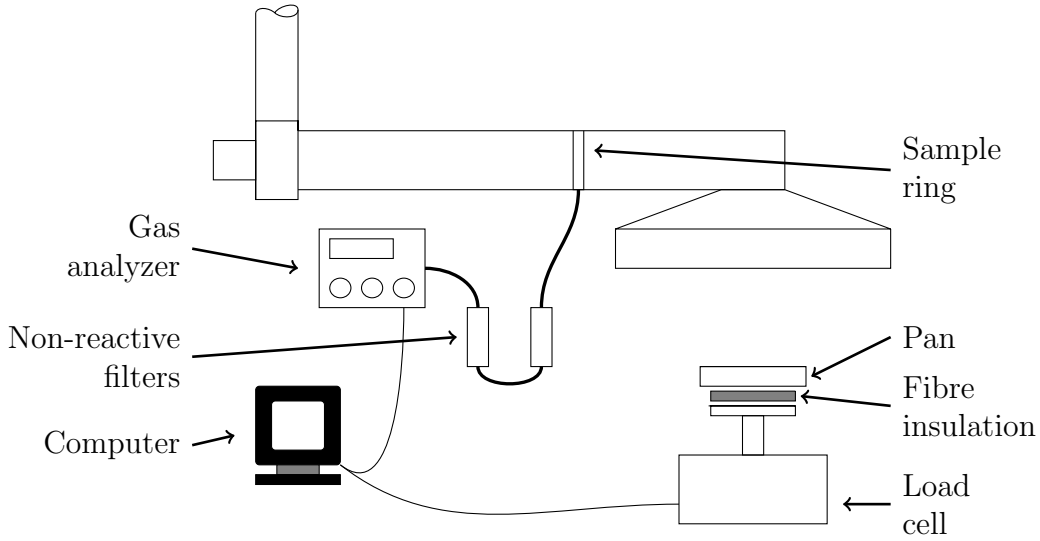

Figure 3.6: Oxygen consumption calorimetry experimental apparatus.

During the experiments, there was some heat transfer from the flame through the test pan and, in the case of the heavy gas oil samples, small droplets of fuel were ejected from the pan during the tests. Therefore, a layer of insulation was placed beneath the pan to protect the load cell and platform. Finally, since the cone heater was not used in these experiments, the spacing between the heater and the sample was increased to the maximum possible extent to protect the cone from excessive heating and soot deposition from the fire plume, as well as to decrease interference from the cone heater to the fire.

The cone calorimeter testing was conducted in sets of three samples. In each test the fuel was poured into the petri dish immediately prior to the start of test and the total fuel mass was recorded. The test pan was placed on the load cell, and the fuel was ignited with a propane torch. Data was acquired once per second, and was recorded throughout the burning period.

The kerosene was tested at room temperature in each test, while the heavy gas oil was tested at initial fuel temperatures varying from 40 °C to 90 °C. It was found experimentally that tests conducted with heavy gas oil at initial temperatures below 40 °C could result in violent fuel ejections from the pan and consequently the tests could not be performed without damaging the apparatus. For initial fuel temperatures above 40 °C, moderately well-behaved pool fire behaviour was observed, with infrequent ejections of oil, allowing for more consistent measurements.

The cone calorimeter test system is constrained to sample sizes to 0.15 m diameter, and to heat release rates of below approximately 5 kW for long duration burning. Therefore the medium-scale furniture calorimeter at the UWLFRF was used to measure the heat release rate of heavy gas oil and kerosene pool fires at larger diameters. The medium diameters allowed for the comparison of the diameter dependent fire characterization correlations, as well as document the fire behaviour at larger scale.

The furniture calorimeter at UWLFRF is manufactured and supplied by FTT and is constructed to the FTT guidelines. The furniture calorimeter is regularly calibrated with a methane burner and is experimentally rated to a maximum heat output of approximately 1 MW. This furniture calorimeter utilizes a separate duct system from the cone calorimeter to exhaust the combustion gasses from the building. However, an attachment for the furniture calorimeter allows the gas analysers for the cone calorimeter to be used on the furniture calorimeter. The sample gas pump from the cone calorimeter is therefore attached to the sampling port of the furniture calorimeter exhaust duct, and representative samples of the combustion products are drawn from the exhaust duct. These gases are then analysed using the same gas analysers as are used in cone calorimeter tests.

This system, then, shares many of the components with the cone calorimeter. Since these were discussed above, they will not be discussed again here. The furniture calorimeter also has several unique components. A large scale load cell, rated for a maximum mass of 500 kg and precision of ± 1 g, is used to measure the instantaneous mass of the samples. The extraction fan system is adjustable to accommodate different size fires without diluting the sample gas, and has a combustion gas extraction flow rate range of 0.6 to 3.0 m^3/s. Finally, data is recorded using the same computer as for cone calorimetry and uses the *LSHRCalc* software produced by FTT to record and analyse the data.

Test pans of 0.19 to 1.12 m in diameter were used for the heat release experiments conducted in the furniture calorimeter, and both kerosene and heavy gas oil were used as fuel in these pool fire tests. Kerosene tests were conducted with the fuel at ambient temperature, while the heavy gas oil was heated in the test pan to the designated initial temperature in an industrial oven. Before each test, the initial fuel mass was recorded, and the pan was placed on the load cell, under the furniture calorimeter exhaust hood. The fuel was ignited using a propane powered *tiger torch*, and the fuel was allowed to burn for a pre-determined length of time, typically 40 minutes. Data was collected throughout the burning period at a frequency of 3 s.

Whether measured in the cone or the furniture calorimeter, the heat release rate of a liquid fuel, as measured by oxygen depletion calorimetry, shows three distinct phases. These burning phases are shown in Figure 3.7, a characteristic heat release rate plot as

measured from a kerosene pool fire using the cone calorimeter. Initially, the propane fuelled ignition torch causes a significant increase in the heat release rate as evident from approximately 1 to 2 minutes on the figure. Upon removal of the flaming ignition source, the liquid fuel enters into a steady burning phase, from approximately 2 to 18 minutes in the figure, with a uniform heat release rate. Finally, as the fuel level becomes low, the heat transfer and resulting losses to the pan becomes significant, and the fire decays and eventually burns out, from 19 to 22 minutes in Figure 3.7.

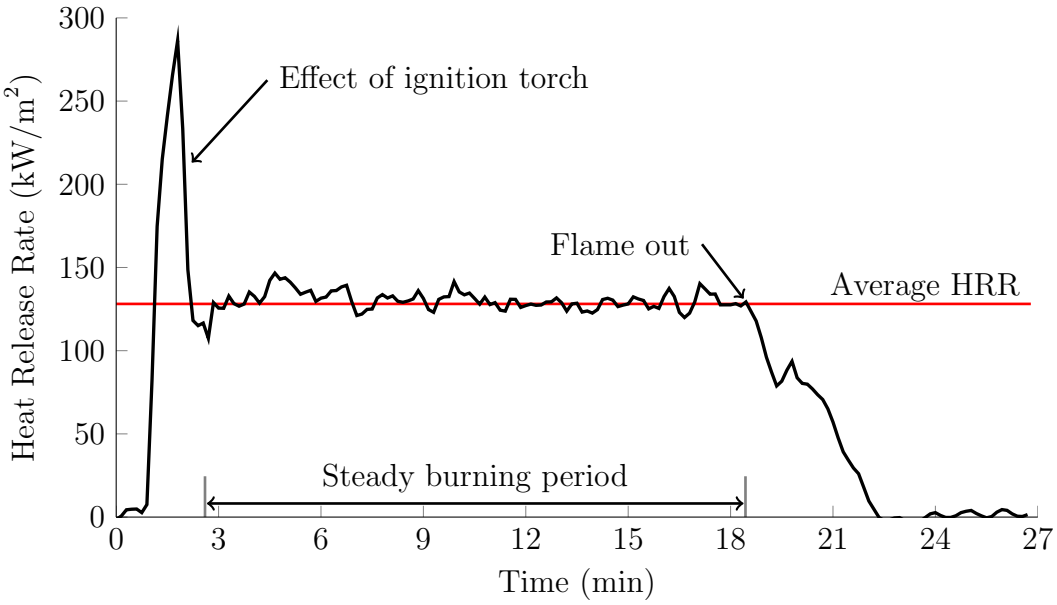

Figure 3.7: Characteristic heat release rate profile for liquid pool fire as measured by oxygen consumption calorimetry.

As can be seen from this plot, the duration of the steady burning period had a well defined average heat release rate, and the duration of this period greatly outweighs the initial period of ignition and flame spread, as well as that of fire decay. The average heat release rate was therefore taken as the heat release rate measured during the steady burning period, as shown in equation 3.10, thus neglecting the effects of the ignition and burn-out periods.

$$HRR_{\text{avg}} = \frac{f}{t_{\text{s,e}} - t_{\text{s,s}}} \sum_{i=1}^{t_{\text{s,e}}} (HRR(fi)) \tag{3.10}$$

where f is the recording interval of the tests, $t_{\mathrm{s,s}}$ and $t_{\mathrm{s,e}}$ are the time at the start and end of the steady burning period, and $HRR(i)$ is the heat release rate at time $t = i$.

Similarly, the total energy released per unit mass – or effective heat of combustion – was measured based on the total energy released during the steady burning period divided by the mass lost in the same period. This is determined from the integral of the heat release rate versus time curve, or

$$\Delta H_{\mathrm{C,eff}} = \frac{1}{m_{\mathrm{s,e}} - m_{\mathrm{s,s}}} \int_{t_{\mathrm{s,s}}}^{t_{\mathrm{s,e}}} (HRR(t))\, dt \tag{3.11}$$

where $m_{\mathrm{s,s}}$ and $m_{\mathrm{s,e}}$ is the recorded mass at the start and end of the steady burning period. However, as shown in Figure 3.7, the heat release rate during the burning period is well represented by the average heat release rate; therefore, equation 3.11 can be simplified to

$$\Delta H_{\mathrm{C,eff}} = \frac{HRR_{\mathrm{avg}}\,(t_{\mathrm{s,e}} - t_{\mathrm{s,s}})}{m_{\mathrm{s_o}} - m_{\mathrm{s_i}}} \tag{3.11.b}$$

The rate of mass loss is derived from the instantaneous recordings of mass with time, and is reported as a 5-point backwards difference average by *ConeCalc*. Similar to equation 3.10, the test average mass loss rate in a given test can be calculated as the average of the mass loss rate during the steady burning period. However, due to the inherent noise in the mass loss rate data, a true representation of the average mass loss rate for a given test is given by

$$MLR_{\mathrm{avg}} = \frac{m_{\mathrm{s,s}} - m_{\mathrm{s,e}}}{t_{\mathrm{s,s}} - t_{\mathrm{s,e}}}. \tag{3.12}$$

Finally, knowing the actual heat of combustion as measured by the bomb calorimeter as described in Section 3.3.1, an experimental measurement of the combustion efficiency was derived. The combustion efficiency is defined as the ratio of actual heat of combustion to effective heat of combustion, or

$$\chi = \frac{\Delta H_{\mathrm{C_{eff}}}}{\Delta H_{\mathrm{C}}} \tag{3.13}$$

where ΔH_{C} is the theoretical heat of combustion. The combustion efficiency therefore has a value of 1.0 or less, as $\chi = 1$ when $\Delta H_{\mathrm{C,eff}} = \Delta H_{\mathrm{C}}$. Experimentally, this is the ratio of

the measured value of heat release to the rate of maximum possible energy production as shown in equation 3.13.b.

$$\chi = \frac{HRR_{\text{avg}}}{MLR_{\text{avg}} \times \Delta H_{\text{C}}} \tag{3.13.b}$$

The heat release rate was therefore measured using two distinctly different methods, and the results of the measurements were compared. The heat of combustion measured using a bomb calorimeter represents the total theoretical energy available in the material, while the heat release rate measured from oxygen consumption calorimetry represents the actual energy release during free burning conditions. The results of these measurements are presented in Section 4.2.

3.4 Flame Spread Rate

Due to the relatively small pool surface areas of the test pans used in both the heat release rate measurements and the pan burner instrumented for thermal measurements, a different configuration of pan was required to measure the rate at which the flame front propagated across the pool surface. As a result, a long and narrow pan was used to measure one dimensional flame spread rate. This provided sufficient distance to obtain a good measurement of the rate of flame spread across the fuel surface, whilst minimizing the fuel consumption in each test. Experiments were conducted using heavy gas oil as well as kerosene as fuel. This section details the apparatus and methods used to quantitatively assess the flame spread rate.

The flame spread rate experiments were conducted in a 3.6 m rectangular pan outdoors at the UWLFRF. A schematic of the flame spread rate apparatus is shown in Figure 3.8. To optimize fuel usage, the large pan was tilted at a 60° angle to produce a trench of 0.25 m width, 3.6 m length and maximum fuel depth of 0.12 m. This pan geometry allowed for a pool with a width of 0.2 m and depth of 0.1 m in the center of the triangle formed by the pan wall and bottom. Further, this configuration created a rectangle inside the triangular cross-sectional area of 0.5 m wide by 0.04 m, thereby exceeding the minimum fuel layer width and thickness for the approximation of infinite fuel layer dimensions as established by Mackinven et al. [54]. Lastly, position markers were spaced at 0.5 m intervals along length of the test pan to allow for time-resolved flame position measurements.

The time for the flame to reach each marked interval was visually observed and recorded by hand, while a digital camera was used to simultaneously record the flame position. It

is well documented that ambient wind speed has a significant effect on the rate of flame spread [44, 57]. Therefore, since the experiments had to be conducted outside, all of the flame spread rate experiments were conducted on days with low ambient wind speeds. In addition, a wind sock was placed within view of the camera to qualify the wind direction and the relative strength of the wind in order to identify and explain any anomalies in the recorded results. Finally, experiments were also conducted in both concurrent and counter current wind directions, to achieve an average, wind-neutral flame spread rate.

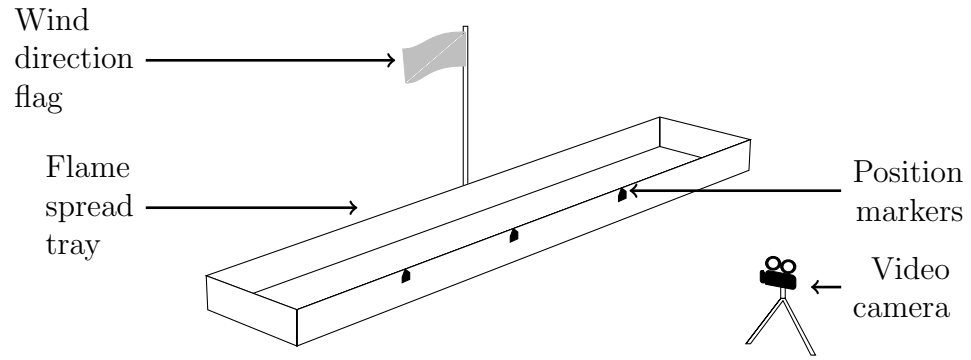

Figure 3.8: Schematic of the flame spread rate experimental apparatus.

In each experiment, the fuel was poured into the flame spread trench to a maximum fuel depth of 0.1 m at the center of the trench. At the designated time, the fuel was ignited using a propane tiger torch at one end, approximately 0.2 m from the first position marker. Once established, the flame was allowed to spread freely across the fuel surface, and time zero was recorded when the flame front passed the first marker, allowing 0.2 m distance for the flame to fully develop. The time at which the flame front passed each subsequent marker was recorded, as well as the time for the flame to reach the end of the trench. Steel sheets were then used to suffocate the fire, and the fuel was allowed to cool to the designated initial fuel temperature prior to commencing the next test. Additional fuel was added to the tray after each experiment to ensure the consistency of the fuel.

For these experiments, the wind speed and direction at the start, midpoint, and end of test was measured using a *Kestrel* hand-held wind meter. The ambient temperature and temperature of the fuel were also recorded prior to each test. Finally, video recordings of the flame propagation were taken, with a view of the wind direction flag in frame to compare to the wind conditions measured throughout the test.

The rate of flame spread is defined as the rate of propagation of the flame front across the fuel surface. The flame front location is taken as the position of the flame front at the

level of the fuel surface, rather than at the upper tip of the flame, since the position of the tip of the flame relative to the surface is dependent on the wind and rate of spread. The flame front position over the test time was then measured from the instantaneous recordings of each experiment. A representative plot of flame position versus time as measured in the flame spread trench is shown in Figure 3.9.

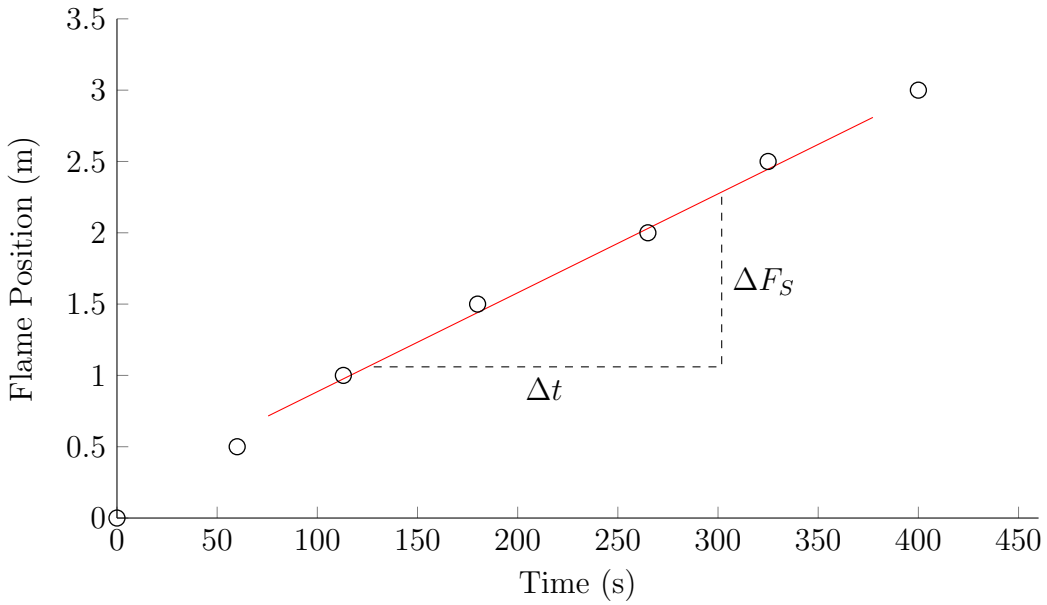

Figure 3.9: Characteristic flame position versus time plot as measured in flame spread rate experiments.

The rate of flame spread was found using the measured value of distance travelled by the flame, divided by the time required for the flame front to propagate that distance. As there were multiple position markers along the length of the flame spread tray, the average flame spread rate was found as the average of the flame propagation between each sequential set of position markers, or

$$FSR = \frac{1}{n}\sum_{i=1}^{n}\left(\frac{s\left(\mathrm{t}_{i+1}\right) - s\left(\mathrm{t}_{i}\right)}{t_{(s(t_{i+1})} - t_{(s(t_i)}}\right) \tag{3.14}$$

As is seen in Figure 3.9, the flame position as a function of time was found to be linear for each of the fuels, therefore the flame spread rate was simplified to

$$FSR = \frac{3.0 \text{ m}}{t_{(F_s=3)} - 0 \text{ s}}. \tag{3.14.b}$$

Finally, to account for the effect of ambient wind on the data, flame spread rate measurements were taken for flames travelling in both up and down–wind directions during periods with comparable and fairly constant, low magnitude winds. The average flame spread rate was then taken as the average of the average result of the tests in each wind direction.

$$FSR_{\text{avg}} = \frac{n_{\text{up}} FSR_{\text{up}_{\text{avg}}} + n_{\text{down}} FSR_{\text{down}_{\text{avg}}}}{n_{\text{up}} + n_{\text{down}}} \tag{3.15}$$

This method of measuring the flame propagation rate was derived from the standardized method proposed by Mackinven et al. [54], and is similar to the methods used by other researchers [44, 47, 51, 57]. The flame spread rate measurements for both heavy gas oil are documented in Section 4.3. Where possible, the results are compared with values obtained from literature.

3.5 Water Suppression Spray

Due to renewed interest in suppression of hydrocarbon pool fires, the final set of experiments in this research was designed to investigate the effects of water suppression spray on both heavy gas oil and kerosene pool fires. For this, a series of experiments were conducted to qualitatively study the interaction of water sprays with the heated fuel surface in pool fires established on large diameter pans. The suppression water was supplied from a hose stream with a well-defined flow rate and spray pattern.

Water suppression experiments were conducted using both 1.12 and 2.0 m diameter steel pans, as described in Table 3.2. Due to the scale and potential consequences of these large scale experiments, all of the experiments were conducted outside, again on days with low ambient wind conditions. In each test, the test pan was placed inside a larger, square stainless steel pan of 3.0 m side length to contain any spills or frothing. A schematic of the water suppression spray experimental apparatus is shown in Figure 3.10 with the relevant components labelled.

The water for the suppression spray was sourced from a municipal hydrant. Three 15 m (50 ft) lengths of 44.5 mm ($1\frac{3}{4}$ in) diameter fire hose was used to connect the nozzle to the

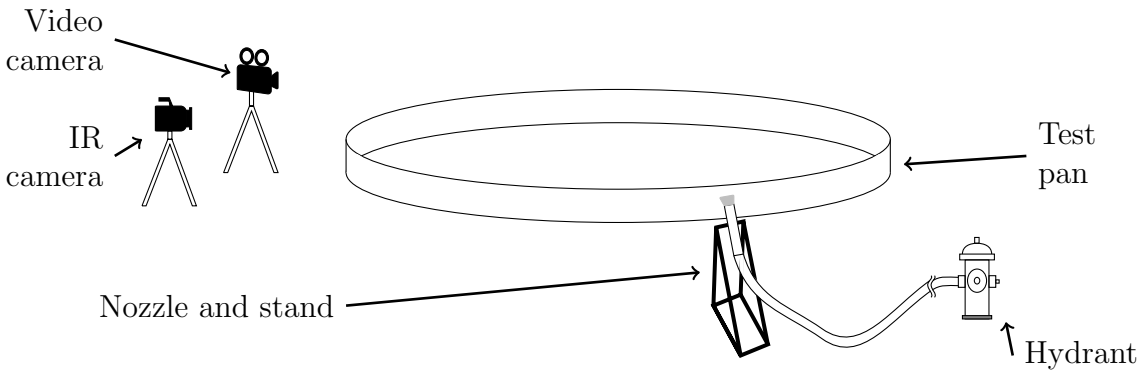

Figure 3.10: Schematic of the water suppression spray experimental apparatus.

hydrant. A standard 63.5 mm (2.5 in) adjustable flow rate fire fighter handline nozzle was used to produce the suppression stream. The nozzle was attached to a stand to produce a constant and reproducible suppression stream for the experiments. The water from the hydrant was at a temperature of approximately 10°C, and this temperature was found not to significantly change over the duration of a suppression experiment.

A ball-valve gated wye was connected to the hydrant before the fire hose. The adjustable valve was used to reduce the operating pressure in the hose and therefore reduce the flow rate. The flow rate from the nozzle that was prescribed in each experiment was achieved by adjusting the nozzle flow rate, as well as by adjusting the ball-valve at the handline nozzle shut-off.

A digital video camera was positioned to visually record a wide angle view of all suppression experiments. A second video camera was installed at a height of 4 m above the pan and was zoomed in and focussed on the fuel surface. This camera recorded the physical interaction between the water and the heated fuel at the surface. Finally, an infrared camera was focused on the pan side walls and was used to measure the fuel regression rate, and fuel surface temperature during each experiment. Initial fuel temperature, ambient temperature, and water temperature were recorded before and after each test. Wind speed and direction was monitored periodically throughout the test period.

A guideline for the water application rate required for fixed fire protection systems is provided in NFPA 15: *Water Spray Fixed Systems For Fire Protection* [133]. The area normalized flow rates range between 6.11 and 20.4 L/min/m^2 (defined in [133] as between 0.15 and 0.5 gpm/ft^2), with a recommended application rate of 0.3 gpm/ft^2 for control of large, open hydrocarbon pool fires [133]. The design flow rates for this series of experiments was based on the above criteria and is shown in Table 3.3.

Table 3.3: Design water flow rate for water suppression experiments, based off requirements from NFPA 15 for control of large, open hydrocarbon fires [133].

Test Pan	**Surface Area**	**Normalized** (L/min/m^2)		**Actual** (L/min)	
	(m^2)	*Min*	*Max*	*Min*	*Max*
1.13 m	1.0	6.11	20.4	6.1	20.4
2.0 m	3.1	6.11	20.4	18.9	63.2

Prior to each test, the flow rate through the nozzle was calibrated by systematically adjusting the nozzle flow rate and measuring the time required to fill a 150 L (40 gal (US)) drum. For the 1.12 m pan experiments, a smaller 20 L drum was used instead. The flow rate was considered adequate when the time required to fill the pail deviated by less than 5% from the prescribed time. For each flow rate, it was further ensured that the water spray pattern had a footprint wide enough to cover the entire surface area of the pan, but not beyond the pan walls. It is possible that the water flow rate varied during a test due to fluctuations of pressure in the water main; however, any fluctuations in water supply were small compared to the overall flow rates used.

For each test, a 0.05 m thick fuel layer was added to the fuel pan. The video camera was set to record at 30 frames per second, and the infrared camera was set to capture images every 15 seconds, and the recordings started. The fuel was ignited at one edge of the pan using a propane tiger torch, and the fire was left to spread across the surface. Once full flame cover was achieved, the fire was given five minutes of steady, pre-burn time prior to the start of the suppression experiments. The design flow rate and water spray pattern were defined for each experiment, as well as measurements of the wind speed and initial fuel temperature. Documentation of time at the start of suppression, time at flameout, and time of any extraordinary events were recorded throughout the experiments.

This chapter presented the experimental methods used to measure and characterize the burning behaviour of untreated heavy gas oil. An instrumented pan burner was used to measure the burning properties of thick layer pool fires. Other pan configurations were employed to assess the rate of flame propagation, boilover, and water interaction properties of the fuel. In all cases, experiments were conducted on kerosene to validate the experimental methods as well as compare the heavy gas oil results to those of a well documented fuel. The results of these experimental measurements are presented in Chapter 4. A further analysis on the boilover characteristics of heavy gas oil is presented in Section 4.8.

Chapter 4

Experimental Results

This chapter presents the results of the experiments completed to characterize the burning behaviour of kerosene and untreated heavy gas oil using the methods and measurements discussed in Section 3. Experiments were conducted to determine the global burning characteristics of each fuel using an instrumented pool burner, and secondary experiments were conducted, as necessary, to investigate other specific fire characteristics of the fuels.

A significant issue in preliminary experiments with heavy gas oil as fuel was the emulsification of water in the oil. The small pockets of water superheated due to the heat from the fire, which caused a rapid evaporation of the water and a sudden generation of steam. This caused a series of micro-explosions, wherein small amounts of oil were ejected from the pan. The results discussed in the following sections were obtained using dried oil. For this, the oil was heated which allowed the water to separate from the oil. The remaining oil was used as fuel so that the fuel ejections were mitigated. Any reference to heavy gas oil refers to dried oil, unless otherwise stated. A subset of experiments conducted with undried oil were also conducted to determine the effects of the fuel ejection phenomenon on the measured results. The results from these latter experiments are discussed in Section 4.6.

This chapter covers the experimental measurements of fuel regression rate done with dried heavy gas oil and kerosene, followed by a discussion of the measurements of heat release rate for both fuels. The flame spread rate and water suppression experiments are detailed, along with a discussion of the fire behaviour as related to the individual measurements. Then, an investigation into the effects of water emulsification and fuel weathering in the heavy gas oil is documented. Lastly, a discussion on the propensity for, and behaviour during boilover is presented.

4.1 Fuel Regression Rate

A series of experiments was conducted on kerosene and heavy gas oil pool fires to determine the rate at which the fuel surface regressed in reference to the top of the pan wall. A characteristic plot of the change in fuel mass over the course of the burning period for a heavy gas oil pool fire is shown in Figure 3.3. Similar profiles were found for all experiments conducted on kerosene, as well as those conducted on heavy gas oil. A nearly constant value of mass burning rate was measured throughout the burning period for both the heavy gas oil and kerosene, and there was no evidence to suggest that the burning rate decreased over the course of the burning period for either fuel. A decrease in the regression rate would be expected if either of these fuels behaved in a manner similar to that previously noted for complex hydrocarbon mixtures [62], where light fractions are combusted preferentially. The remainder of this section discusses the regression rate results obtained for heavy gas oil and kerosene as amalgamated from each of the different experimental methods employed for the measurements.

The four methods utilized in this work to measure the liquid fuel regression rates are described in detail in Section 3.2.1. Since each measurement method used a distinct apparatus and data analysis technique, a comparison of results from each of the methods for a given experiment is presented in Table 4.1 to validate the accuracy of the different methods. The results shown in this table are from a 0.6 m diameter heavy gas oil experiment with an initial pool depth of 0.3 m and a steady burning period of three hours. For purposes of the comparison, the fuel regression rate calculated directly from the measured initial and final fuel depths (Visual) was taken to be the baseline value. The measured values and the percent differences for each of the other methods were calculated from this reference value. It is understood that direct visual measurement of the level of the oil before and after the steady burning period did not account for the initial fuel preheat period, nor any fire decay period at the end of the steady burning time. However, it can be argued that these two periods combined accounted for less than 5% of the total burning duration for the lengthy fire considered in this comparison; therefore, this deviation is expected to represent a small error in the measurement. On the other hand, each of the other methods involved an indirect calculation of the fuel regression rate based on either (1) a characteristic parameter not directly indicative of the level of the fuel (i.e. temperature at which the fuel surface passes a thermocouple) or (2) an assumed constant material property (such as constant fuel density). It is hypothesized that despite the limitation noted above, the method based on measured fuel depth best reflects the true regression rate.

As expected, examination of Table 4.1 indicates that the values of regression rates calculated using any method based on consideration of only the steady burning period of the

Table 4.1: Comparison of fuel regression rate measurement methods using a 0.6 m diameter heavy gas oil experiment as a reference.

	Volumetric	**Mass Loss**	**Thermocouple**	**Infrared**
FRR (mm/min)	1.28	1.33	1.32	1.41
Uncertainty	±0.01	±0.10	±0.1	±0.25
$\%_{\text{diff}}$ (%)	0.0	3.9	3.1	10.1

fire are higher than the reference regression rate values obtained via visual measurement of the fuel level during the entire burning period. Nonetheless, it is clear from the values in this table that each of the methods used in this work were effective at measuring the fuel regression rate, with only a small deviation, less than 4%, between the mass loss and thermocouple methods and the reference value, and a slightly higher difference, approximately 10%, between the visual and infrared methods.

Possible errors inherent in each of the other measurement methods should also be noted and are discussed briefly here. The regression rate derived from the mass measurements was directly scaled by the density of material; therefore, a change in the density of the fuel during the burning process or errors in the measurement of the density were directly translated to the calculated value of regression rate. The measurements using the thermocouple readings relied on a constant spacing between the thermocouple beads; however, due to human error and the accuracy of measurements while arranging the array, it is expected that spacing of the thermocouples was subject to a degree of uncertainty. Finally, the infrared camera was subject to calibration errors, as well as measurement errors that arose from interferences in the captured images due to flame impingement on the side of the pan at the measurement location. Given the relatively minor errors associated with each method, the precision of each fuel regression rate measurement method is deemed sufficient for the purposes of this study. Values of regression rate as measured by any one of the methods is therefore referred to interchangeably as 'the fuel regression rate' and no further distinction as to the measurement method will be made in the remainder of this work.

The fuel regression rate was measured during each of the instrumented pan burner tests, as well as during the heat release rate and water suppression experiments. A set of regression rate data was acquired for pan diameters ranging between 0.11 to 2.0 m, across a wide range of initial fuel temperatures. The regression rate data reported in this section are from experiments conducted at an initial temperature of 60 ± 20 °C. Some variations

in measured results are anticipated based on possible differences in fuel regression rate as a function of the initial fuel temperature. To demonstrate the potential effect, it was found in large scale experiments conducted by Randsalu that a 10 °C increase in the initial fuel temperature resulted in a 10% increase in the fuel regression rate in Jet-A pool fires. This observation was based on a very limited set of experiments, and it is not clear if the observed differences in regression rate were statistically significant [72].

Values of the measured experimental regression rate for each pan diameter with corresponding uncertainty are shown for heavy gas oil in Figure 4.1. Also in the plot is a line showing the best fit for Burgess' correlation (equation 2.2.b) to the present experiments, where the values of the empirical coefficients, $\dot{m}_\infty$ and $k\beta$ in the relation by Burgess [22], were determined using a two variable least squares fit to the experimental data. The experimental results are compared with values of regression rates documented in the literature for similar fuels, in particular a spline fit to the values of regression rate measured by Blinov and Khudyakov [38] for solar oil, and results calculated using Burgess' correlation using his published values of $\dot{m}_\infty$ and $k\beta$ for heavy fuel oil [22].

In much the same way, Figure 4.2 shows the measured values of fuel regression rate for kerosene in the present experiments, again with a plot of Burgess correlation [22] using the calculated best-fit parameters for the present experimental data. The curve obtained using Burgess correlation with his published values of $\dot{m}_\infty$ and $k\beta$ for kerosene [22] and the spline fit of Blinov's measured values of fuel regression rate for tractor kerosene [38] are also shown.

The values of regression rate for heavy gas oil measured in the present work show some agreement to the results for 'solar oil' as documented by Blinov and Khudakov [38], including that they appear to approach the approximate value of the infinite diameter regression rate of 3.6 mm/min. The measured regression rates for the kerosene fires in the present experiments, on the other hand, appear to be consistently lower than measured values for kerosene reported by Blinov [38]. This might well be explained by the fact that the experiments by Blinov were conducted in Russia prior to 1961, so it is likely that composition and additives in the two kerosene fuels were quite different. Furthermore, the results by Blinov used tractor kerosene, whereas the present experiments were conducted using lantern kerosene. While there is little difference between the heats of combustion, the latent heats of vaporisation, and the densities of the various blends of kerosene, any small differences help to account for the discrepancies seen in Figure 4.2.

The regression rate correlation developed by Burgess [22] and presented as equation 2.2.b in Section 2.1 represents an empirical fit to experimental data for pool fires of a range of diameters for various fuels. It uses two fit parameters: the experimentally measured in-

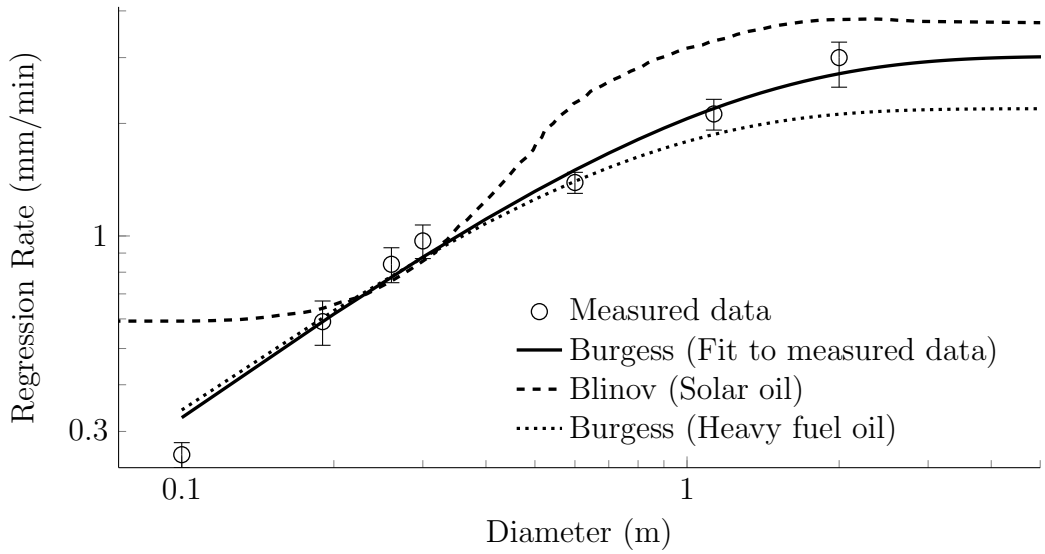

Figure 4.1: Measured fuel regression rate as a function of pan diameter for heavy gas oil compared with data from Blinov (solar oil) [38], and correlation by Burgess [22] with values from Table 4.2.

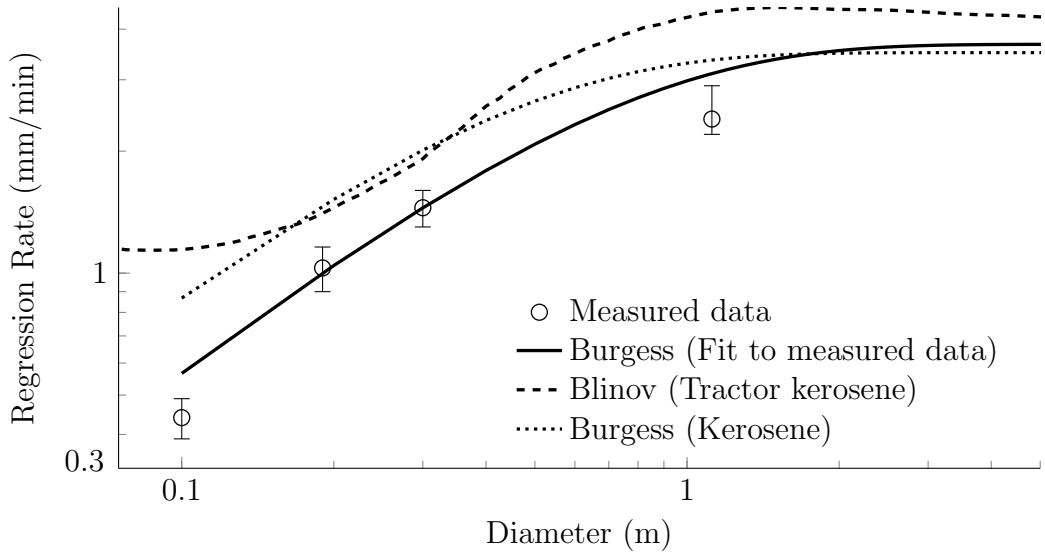

Figure 4.2: Measured fuel regression rate as a function of pan diameter for kerosene compared with data from Blinov (tractor kerosene) [38], and Burgess correlation [22] with values from Table 4.2.

finite diameter regression rate, R_∞, and a diameter correction $k\beta$. As mentioned above, a two-variable least squares fit to Burgess' equation was performed for the measured fuel regression rate results for the heavy gas oil and kerosene to determine the empirical fit coefficients of the measured data. The values of R_∞ and $k\beta$ determined in this analysis are shown in Table 4.2, and compared with values found in the literature for similar fuels [22]. From this table and the curves shown in Figure 4.1 and Figure 4.2, it is seen that the coefficients presented in the literature for heavy gas oil and kerosene do not well represent the present measured results. In particular, a remarkable difference between the infinite diameter regression rate is clear between the measured and literature data. This is unexpected, as most fuels typically reach a steady burning rate of nearly 4 mm/min at large diameters, as previously noted by Blinov and Khudakov [38]. That the infinite diameter burning rate for heavy fuel oil as determined via a direct fit of the correlation to the present data is different than the results given by Burgess for heavy oil is perhaps not unexpected, as the present fuel is significantly different than the heavy oil and crude oil used in those experiments. More notable is the 22% difference between the infinite diameter regression rate reported in the literature for kerosene and the best-fit value for the same fuel in the present results. The discrepancy between the calculated infinite diameter regression rate and those reported in the literature, then, warrants further investigation.

Examination of the regression rate data used to derive these fit coefficients points to fact that the fit coefficients, in particular for the heavy gas oil, may be largely influenced by the data obtained in the 2.0 m diameter experiment, where the regression rate was measured using the infrared camera. This value for regression rate may have been artificially high, leading to a similarly high value for the calculated coefficient of R_∞. It was shown in Table 4.1 that, in general, regression rates determined using data from the infrared camera were up to 10% larger than comparative values measured using the other techniques. This, coupled with the difference in fuel properties, may explain the difference in R_∞ between the present heavy gas oil and heavy fuel oil – for example. In the case of kerosene, no data was obtained for diameters larger than 1.12 m, so the fit was significantly influenced by the regression rates measured at the small pan diameters. It is possible that the 1.12 m pan was not large enough to fully approximate the infinite diameter conditions, resulting in a measured R_∞ lower than those documented in literature. Furthermore, the square geometry of the 1.12 m pan may have had an affect on the measurements in these experiments, and could have contributed to the lower value.

An additional explanation for the noted discrepancy in the R_∞ values lays in the reality that there exists a wide discrepancy in pool burning correlation values for a given fuel reported by different researchers. Data tabulated by Laboureur [23] for diesel oil shows a variation from 0.034 to 0.062 kg/m^{2}s in estimates of the mass burning rate at infinite diam-

Table 4.2: Empirical fit coefficients to equation 2.2.b for fuel regression rate, comparing experimental measurements and literature values [22].

Fuel	$\dot{m}''_\infty$ (kg/m^{2}s)	ρ (kg/m^3)	R_∞ [a] (mm/min)	$k\beta$ (m^{-1})
Heavy Gas Oil (Best-fit)	0.047	940	3.0	1.1
Heavy Fuel Oil [23]	0.035	960	2.2	1.7
Crude Oil [23]	0.039	850	2.8	2.8
Kerosene (Best-fit)	0.050	820	3.7	1.7
Kerosene [23]	0.039	820	2.9	3.5

[a] Calculated using equation 2.1

eter, and 0.63 to 2.8 m^{-1} for the extinction coefficient as measured by different researchers. This range of values, which bracket measurements by four different researchers, is similar to those seen in Table 4.2 and helps to show the difficulty in measuring the regression rate in liquid fuelled pool fires. Again, it is clear that variations in the fuel composition, as well as the various experimental parameters used in the tests, can also have a significant effect on measured values of the fuel burning rate. Such differences, together, help to account for the discrepancy seen in the present results.

As mentioned, the regression rate is largely affected by several experimental parameters including, but not limited to the fuel temperature, freeboard height, and ambient temperature [67]. Within the present experiments, pans of glass and metal were used, as well as pans with different wall heights. A full description of each of the test pans is shown in Table 3.2. While the pan material is not considered to have greatly affected measured values of regression rate, the initial temperature of the fuel and the pan freeboard height did have some impact, as discussed below.

To examine the impact of initial fuel temperature on measured values of regression rate, Figure 4.3 shows the normalized regression rate of heavy gas oil plotted against the initial fuel temperature. To compare the results across multiple pan diameters, the results are presented as the regression rate measured for a given initial fuel temperature, normalized by the average regression rate for a 40 °C fuel temperature at the same pan diameter. Therefore, the spread of values at each temperature represents the spread of experimental measurements at that temperature. Due to the limited number of tests at each fuel temperature, the experimental variability is large and there is insufficient data to make a meaningful statistical analysis of the effect of fuel temperature on burning

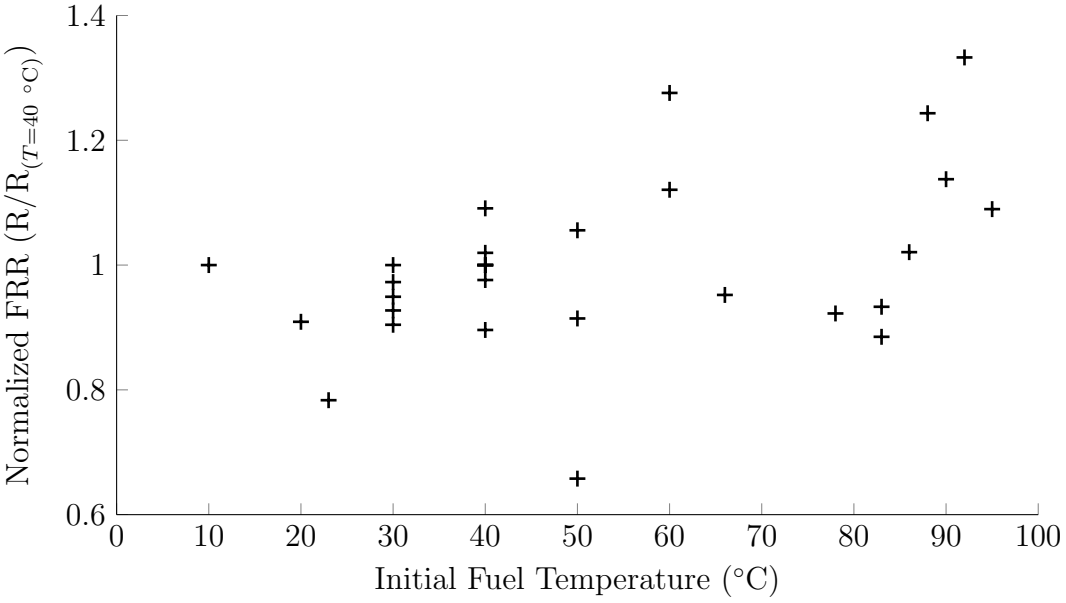

Figure 4.3: Temperature dependence on fuel regression rate for 40 °C normalized temperature and regression rate at that temperature.

rate. Nonetheless, Figure 4.3 demonstrates an increased fuel regression rate increased with increasing initial fuel temperature. This is as expected since, at higher initial temperatures, the fuel was heated to a temperature closer to the vapourisation temperature, and therefore less energy was required to heat the fuel to the vapourisation point. This energy was then available to vapourise the fuel, which caused an increased fuel burning rate.

From Figure 4.3, an increase in average fuel regression rate of approximately 10% can be seen for an increase in fuel temperature from 40 to 80 °C. This trend is comparable to results by Hall, who found a 0.2 mm/min increase in regression rate per 10 °C change in temperature for benzene [58], and with Randsalu who found a similar 0.25 mm/min increase for Jet-A pool fires [72] over a similar temperature increase. Since the data in Figure 4.3 incorporates regression rate measurements from all pan diameters, from 0.106 to 0.6 m, it can further be concluded that the influence of temperature on fuel regression rate is not dependent on pan diameter, at least for the present experiments. Finally, in terms of the scatter in the data, it should be noted that the temperature of the fuel was not maintained constant, and consequently decreased through the burning period for every experiment. The decreasing fuel temperature throughout the experiment likely caused a similar decrease in the regression rate, thus affecting the calculated average regression rate.

Table 4.3: Coeficients for the experimental fit to equation 2.4 showing the effect of lip height on burning rate.

Fuel	d (m)	$\dot{m}(H=0)$ (kg/s)	$min\,(H/d)$ (–)	η (–)	R^2 (–)
Heavy Gas Oil	0.19	0.00024	0.01	0.11	0.901
	0.26	0.00065	0.133	0.17	0.887
	0.60	0.0058	0.133	0.17	0.927
Kerosene	0.19	0.00042	0.01	0.05	0.981

It is possible that maintaining the fuel temperature at the higher temperature throughout each experiment would have helped to increase the correlation of the data, particularly for initial fuel temperatures above 64 °C, where the heat loss seems to become significant.

The pan freeboard height is also known to have an effect on the fuel burning rate, as the heat loss from the flame column to the pan walls becomes significant at large pan lip heights, coupled with the increased wall height limiting the oxygen availability. Equation 2.4 has been proposed to model the decrease in burning rate with increased pan wall height, where the coefficient η is a fit parameter that is found through a fit to experimental results [67]. For the mass measurements recorded for each of the pool fire experiments, a single parameter least squares optimization algorithm was run for the mass loss rate measurements, which solved equation 2.4 for *eta* using the calculated mass loss rate at each time interval.

Table 4.3 shows the experimental fit parameter for heavy gas oil and kerosene for the range of pan diameters in the present work. This value represents the net effect of an increased lip height on fuel regression rate, with values near 0 indicating that the lip height had little effect on the burning rate. It is seen that the fit coefficient is dependent on the type of fuel, with kerosene having a lower value than heavy gas oil. This is consistent with the expected burning behaviour of the two fuels, since kerosene is more volatile than heavy gas oil, therefore increased heat loss to the walls in a kerosene fire does not affect the rate of fuel vapourisation – and thus mass burning rate – as much as for heavy gas oil. The fit parameter was calculated to be somewhat independent of pan diameter and pan material; however, there are too few data points to make a conclusive remark on the possible effects of different pan diameter configurations.

A further discussion on the fuel regression rate is found in Section 4.5, as related to the overall burning behaviour of heavy gas oil. The effect of water emulsification on the fuel regression rate is discussed in Section 4.6.

4.2 Heat Release Rate

Experiments were conducted to measure the rate of heat release in various diameter heavy gas oil pool fires in efforts to compare the burning characteristics of the fuel with values reported in literature. Reference experiments were also conducted with kerosene to validate the experimental methods, as well as facilitate comparison of the properties of the two fuels. The results of the heat release rate measurements are presented here.

To effectively compare the rate of heat release of the liquid fuels to the theoretical values, as well as to values presented in the literature, the heat of combustion for each fuel was measured using an adiabatic bomb calorimeter. The measured values of heat of combustion for the heavy gas oil and kerosene are shown in Table 4.4, and compared with literature values for similar fuels from [20, 79, 134, 135].

Table 4.4: Comparison of the measured heat of combustion of heavy gas oil and kerosene to values documented in literature [20, 79, 134, 135].

Fuel	ΔH_C (MJ/kg)		**Reference**
	Measured	*Documented*	
Heavy Gas Oil	43.5	–	
Kerosene	45.8	44–47	[20, 79, 134]
Crude Oil	–	45–46	[79, 134]
Heavy Fuel Oil	–	42–45	[20, 79, 134, 135]

The measured value for the heat of combustion of kerosene at 45.8 MJ/kg closely matches that commonly found in literature [20, 79], and is similar to the referenced value of 43 MJ/kg for the general class of hydrocarbon fuels used in fire safety design calculations [136]. Similarly, the heavy gas oil has a heat of combustion within the common range of values for hydrocarbons and specifically in the range normally reported for heavy and complex fuels. The measured heat of combustion of heavy gas oil, 43.5 MJ/kg, is in the range of those for both heavy fuel oil and for crude oil, $42 - 45$ and $45 - 46$ MJ/kg,

respectively, as documented in literature [20, 79, 134, 135]. The above-noted difference in heat of combustion values between crude oil and heavy fuel oil, while not insignificant, is similar with other fuels. Gasoline – a comparatively volatile fuel – for example, has a heat of combustion only 10% higher than that of heavy fuel oil [79], a far heavier and more complex hydrocarbon.

Measurements of the rate of heat release from both kerosene and heavy gas oil fires were obtained from the cone calorimeter and furniture calorimeter using the method of oxygen consumption calorimetry. An introduction to the testing method is presented in Section 3.3, and a complete description of the apparatus and calculation methods is presented in [107]. In each experiment, the pan of fuel was ignited with a propane torch and allowed to freely burn for a time of 20 to 45 minutes. No correction was applied to filter out the spike in heat release rate from the ignition torch, but this did not impact the data since the reported heat release rate was calculated from the average heat release rate determined during the steady burning period. Furthermore, as fuel was not replenished during the burning period, the tests were truncated such that possible effects on the data of increasing pan wall height due to the regression of the fuel surface did not affect the repeatability of the results, as discussed in Section 4.1.

Much like the fuel regression rate, a primary concern for the modelling of storage tank fires is the effect of diameter on heat release rate. Measurements of heat release rate were therefore taken during the experiments in the instrumented pan burner, and additional measurements were taken across a range of pan diameters to globally assess the burning characteristics. Pool diameters of 0.06 to 1.12 m are considered in this work, with the cone calorimeter used on the 0.106 m diameter pans and smaller, and the furniture calorimeter used on the 0.19 m diameter pans and larger.

Similar to the previously reported regression rate results, results of the heat release rate experiments are grouped in 40 °C initial fuel temperature brackets, and the following discussion considers results only for tests in which the fuel temperatures were 40 ± 20°C. There were insufficient measurements of heat release rate made at different initial fuel temperatures to make a statement on the effect of temperature on heat release rate.

The measured heat release rate was found to correlate approximately with the pan diameter; however, a more effective relation was found between the area normalized heat release rate and pan diameter. Measured values of the area normalized heat release rate are plotted as a function of pan diameter in Figure 4.4 for heavy gas oil fires and in Figure 4.5 for kerosene fires. Also plotted are the curves for area normalized heat release rate versus fire diameter calculated using the heat release rate model presented in equation 2.5.b, with

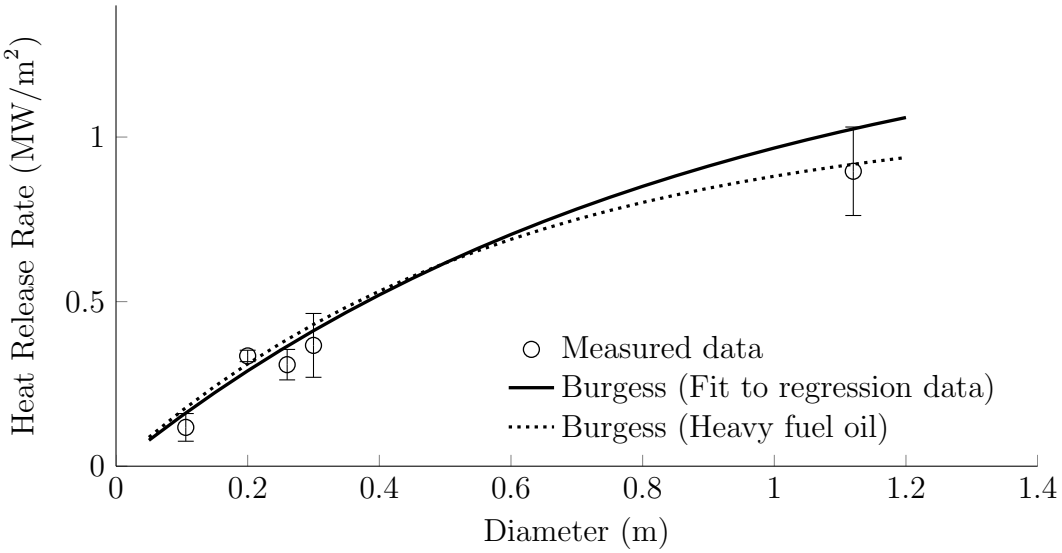

Figure 4.4: Measured heat release rate as a function of pan diameter for heavy gas oil compared with Burgress corelation using values from Table 4.2.

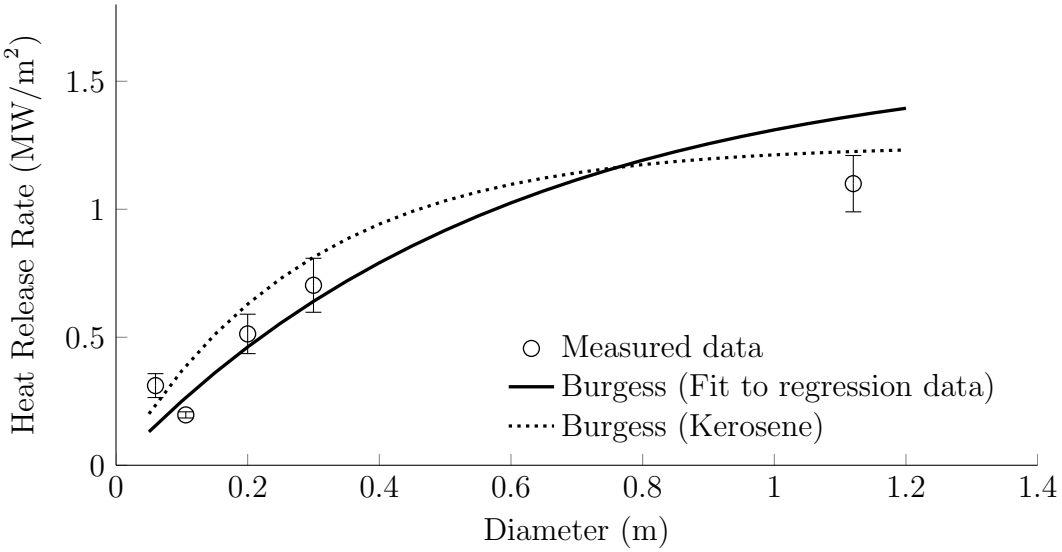

Figure 4.5: Measured heat release rate as a function of pan diameter for kerosene compared with Burgress corelation using values from Table 4.2.

Table 4.5: Experimental parameters as measured by the cone calorimeter for 0.106 m diameter pan at 40 °C.

Fuel	**HRR** (kW)	**MLR** (g/s)	**FRR** (mm/min)	χ ($-$)
Heavy Gas Oil	1.12 ± 0.07	0.035 ± 0.002	0.26 ± 0.01	0.72 ± 0.05
Kerosene	1.74 ± 0.15	0.046 ± 0.005	0.39 ± 0.03	0.82 ± 0.01

both the least squares fit data determined from the regression rate experiments tabulated in Table 4.2 and the values reported in the literature [22].

It can be seen that this model provided a reasonable fit to the measured results, where the area normalized heat release rate values predicted for both heavy fuel oil and kerosene based on values of $\dot{m}_\infty$ and $k\beta$ from the literature closely approximate the measured results. Conversely, the best-fit parameters from the regression rate experiments show a good fit to the experimental heat release rate data using equation 2.5.b, however are consistently slightly higher at the 1.12 m diameter. In this experiment, a thin fuel layer was used to limit the volume of fuel consumed, which may have caused some heat loss to the pan walls and bottom. This would have resulted in a measured heat release rate lower than expected, and could explain how the measured values for both fuels are lower than the model. Nonetheless, the close agreement of the measurements and the predictions demonstrates the self-consistency of the measured values in this work, since the liquid fuel regression rates and the heat release data were independently measured using a variety of different techniques.

At this point in the discussion, it is of interest to further focus on measurements made using the cone calorimeter, as this apparatus presents a relatively standardized testing apparatus amongst researchers. The severe limits on the sample size and pan configuration provide a relatively constant pool area and set of experimental conditions, allowing the results presented in literature to be directly compared to the present results. As well as the heat release rate, the mass loss rate, and therefore fuel regression rate were also measured in the cone calorimeter. Using the independent measurement of the heat of combustion obtained in the bomb calorimeter, an estimate of the combustion efficiency of the burning fuel was also made for these small scale fires. Table 4.5 shows a summary of the cone calorimeter measurements for heavy gas oil and kerosene in the present work.

From Table 4.5, as well as comparison of Figure 4.4 and Figure 4.5, it can be seen that the measured heat release rate of kerosene was higher than that for heavy gas oil across

Table 4.6: Experimental heat release rate measurments for liquid fuels as measured using a cone calorimeter by different researchers in pans of approximately 0.0284 m^2 [65, 71, 91].

Fuel	HRR (kW)			
	Measured	**Jianghong** [91]	**Iwata** [65]	**Mealy** [71]
Kerosene	16	13	18	12
Heavy Gas Oil	11	–	–	–
Crude Oil	–	–	8.5	–

all experimental diameters. This is not unexpected, due to the similar heat of combustion of the two fuels, but higher volatility and thus the greater mass burning rate of kerosene. Further, kerosene was noted to burn with much less smoke than the heavy gas oil, indicating that the combustion was more complete, which in itself would lead to greater heat release in the kerosene fires.

To further assess the data from the present measurements, it is of interest to compare the cone calorimeter measurements in Table 4.5 to those made in other test laboratories. Since there is no formal testing standard for the use of the cone calorimeter to test liquid fuels, there may be a wide variability in values for the same materials. Nonetheless, the cone calorimeter provides the best experimental apparatus for highly controlled heat release rate measurements. Table 4.6 shows the steady state heat release rate as measured under the cone calorimeter for common fuels, as reported by different researchers under similar test conditions. On first examination, the differences in the results amongst researchers appears to be quite small. However, this is misleading as it must be noted that the results are scaled by a small sample area of 0.0284 m^2. Therefore, the difference in values becomes significant when using these values to compare estimated heat release rates in a large scale fire. The heat release rate measured for kerosene by Mealy would predict the heat release rate from a 1 m^2 fire to be 423 kW, while Iwata would predict 630 kW for the same fire, giving a 50% difference between the two predictions. The wide discrepancy in the measured values can likely be explained by differences in the experimental procedure used by different researchers, as the results at small scale are greatly influenced by the various factors affecting the burning rate described in Chapter 2, as well as by small variations in the fuel composition or weathering of the samples.

Unfortunately, there is little reported data relating to well controlled measurements of heat release rate of kerosene or heavy gas oil fires at a larger scale, for instance using a furniture calorimeter or other more standardized method. Since the other heat release

rate determination methods, including radiative flux and flame height measurements, are dependent on the experimental conditions and are often not well documented, there is little value in making a comparison to the current results. However, as the heat of combustion is well defined, and the regression rate measurements presented in Section 4.3 are in good accord with measurements found in literature, it can be concluded that the heat release rate behaviour of heavy gas oil is comparable to those of other heavy hydrocarbon fuels. As well, the calculation method shown in equation 2.5.b, coupled with accurate material properties appears to provide an accurate prediction of the heat release rate, at least for the diameters considered in these experimental measurements.

4.3 Flame Spread Rate

The next burning characteristic to be studied in this work was the rate at which the flame front propagated across the fuel surface, for both kerosene and heavy gas oil. Due to the small surface area of the pans used in the instrumented pool burner experiments, a custom configured, elongated pan was used to make these measurements. The full experimental method is provided in Section 3.4; however, a brief reiteration is provided here. The experiments were conducted in a trench pan, 3.6 m long and 0.25 m wide, with a depth of 0.1 m. A layer of fuel 0.05 m deep was added to the pan, and the fuel was ignited from one side. The time at which the flame front progressed along the fuel surface was recorded at regular intervals. The rate of flame spread was derived from the length of each interval divided by the time taken to cover that distance. Additional measurements of the rate of flame spread were derived during suppression experiments in the 1.12 m and 2.0 m diameter pans, as detailed in Section 3.5.

Figure 4.6 shows plots of flame front position as functions of time for both heavy gas oil and kerosene for experiments conducted in the flame spread trench apparatus. It is clear from this plot that a linear trendline well represents the flame positions versus time data for both fuels, indicating that the rate of flame spread was consistent through the entire measurement period. The differences in slope of the lines for the two fuels indicate a higher value of flame spread rate for kerosene than for heavy gas oil. The constant slope of the flame position plot indicates that the flame spread is a steady phenomenon, and that the average flame spread rate is well represented by the slope of these curves.

The measured rates of flame spread were found to be independent of the fire size based on comparison of values determined using the constrained flame spread tray experiments and those found under unconstrained spread in the large scale experiments conducted in the 1.12 and 2 m pans. For the tray experiments, Figure 4.7a shows a comparison of the flame

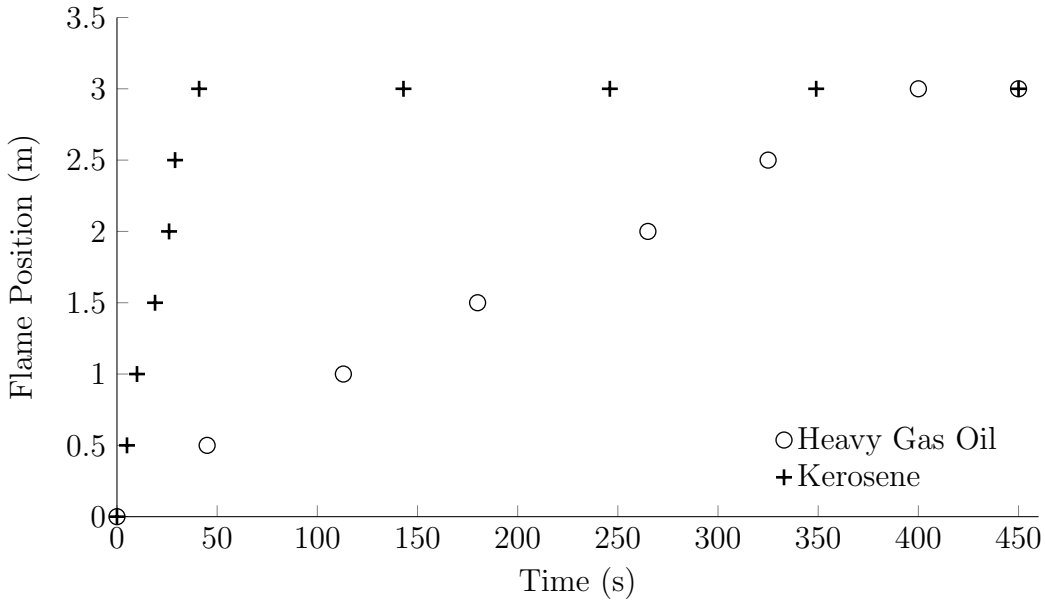

Figure 4.6: Flame front position versus time as measured for heavy gas oil and kerosene.

shape at the start of the flame spread, 60 seconds after ignition, and Figure 4.7b shows an image where the flame had propagated two thirds of the length of the tray, 310 seconds after ignition. In each of the images, the flame shape and size are roughly constant, with only a small increase in flame height as the flame propagates along the tray. It is therefore evident that the flame height, or fire size, did not grow appreciably as the flame spread across the fuel surface, and thus there was a relatively constant heat flux from the flame to the fuel surface ahead of the fire. In contrast, during unconstrained flame spread experiments in the 1.12 and 2 m diameter pans, both the flame area and flame height steadily increased with time after ignition as the fire spread across the pool surface. The flame spread rate observed in these experiments was found to closely match that measured in the constrained tray experiments, which confirms the findings of Mackinven et al. [54], who found that the driving mechanism of flame spread in fuels below the flashpoint temperature was the sub-surface mixing, rather than the radiative flux to the fuel surface. The remainder of this discussion will thus be focused around those values obtained by averaging the flame spread rates measured under concurrent and countercurrent wind conditions in the trench apparatus.

In the trench experiments, the measurements of flame position in each experiment were recorded by visually verifying the flame position as the front crossed over the various posi-

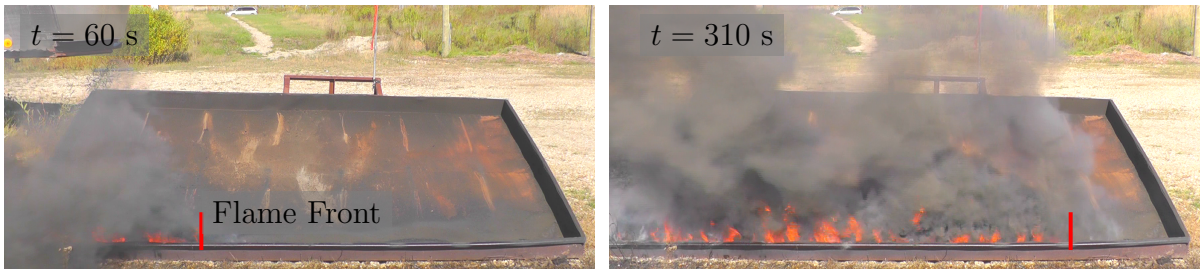

(a) $FS = 0.6$ m (b) $FS = 2.5$ m

Figure 4.7: Comparison of the flame shape during the flame spread rate experiments at during initial and developed flame spread.

tion makers labelled on the pan. This method has been used by several other researchers, including in the standardized method proposed by Mackinven et al. [54], and has been found to be accurate enough to make good determinations of flame spread across a range of liquid fuels. In the present results, the measurements of flame position were verified using the recorded videos and were found to differ only in cases where the wind caused smoke to obstruct the marker lines during the experiments. Nonetheless, the overall variation from the physical measurements was less than 5%. A summary of the measured results for kerosene and heavy gas oil are shown in Table 4.7 for both con-current and counter-current flame spread.

Table 4.7: Rate of flame spread measurements as measured in the flame spread test pan for heavy gas oil and kerosene in up and down-wind directions.

Fuel	**Flame Spread Rate (cm/s)**		
	Countercurrent	**Concurrent**	**Wind Neutral**
Heavy Gas Oil	0.7 ± 0.05	0.8 ± 0.05	0.8 ± 0.1
Kerosene	9.0 ± 0.1	9.7 ± 0.15	9.3 ± 0.25

As is expected, the rate of flame spread in the down wind direction was greater than the rate of spread in the up wind direction. As has been documented, in concurrent spread the wind tilts the flame column towards the fuel, enhancing the heating and vaporisation of the fuel ahead of the flame front, thus increasing the spread rate. In the present experiments, there was insufficient variability in the wind speeds to comment on the effect of wind speed on the rate of flame spread. Rather, the average wind speed was 2.1 m/s during the

most wind-affected experiments; therefore, there was good consistency in the experimental conditions. As such, an average of the con- and counter-current flame spread rates - representing the wind neutral flame spread rate – are compared to values in the literature for wind neutral conditions.

The flame spread rate of 0.8 cm/min for the heavy gas oil is comparable to that previously measured for flame spread across other heavy fuels, notably values of approximately 6 cm/min for SAE 30W motor oil [137]. As these fuels are both far below their respective flashpoint temperatures, it anticipated that the flame spread in both of these fuels would be similar as it is driven by subsurface mixing of the fuel, rather than through heating of vapours above the fuel surface [54]. Since heavy gas oil has a flashpoint of over 150 °C, it is logical that only sub-flashpoint flame spread would occur in the event of an actual fire, and the vapour-driven flame spread was not considered in this study.

The flame spread rate of the kerosene as measured in the present experiments is comparable to values reported by Mackinven et al. [54] and Guo et al. [138] for a fuel temperature of 20 °C, well below the flashpoint temperature. It is understood that the variability in measured values of flame spread increases as the fuel temperature approaches the flashpoint. However, consistency of the present data with that of Mackinven et al. [54] at low temperature increases the overall confidence in the determination of wind neutral flame spread rate based on the averaged values used here.

This concludes discussion of the flame spread rate experimental measurements. Further discussion of flame spread is presented in Section 4.5, as related to the general burning behaviour of the oil. A significant increase in the flame spread rate was noted for undried oil, where the fuel ejections aided the preheating and enhanced mixing of the fuel ahead of the fire. This effect is discussed further in Section 4.6.

4.4 Suppression

An important aspect of fire suppression systems design is the effect that water suppression sprays have on the hot surface of a burning liquid fuel. For example, a potentially hazardous situation can occur if heated oil from the fuel surface mixes with the suppression water, creating a mixture of steam and oil, that expands in volume and can potentially overflow the storage tank or test pan.

Due to the known occurrence of hazards such as that above, as one section of the present research, a series of experiments was conducted in the 1.12 m and 2.0 m diameter pans to evaluate the effectiveness of water suppression sprays on heavy gas oil and kerosene

pool fires. For all tests, a 0.1 m thick fuel layer was added to the pan and the fuel was ignited and allowed to burn freely for five minutes prior to the suppression attempts. The volume of water applied during suppression and the time to flame extinction were recorded for each test. A reference experiment was also conducted on suppression of a kerosene fire in the 1.12 m pan. The full experimental method for this series of tests is presented in Section 3.5.

Initial experiments were conducted following the recommended water application rates from NFPA 15 [133], for the control of large, open hydrocarbon pool fires, with a range between 0.10 to 0.34 L/s/m^2. Values within this range were used in the present experiments in the effort to establish the effectiveness of a defined area normalized flow rate on the heavy gas oil fire properties, with the intent to control and extinguish the fire. Further attempts were made to establish whether the flame spread rate was sufficient to overcome the suppression capabilities of the water stream.

The suppression spray was calibrated to a designated flow rate before each of the experiments. It was ensured that for each flow rate, the spread of the suppression water covered the entire pan surface. Water loss due to ambient wind was not accounted for, but instead was assumed to be minor relative to the total volume of water in the spray.

Table 4.8 summarizes fire diameters and water flow rates used for each of the experiments and the time to suppression, for both heavy gas oil and kerosene fires. As mentioned in Section 3.5, the minimum area normalized water flow rate recommended by NFPA 15 for the control of open hydrocarbon pool fires is 6.1 L/m^{2}s.

Table 4.8: Results of suppression experiments on heavy gas oil and kerosene.

Fuel	**Diameter** (m)	**Flow Rate** (L/m^{2}s)	**Time** (s)	**Comments**
Heavy Gas Oil	1.12	6.1	30	Frothed out
	1.12	5.4	30	Frothed out
	1.12	5.4 [a]	45	Frothed out, no overflow
	2.0	18.9	—	Did not control
	2.0	18.9 [b]	45	Frothed out
Kerosene	1.12	20.4	—	Did not control

[a] 4 rounds of 5 s duration spray

[b] Straight steam spray

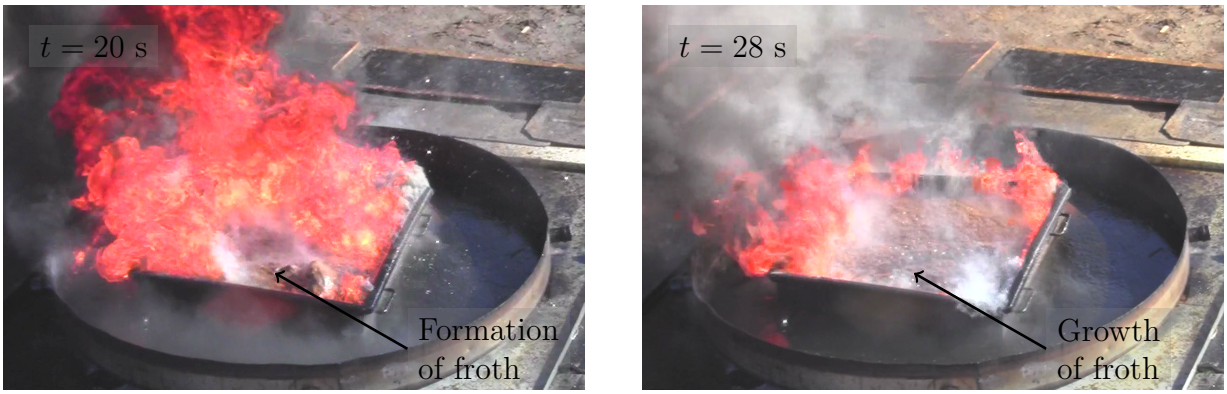

(a) $t = 20$ s (b) $t = 28$ s

Figure 4.8: Formation and spread of steam-impregnated froth layer during suppression experiments on heavy gas oil in 1.12 m pan, and suffocating fire.

A total of three suppression experiments were conducted at the intermediate 1.12 m diameter scale on heavy gas oil pool fires. In each case, the fire was suppressed in less than a minute after initiation of suppression. It was found that upon contact with the heated fuel surface, the suppression water evaporated as it sank into the heated fuel, forming steam. As the steam migrated back towards the surface of the fuel, it mixed with the heated oil, forming a froth mixture, heavily impregnated with water. Due to the volume expansion of water to steam, this froth mixture was much greater in volume than the original oil, and therefore spread across the fuel surface. The froth was sufficiently impregnated with water and steam that it generally would not ignite and therefore the spreading layer of froth aided to suppress the fire.

An example of the formation and spread of the froth layer is shown in Figure 4.8, as recorded during the 1.12 m suppression experiment. The layer of froth growing over time and spreading across the surface is clear from this figure. As well, a significant decrease in flame intensity is noted while the froth spread, as is expected due to the decreasing relative area of the fuel surface. Finally, it should be noted that this frothing phenomenon is not unique to the heavy gas oil. It has been previously documented for interactions of heated oil and water [90, 139], and is the basis for the slopover phenomenon.

Due to the layer of froth aiding the suppression of the flame column, and preventing the spread of flame towards previously suppressed pool surface, the water requirement

for suppression of the heavy gas oil fires was very low. The 1.12 m diameter fires were suppressed at a flow rate below the minimum recommended amount, at 5.4 L/min.

Contrary to the results for suppression of the heavy gas oil fires, a water flow rate of 20.4 L/min, the maximum water flow rate considered in this study, was not sufficient to control or suppress the 1.12 m diameter kerosene pool fire. This is consistent with reports that recommend using Aqueous Film Forming Foam for hydrocarbon pool fires, due to the inability of water alone to control the fires [88, 139]. As discussed in Section 4.2, the heat release rate of kerosene was only marginally greater than that of heavy gas oil, so it would be expected that a 278% increase in water flow rate would be able to suppress the fire. From this data, it is clear that the generation of the froth and subsequent suffocation of the flame column was one of the main driving forces aiding the suppression of the heavy gas oil fire. The direct impact of the water spray on the flame column was therefore considered to be negligible compared to the more effective suffocation effects of the froth layer.

Due to the inability of the highest volume water stream to control the kerosene pool fire at the small scale, a large scale suppression experiment was not attempted for kerosene. However, two larger scale suppression experiments on 2.0 m diameter fires were conducted using heavy gas oil as fuel. Again, the suppression water nozzle was configured to allow the water stream to spray across the entire fuel surface, and the minimal area normalized water flow rate was used. In this situation, the droplets of the water spray were overcome by the heat in the flame column, and the spray was ineffective at controlling the fire at this scale. It is hypothesized that the water droplets were vapourised prior to reaching the fuel surface, and therefore the frothing suffocation of the fire seen in the tests on the 1.12 m diameter fires did not occur. A second experiment was conducted, similar to the first, except that the water spray was reduced into a straight steam and directed in an arc towards the flame column, generating larger sized droplets and imparting more momentum into the water droplets in the suppression spray. In this case, the water did appear to reach the hot surface of the fuel and the fire was extinguished in a time and fashion similar to that seen in the small scale experiments. Again, the generation and spread of a water impregnated froth layer was determined to be the cause of the suppression.

While it is expected that the increased strength of the flame column in the larger fire had an effect on the suppression water requirements, the effectiveness of suppression in the large pan test was also affected by the distribution of the water spray to the fire. For the small pan, the flow of water was sufficiently low that the nozzle had to be placed very near the test pan to deliver the water to the fire, and the angle of nozzle was low enough to ensure that all of the full volume of water used hit within the pan, and interacted with the fire column. On the other hand, with the larger diameter pan, the nozzle had to be placed further from the pan to deliver the water, and the nozzle angle was much greater.

These conditions combined likely resulted in the water spray being affected much more by the wind at the large scale than for the smaller fires, which would further decrease the effectiveness of the suppression spray.

Of note from the successful heavy gas oil suppression experiments was the volume of steam-oil mixture, or froth, generated as a result of the spray interacting with the hot surface of the oil. In each of the experiments, sufficient froth was generated to smother the fire; however, this volume was also sufficient to overflow the test pan and cause flaming oil to spread into the containment pan. It is clear that while the froth may reduce one hazard, fire spread to the surroundings presents another hazard in the case of actual storage tank fires. Further experiments indicated that the volume of froth generated could be mitigated by using a pulsating suppression spray, where a five second break in the spray allowed for some of the froth to subside prior to commencing a new burst of spray. This approach might be optimized in a real system to achieve the best balance between generation of froth to aid suppression of the fire, while minimizing the potential for any overflow of flaming oil to the surroundings. It remains unclear, though, if this behaviour would also occur in real-scale fires, and may not be practical in many situations.

After the surface fire was contained, a layer of the froth remained over the fuel surface for approximately 20 minutes, and subsided as the steam migrated out of the oil. This froth layer acted as a fire break while there was a sufficiently thick layer on top of the fuel, as there was enough water contained in the froth to prevent ignition of the fuel, even with application of a high intensity propane torch. Furthermore, once the water evaporated from the froth in the surface layer, the fuel returned to a state resembling the original oil, having a similar colour and viscosity. It would likely be possible to introduce the residual oil back into the upgrading process without much alteration, therefore wasting minimal product in the case of a fire.

While this study only considered the basic interaction of water suppression sprays on heavy gas oil pool fires, it is believed that the phenomenon exhibited in the small scale experiments could resemble the behaviour of actual tanks. The formation of the froth layer during suppression of heavy oils should be studied in larger scale experiments, as this behaviour could reduce the requirements for foam and suppression water reserves for industrial instalments. This inerrant suppression mechanism could represent an area of cost savings in the case of a fire, as the froth layer reduces the volume of water reserves required, as well as the necessary volume flow rate of the suppression pumps.

4.5 Fire Behaviour

The overall burning behaviour and thermal distributions developed in the fuel for the heavy gas oil and kerosene fires were investigated in more depth using the instrumented pan burner described in Section 3.2. In this series, experiments were conducted to monitor the temperature through the depth of the fuel in an attempt to determine whether a hot-zone formed within the fuel, while also tracking the development of the characteristic burning behaviour of the fire. Experiments were conducted in pans of 0.19 m to 0.6 m in diameter both with and without a water sublayer. This section discusses the burning characteristics of the fire for experiments in which there was no water sublayer. The results are also used, with theory where possible, to shed further light on the development and behaviour of the fires studied in the present work. A discussion of the experiments conducted with a water sublayer relate to the the potential for boilover and are presented in Section 4.8.

A number of experiments were conducted to measure the temperature history through the depth of the heavy gas oil and kerosene fuels using the instrumented pan burner as shown in Figure 3.1. In each experiment, the linear thermocouple rake shown in Figure 3.2a or the grid thermocouple rake shown in Figure 3.2b were inserted into the pan and a thick layer of fuel, ranging in depth between 0.06 and 0.30 m, was added to the pan. The fuel was ignited with a propane torch, and then allowed to burn freely until all of the fuel was consumed. For each experiment, the time history of fuel mass loss and temperature distribution in the fuel were recorded, as were the overall fire characteristics. A full experimental set-up and description of the apparatus is shown in Section 3.2.

Preliminary experiments were conducted to analyse the temperature distribution into the depth of each fuel, using the linear thermocouple rake shown in Figure 3.2a. Figure 4.9 shows a characteristic plot of the temperature history in a heavy gas oil fire as measured during an instrumented experiment. As this plot is characteristic of the results obtained in each of the experiments, regardless of fuel, fuel temperature, or pan diameter, this figure is referenced throughout the following sections.

As can be seen in Figure 4.9, the temperature at each thermocouple bead remained constant at a value equal to the initial fuel temperature while a sufficiently thick layer of fuel remained above the thermocouple bead. As the fuel surface regressed and the depth of the fuel layer above the topmost thermocouple decreased, the measured temperature at the upper thermocouple gradually increased as the heated fuel surface approached that thermocouple bead. The temperature at that thermocouple then registered a constant value of approximately 460 °C for a short period of time, as the fuel surface passed over the bead. The temperature of the thermocouple then quickly climbed to the range of 600

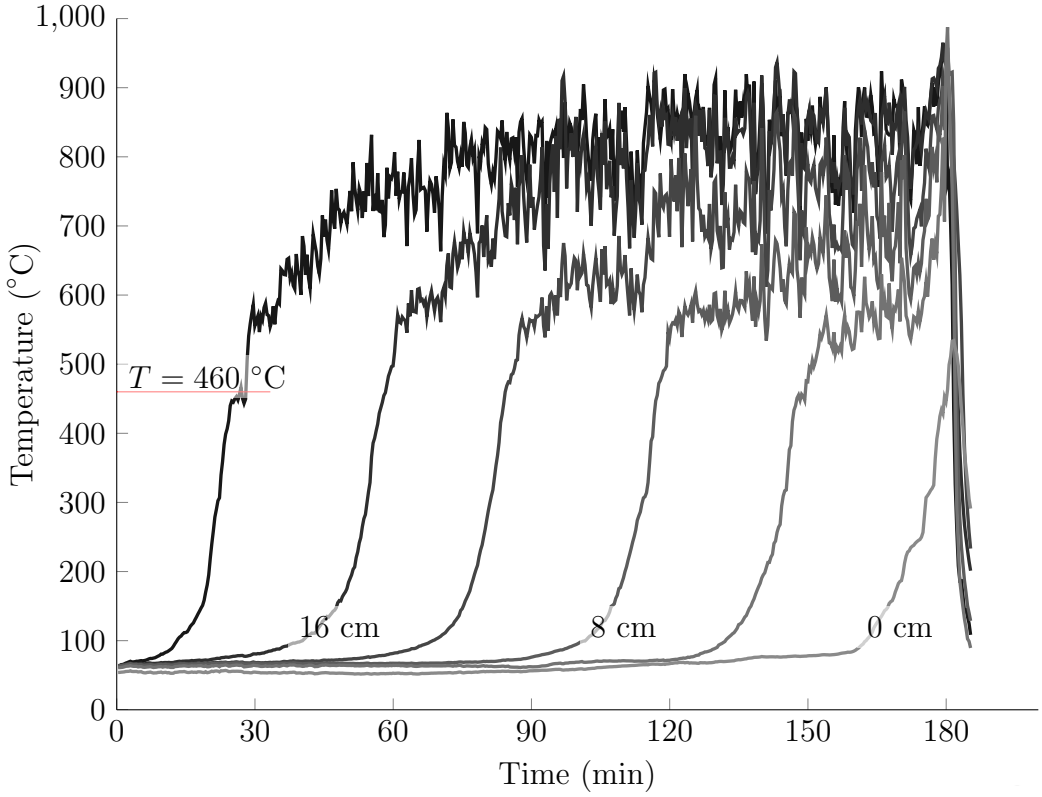

Figure 4.9: Characteristic temperature history at various depths into fuel, as measured in 0.6 m diameter heavy gas oil pool fire.

to 900 °C as the thermocouple bead entered the flame zone. This trace then repeated at a later time for the next thermocouple down the rake. Due to the long time scale of this plot, the constant temperature regions are compacted; however, as is evident in the example of Figure 3.4, showing a shorter time period, the temperature during this time was at or very near the boiling point of the fuel and was consistent throughout the duration of the burn.

Initial experiments conducted using the grid thermocouple rake shown in Figure 3.2b facilitated measurement of the temperature distribution through the depth of the fuel as well as through the fuel radially from the center of the fire to near the edge of the pan. In these experiments the infrared camera was also used to thermally profile the walls of the test pan. From these experiments, the thermocouple measurements indicated that there was a net heat loss from the fuel to the pan walls, that decreased with distance below the fuel surface. This effect is captured in the contour plot of the temperature distribution

along a radial slice through the heavy gas oil during a surface fire, as shown in Figure 4.10a for a time of 20 min after ignition – well into the steady burning period. This figure shows a layer of heated fuel near the surface, and a layer of cold fuel below, with the fuel near the pan walls and bottom cooler than that in the center. From this data, it is of interest to note the relative direction and mechanisms of heat transfer around the walls of the pan. Figure 4.10b shows the difference in temperature between the fluid temperature measured nearest the wall via the thermocouple rake from Figure 4.10a, and the wall temperature measured via the infrared images of the pan wall at the same time. Since the initial fuel temperature was 30 °C and the ambient air was approximately 10 °C during this experiment, there was convective cooling of the pan walls to the surroundings. This can also be seen in the contour plot where the temperature is colder around the pan walls and pan bottom. It can also be seen that there was a net heat transfer from the pan walls into the fuel only very near the fuel surface, in the region where the flame was attached to the pan walls, which caused intensified localized heating of the wall. At increased depth into the fuel, the temperature differential between the pan walls and fuel became negative. This indicates, then, that there is some heat transfer from the flame to the fuel at a distance near the flame attachment, while the bulk fuel experiences a net heat loss to the pan walls, which is cooled by the surroundings.

The observation that there is a net heat transfer into the fluid near the fuel surface and net heat transfer out of the fuel to pan walls towards the bottom of the pan is in accordance with experimental measurements reported by Nakakuki [18] and Alireza et al. [140], as well as in analytical models by Alnasser [85]. This also supports the hypothesis proposed by Hall [58] that the formation of heated layers in the liquid fuel of pool fires is not based on preferential heating of the pan walls. Thus, even though the calibration of the infrared camera may have introduced some error into the temperatures measured along the pan wall, the general trend seen in these experiments matches the expected trend and measured temperatures are accurate enough to conclude that heat transfer into the fluid from the pan walls does not occur past a small distance from the surface in these experiments. Based on this observation, it was deemed that further radial temperature measurements were unnecessary, and only the linear rake was used in subsequent experiments to allow for more resolution of thermal profiles into the fuel depth along the pool centerline.

With this introduction, the following sections describe other overall aspects of the burning behaviour of heavy gas oil, as measured in the described experiments. As the heavy gas oil fires exhibited a number of interrelated phenomenon, the results are presented in terms of the observed behaviour during each of the three characteristic burning periods of the fire. This section also makes frequent reference to the results described in Section 4.1 through Section 4.4; additional information and detail can be found in those sections.

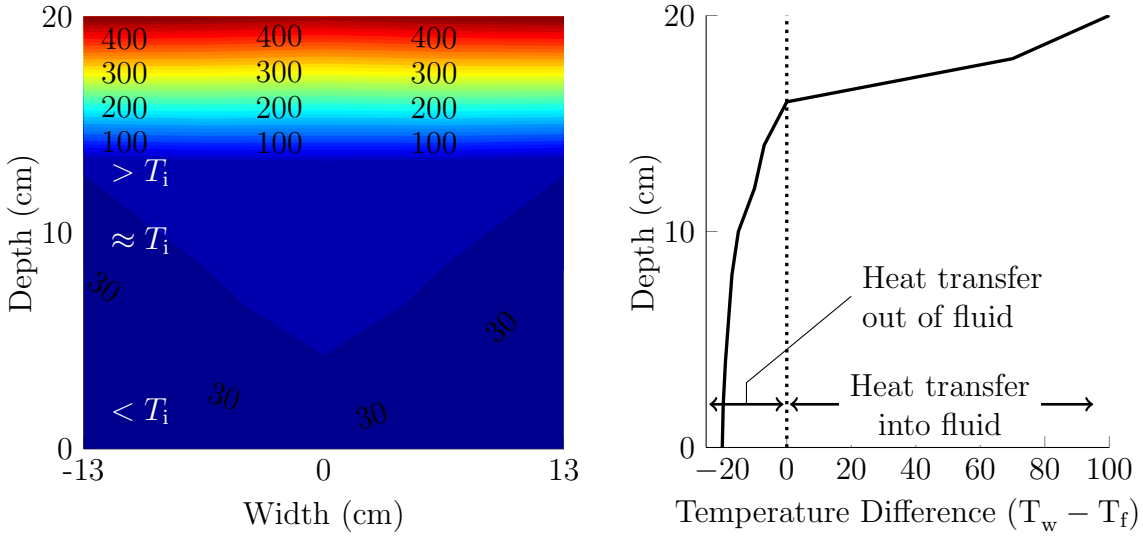

(a) Contour plot.

(b) Temperature difference.

Figure 4.10: Contour plot of fuel temperatures through cross section of oil as measured by grid thermocouple rake shown in Figure 3.2b (a); and difference between pan wall temepratures measured by infrared camera and temperature measured by thermocouples closest to wall location (b).

4.5.1 Burning Periods

A number of experiments were conducted to quantify the overall stages of burning observed in the untreated heavy gas oil fires. Since the heat release rate can be directly derived from the fuel regression or mass loss rates, and the regression rate was recorded for each experiment, the measured values of the fuel regression rate are used as a basis for discussion of the fire behaviour during the different burning periods. Figure 4.11 shows the instantaneous recordings of sample mass in a 0.6 m diameter heavy gas oil fire experiment superimposed with the calculated mass loss rate data throughout the experiment. While the calculated average decrease in mass is relatively linear through a large portion of the fire, there is significant noise in the instantaneously calculated values of mass loss rate. It is hypothesized that this is due to the measurable impact of the ambient wind on the mass measurements. As a result, the mass loss rate data has been smoothed with a thirteen-point smoothing algorithm to reduce the noise and better demonstrate general trends in the values. The 0.6 m diameter test shown in Figure 4.11 was the longest duration experiment conducted

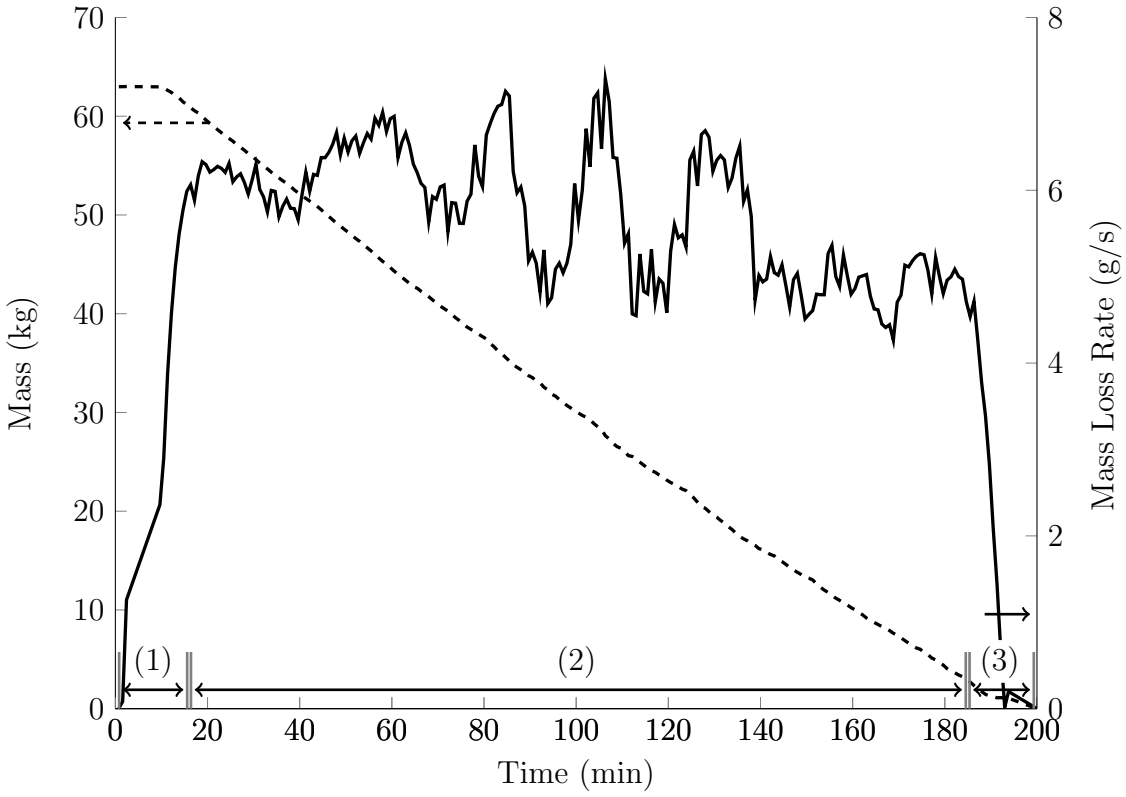

Figure 4.11: Fuel mass history as recorded during 0.6 m diameter heavy gas oil pool fire, experiment labelled with the distinct burning periods.

on the heavy gas oil, and will therefore be used throughout this section for demonstration purposes.

Examination of Figure 4.11 shows that the free burning behaviour of the heavy gas oil exhibits three distinct burning phases: period (1) which ran from ignition to steady burning and is characterized by an increased mass loss rate, period (2) which was a long period of relatively steady burning lasting from 18 to 185 minutes into the test and period (3), a decay period characterized by a rapid decrease in mass burning rate as the fuel burned out. More information on the general burning characteristics for each of these periods are presented with comparison to relevant literature and theory in Sections 4.5.2 through 4.5.4 for steady burning of heavy gas oil pool fires, in which there was no water sublayer and no attempt to suppress the fire. Unique characteristics were observed for fires in which there was a water sublayer beneath the fuel, as well as in the event of suppression of the

fire, so discussion of these phenomena are excluded from the sections on general burning behaviour here and are instead discussed in detail in Section 4.4 and Section 4.8.

4.5.2 Ignition and Flame Spread

In each experiment, the fire was ignited using a propane fuelled torch. Since ignition was localized to the point of application of the torch, the initial burning period, period 1 in Figure 4.11, was characterized by radial flame spread from the point of ignition across the surface of the fuel. One main feature of this period that was visually observed, but was not captured in either the mass or thermocouple measurements, was the violent fuel ejections of fuel that took place during this flame propagation, and for approximately 5 to 10 minutes after full flame cover was established. Again, this was caused by the water emulsification and is discussed in Section 4.6.

Ignition was accomplished using a small propane torch when possible; otherwise, a propane fuelled, high intensity 'tiger torch' was applied. Kerosene was easily ignited at pool diameters of 0.1 to 0.3 m using the small propane torch. The heavy gas oil, on the other hand, was ignited in the 0.1 m diameter pan using the small propane torch; however, for pan diameters of 0.19 m and larger, the tiger torch was required. This is counter to the experimental results of Murad [43], who found that the effects of diameter on the energy requirements of the ignition source became negligible past pool diameters of 5 cm. It is likely that the small torch may have produced sufficient flammable vapours from the heavy gas oil to form a small localized flame, but that there was insufficient burning area established around that flame to produce the heat feedback needed to propagate the flame across the fuel surface. This would explain the necessity for the use of a stronger ignition source to establish the fire, and may indicate that the ignition energy requirement is both a function of fuel flashpoint and pan diameter.

Once a sufficiently energetic flame kernel was formed near the fuel surface to initiate ignition, the flame began to propagate across the surface of the fuel. Predicting the behaviour of a fire in this period of initial growth is of interest in many applications since it can be used to estimate incident radiant flux to, and time to failure of, components near the fire, as well as time available for suppression. To aid in predicting the growth of fires, a classic model of early fire heat release rate growth with time has been proposed as a time-squared fit as shown in equation 4.1 [141].

$$Q = \alpha \left(t - t_o\right)^2 \tag{4.1}$$

In this equation, α is a growth coefficient representing laboratory measurements of the rate of fire growth for various classes of materials, and $t - t_o$ is the time elapsed from ignition. In the case of open hydrocarbon pool fires, the growth is generally classified as either 'fast' with a growth coefficient of $\alpha = 0.0469$ kW/s^2, or as 'ultra-fast', with a growth coefficient of $\alpha = 0.1876$ kW/s^2 [21].

Alternatively, the rate of fire growth can be estimated using measured values of the flame spread rate across the fuel surface (Section 4.3) and the heat release of the fire (Section 4.2). It was found from the video recordings of the fire growth, coupled with measurements of the fire heat release rate during the growth period, that the heat release rate increased with increased relative area of fuel burning. Thus, as would be expected, the heat release rate increased with time during the initial fire spread period while the flame front spread from the localized ignition point. A second model was therefore established to assess the increase in the fire heat release rate from ignition to steady state, based on the measurements of flame spread rate and the expected heat release rate. The growth in fire area can be related to the following equation,

$$A(t) = c\pi \left(u_s t\right)^2 \tag{4.2}$$

where u_s is the flame spread rate measured in the flame spread tray, and c is a coefficient representing the location of ignition. In the case of corner ignition – used in this study, the flame propagates radially at a 90° angle, therefore c is equal to one quarter of a full circle, or 1/4. Finally, the heat release rate was found to be well defined by equation 2.5.b, as discussed in Section 4.2, for steady state burning of pool fires with a defined area of A. The growth of heat release rate, was therefore found to be well modelled by the time dependent rate of flaming area increase, as shown in equation 4.3.

$$HRR = \chi \dot{m}''_\infty \Delta H_C \left[c\pi \left(u_s t\right)^2\right] \left(1 - e^{-k\beta \frac{2}{\sqrt{\pi}} \sqrt{c u_s t}}\right) \tag{4.3}$$

In order to test these theories for predicting the early fire growth of the present heavy gas oil fires, Figure 4.12 shows plots of equation 4.3, as well as the standard growth curve in equation 4.1. These models are compared with the growth in heat release rate measured during a 1.12 m diameter heavy gas oil pool fire during the early growth period, as measured using the furniture calorimeter detailed in Section 3.3

From Figure 4.12, it can be seen that the measured fire growth rate varies close to quadratically with time, indicating that the classic time squared heat release rate growth curve well represents the growth of the fire. The growth rate of the fire, as determined

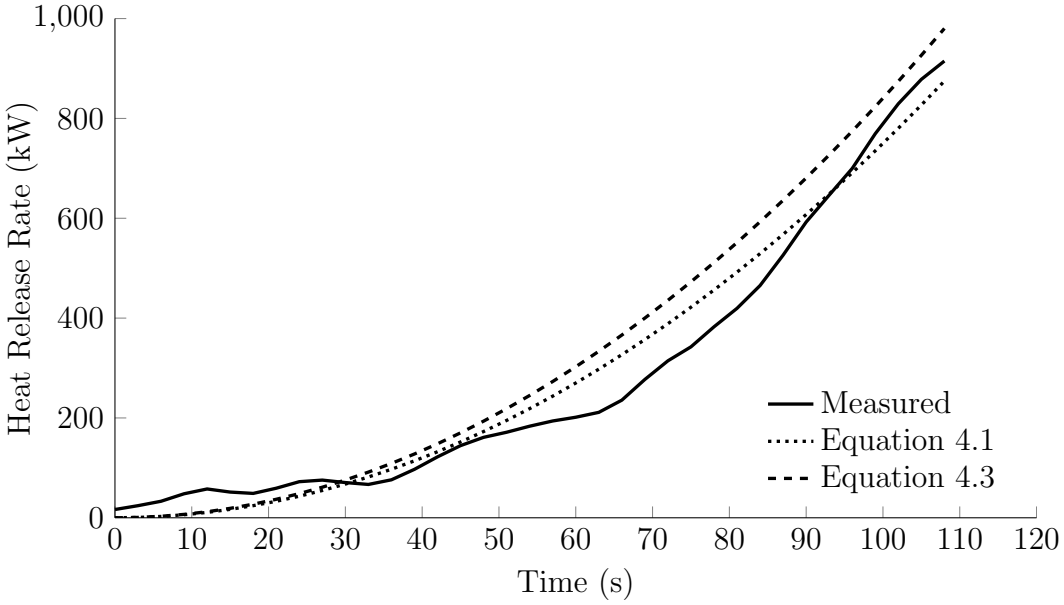

Figure 4.12: Comparison of measured heavy gas oil fire growth during flame spread period and prediction methods using equation 4.1 with $\alpha = 0.075$ kW/s^2, and using equation 4.3.

by adjusting the value of α in equation 4.1, is well represented by a growth coefficient of $\alpha = 0.075$ kW/s^2 and therefore is slightly higher than fast but less than ultra-fast, as might be expected for a heavy hydrocarbon pool fire. Kerosene, by comparison, is much more volatile and therefore has a far greater rate of flame spread and fire growth. The fire growth rate of kerosene in the 1.12 m pan experiment was found to be well represented by equation 4.1 as well, with a growth coefficient of $\alpha = 0.511$ kW/s^2, much greater than the constant assigned to an ultra-fast fire under the classic definition of initial fire growth.

The fire growth rate predicted using equation 4.3 is also effective at estimating the growth of heat release rate with time for the heavy gas oil fires; however, in general it was found to slightly over-predict the heat release rate relative to the measured values – as evident for the 1.12 m diameter fire shown in Figure 4.12. This is likely due to the fact that the time dependent growth of the fire in the empirical relation is accounted for through an estimate of the growth in area of the fire with time, assuming that the value $\chi \dot{m}''_\infty \Delta H_C$ remains constant. Since the measured values of effective heat of combustion for the present fires are based on values taken only during the steady burning period of the fire – when the temperature profile into the fuel depth is well defined - they will tend to be higher than the actual values of heat release that would be characteristic of the fire during

the time while the temperature distribution into the fuel depth is still forming, such as during flame spread and very early fire growth.

Once the flame had spread across the entire fuel surface, a period of fuel pre-heat began, where the fuel under the surface was heated from radiation feedback from the flame. Figure 4.13 shows the temperature distribution into the bulk fuel at various times, plotted against the distance below the fuel surface, as measured by the thermocouple rake (as shown in Figure 4.9). These are plotted for the time period starting at the point of full flame cover, and ending when the period of steady burning begins.

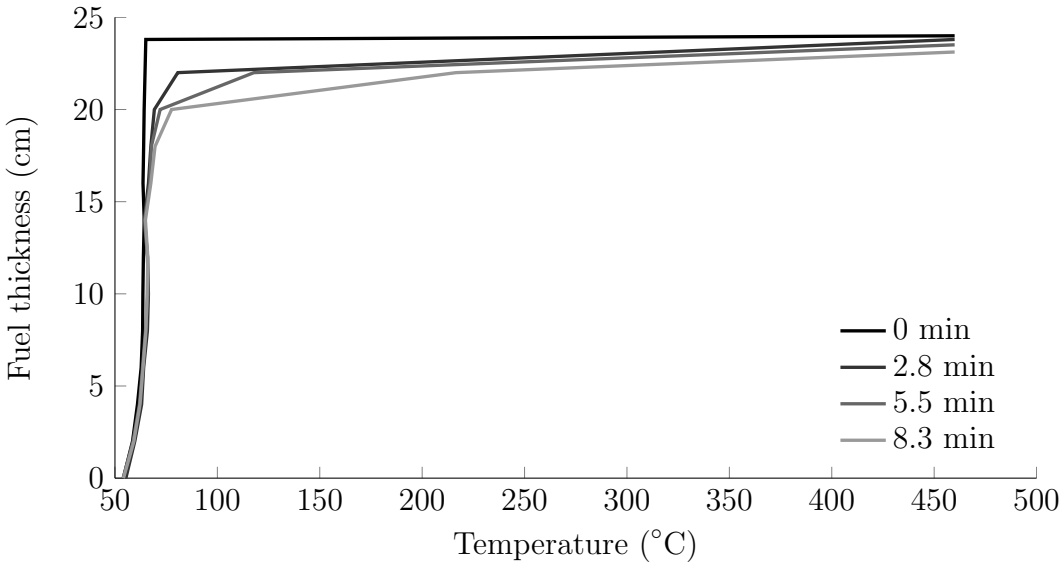

Figure 4.13: Temperature distribution into bulk fuel at various times during the initial burning period following full flame cover.

The temperature profile at the time of full flame cover, shown as 0 minutes, showed a sharp gradient of temperature from ambient into the fuel, since the surface of the fuel had reached the boiling temperature of the fuel, but no heat had been transferred into the fuel below the surface. Over time, the temperature distribution evolved such that there was a high temperature at the surface of the fuel with an exponential temperature decay into the bulk fuel. This occurs as radiated energy from the flame is conducted, over time, into the oil. A constant, well-defined temperature profile into the oil had formed by approximately 8 minutes into the burn, and remained constant throughout the rest of the burning period. This constant temperature profile is discussed further in Section 4.5.3.

It was shown in Section 4.1 that the initial fuel temperature had an effect on the fuel consumption rate; however, it was also found that heat transfer into the oil depth caused an increase in the mass loss rate. The preheating of the fuel during the initial burning phase consumed some of the energy from the flame, thus lowering the energy available for vaporisation of the fuel. This resulted in a decrease in the measured mass loss rate and heat release rate. Figure 4.14 shows the effect of the fuel temperature profile measured in a heavy gas oil fire during the initial burning period, on the various measured parameters. In this plot, the development of the steady-state temperature profile – shown in Figure 4.15 and represented by equation 4.5 – is shown as the development, over time, of the coefficient of determination between the measured temperature profile and equation 4.5. Therefore, in Figure 4.14, while the thermal gradient sharply decreases from the surface following full flame cover and during the early stages of burning, the coefficient of determination is low. However, as the well-defined thermal profile is formed, the coefficient of determination increases, and approaches unity during the steady burning period. Also shown on this plot, for comparison, are measured values of heat release rate and of mass loss rate during the early burning period, while the thermal profile is forming. Each of these values are normalized using the following equation to show a comparison of the values over time, from 0 to 1.

$$x = \frac{x_{\mathrm{i}} - x_{\min}}{x_{\max} - x_{\min}} \tag{4.4}$$

In this equation, x is the value plotted and $x_{\min}$ and $x_{\max}$ are the minimum and maximum values within the plotted time range. This method of normalizing the data shows the trend of each parameter, while removing the differences in magnitude between the different measurements.

It is clear from Figure 4.14 that the mass loss rate and heat release rate increased with time, as the temperature profile into the fuel depth developed. As can be seen in this plot, the timing of the the steady state fuel regression rate coincided with the establishment of the constant temperature distribution into the oil depth, at approximately 160 seconds. This indicates, as expected, that the mass loss rate is directly related to the difference between the energy directed from the fire plume to the fuel surface and the energy transferred into the depth of the fuel. It can be said then, that the steady burning period began when a steady state temperature profile into the fuel depth formed.

Interestingly, it can also be seen in this plot that the mass loss rate and the heat release rate do not approach their steady state values at the same rate. Instead, the mass loss rate reaches a steady state value sooner than the heat release rate. As the heat of combustion is a

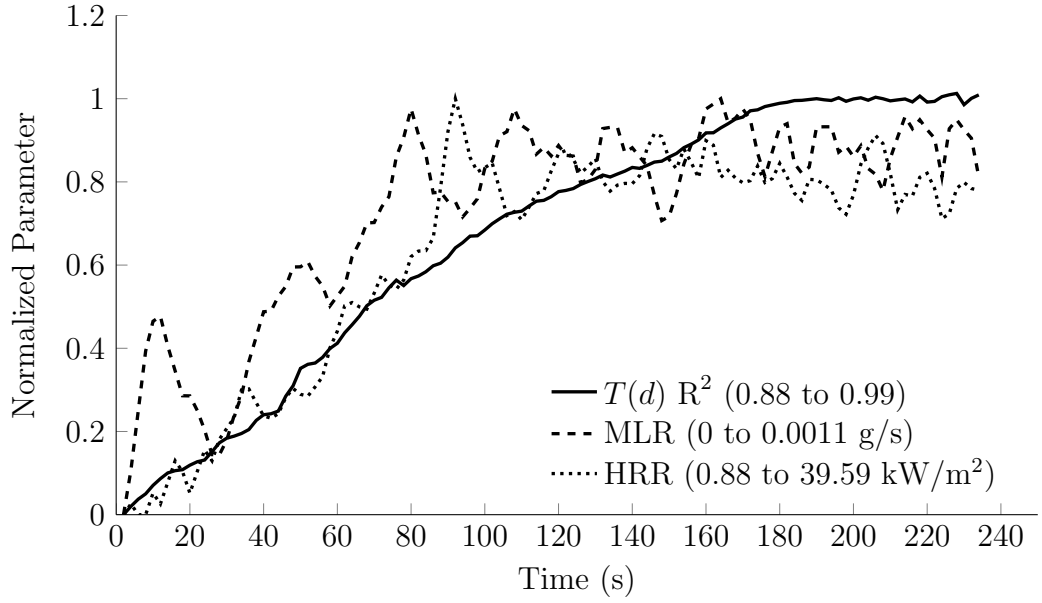

Figure 4.14: Effect of the temperature profile into fuel depth on the measured heat release rate and fuel regression rate. Normalized parameters are plotted using equation 4.4, and the minimum and maximum values used are shown in parenthesis.

defined material property, and there was full flame cover over this period of the experiment, this could indicate that the combustion efficiency is dependent on the temperature of the fuel, with more complete combustion at elevated temperatures. This would make sense, as there is more energy available to vapourise the fuel at higher fuel temperatures, and less of the energy from the flame column is required to heat the fuel. This finding also suggests that a greater combustion efficiency could be measured throughout the burning period for fuels maintained at a higher bulk fuel temperature, thereby possibly resulting in a higher overall heat release rate.

4.5.3 Steady Burning

A period of steady burning commenced once the flame had spread across the full fuel surface, as shown in period 2 of Figure 4.11. During this period, the fuel ejection phase described previously ceased, and the fire burned as a traditional pool fire. This section details the burning behaviour of the fire and temperature distributions in the fuel for a

heavy gas oil pool fire during the steady burning period. Where possible, experimental data are compared to theoretical and empirical models for fire behaviour.

One key characteristic of the steady burning period of the present heavy oil fires that is visible in the characteristic temperature history plot, Figure 4.9, is the vaporization temperature of the fuel of approximately 460 °C. This characteristic temperature is demarcated by the short period of uniform temperature immediately before the steep increase in temperature, that is measured as the thermocouple entered the flame zone. This vaporization temperature of the heavy gas oil does not appear to have changed over the course of the three hour burning period of the experiment. In the case of the kerosene fires, the fuel surface temperature was found to be much lower than that of heavy gas oil, at 240 °C, but still remained constant throughout the duration of the steady burning period. This value of temperature was well matched to the quoted boiling temperature for kerosene of 240 °C [128], and consistent with the different physical properties of the two fuels. In each case, the constant surface temperature of the fuel during the steady burning period is also supported by the relatively constant measurements of measured heat release rate (Section 4.2), as well as consistency in measured values of fuel regression rate (Section 4.3) throughout the duration of the present experiments.

In contrast to the results seen for the present fires, preferential burning of lighter fuel fractions has been reported during steady burning of fires in other fuels, particularly crude oils. This has generally been characterized by a gradual decrease in fuel regression rate and heat release rate, as well as a progressive increase in the vaporisation temperature [29,65] as the fire continued to burn. In this case, the lighter fractions are more volatile, with higher heat release rate, mass burning rate, and are consumed initially. No evidence of these effects were seen in any of the present experiments indicating that both the kerosene and heavy gas oil tested here burned more as pure hydrocarbons, or at least as homogeneous mixtures of their various components. This observation indicates that a hot-zone is not expected to form, and is the basis for the discussion on boilover presented in Section 4.8.

Another key characteristic of the steady burning of both heavy gas oil and kerosene pool fires was the formation of a steady, exponential temperature distribution into the depth of the oil. As can be seen in the time-temperature plot in Figure 4.9, the temperature measured by each thermocouple gradually increased as the fuel surface approached the thermocouple bead, then increased quickly as the bead entered the flame zone. It be seen from this figure that the temperature profile into the depth of the oil remained constant throughout the burning period, and that there was no evidence of the formation of a hot-zone, which would have been characterized by multiple thermocouples measuring a similar temperature at a given time. A clearer representation of the measured temperatures is shown in Figure 4.15, which shows the same temperatures as shown in Figure 4.9, but

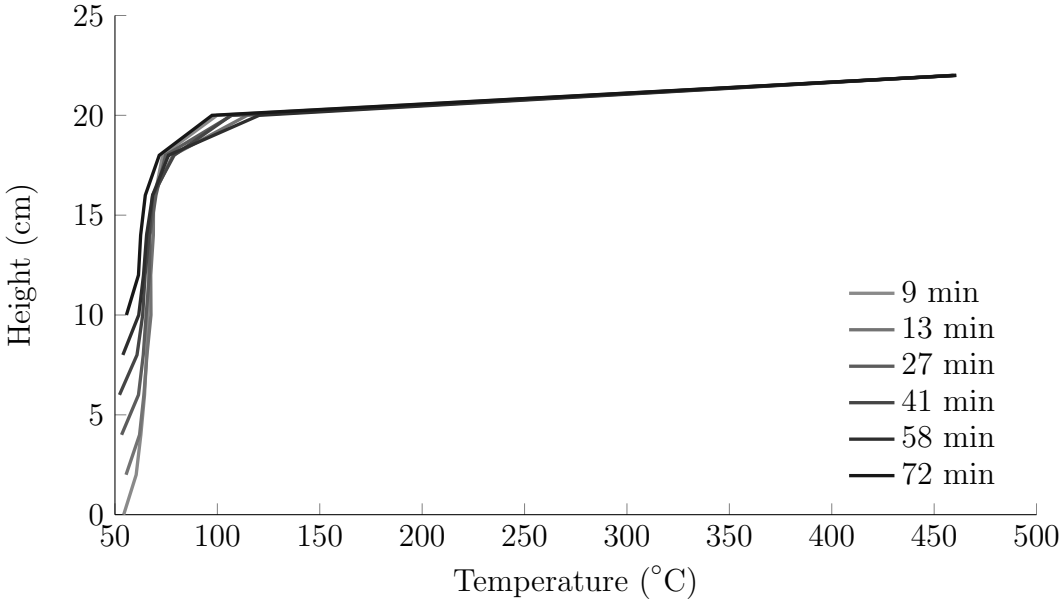

Figure 4.15: Temperature profile through heavy gas oil fuel depth at various times throughout steady burning period in a 0.6 m diameter pool fire.

plotted as a function of depth into the fuel at discrete times throughout the burning period. In this plot, the location of the fuel surface – denoted by a measured temperature of 460 °C, or the fuel boiling temperature – is maintained at a height of 22 cm in order to compare the shape of the temperature profile at each time.

It is clear from this figure that the temperature profile into the depth of the heavy gas oil pool fires assumed a constant shape. This constant temperature profile had formed by the beginning of the steady burning phase, and stayed the same for the duration of the steady burning period. This result is contrary to the expectation that a hot-zone would most likely form during a long burning fire in a fuel comprised of the complex mixture of hydrocarbons such as the heavy gas oil. It is clear that the temperature profile during the steady burning period was characterized by an exponential decay in temperature from the surface into the bulk liquid fuel, with a profile that remained constant throughout the burning period. Further examination of temperature traces in both Figure 4.9 and Figure 4.15 revealed that this exponential temperature distribution progressed downward at a rate approximately equal to the regression rate of the fuel surface. Finally, as can be seen from the overlap in the individual traces in Figure 4.15, the shape and depth of the decay remained constant over the entire burning period. Such a constant temperature profile into the depth of the

fuel is again not unique to the present fuel, but rather has also been observed during fires in single component fuels documented in previous studies [62, 125, 142].

The temperature profile into fuel that is shown in Figure 4.15 was consistently measured for all of the heavy gas oil and kerosene experiments in the present study. For the heavy gas oil fires, it was found to be largely independent of initial fuel depth greater than 4 cm, pan diameter between 0.19 to 0.6 m, and initial fuel temperatures between 20 and 95 °C. Furthermore, while the parameters of the curves differed slightly, the measured temperature distributions with fuel depth for kerosene and heavy gas oil fires exhibited the same distinctive exponential decay from the surface. For both fuels, the temperature profile from the surface into the depth of the fuel was found to be well represented by the equation

$$\frac{T(y) - T_\infty}{T_\mathrm{s} - T_\infty} = \exp\left(-\beta(y_\mathrm{max} - y)\right) \tag{4.5}$$

where $T(y)$ is the temperature at depth y from the surface at y_max, and β is a coefficient of best fit. As discussed in Section 2, this is the same temperature distribution that has previously been observed through the depth of non-hot-zone forming fuels, where the present coefficient was represented by $\beta = \frac{R}{\alpha}$ in equation 2.8, as discussed in Section 2.1. Table 4.9 shows the best fit coefficients determined from the experimental data obtained in each of the test pan diameters for both heavy gas oil and kerosene fires. The column entitled 'measured' is the value of β determined from the present experimental data using the least squares method, while values in the column entitled 'calculated' are the theoretical fit coefficient as proposed by Torero [84], based on the measured fuel regression rate and an estimate of the fuel thermal diffusivity of $\alpha = 9.32(10^{-8})$ m^2/s for heavy gas oil and $\alpha = 9.10(10^{-8})$ m^2/s for kerosene; based on the thermophysical properties of engine oil and kerosene, respectively [143, 144].

The calculated fit parameters were found to be remarkably accurate at predicting the shape of the temperature profile, for both the heavy gas oil and kerosene pool fires. It was seen that the fit coefficients calculated from the measured regression rate were very close to the measured values, except in the case of heavy gas oil fires of 0.6 m diameter. This latter discrepancy is possibly due to the assumed versus the actual value of the thermal diffusivity, which causes a proportional error in the calculation, therefore increasing as the fire diameter increases. As well, the two experiments on smaller diameter fires were conducted inside the wind-controlled facility where the ambient conditions were relatively quiescent. The 0.6 m experiment, on the other hand, was conducted outside which could have caused a difference in the convection cooling of the pan walls, as well as leading to an enhanced burning rate of the fuel due to the effect of wind.

Table 4.9: Fit coefficients to equation 4.5 for temperature profile into fuel depth.

Fuel	d	T_∞	R	β (1/mm)	
	(m)	(°C)	(mm/min)	*Measured*	*Calculated*
Heavy Gas Oil	0.19	65	0.55	1.086	0.98
	0.26	60	0.87	1.389	1.56
	0.60	60	1.34	1.440	2.40
Kerosene	0.19	20	1.10	0.85	0.88
	0.26	20	1.45	0.65	1.16

The ability to model the temperature profile into the depth of the fuel provides a method by which to predict the depth at which the temperature of the fuel exceeds 100 °C. This depth corresponds to that zone in which water emulsified into the fuel might begin to evaporate and form steam, or alternately the fuel layer thickness at which thin-layer boilover might be expected to take place. This can be clearly identified experimentally at approximately 0.02 m beneath the fuel surface in the experiments presented here, as can be seen in Figure 4.15. It can also be determined arithmetically for any tank configuration using equation 4.5, isolated for the 'depth' term, and using a temperature of interest of 100 °C. This is shown in equation 4.6,

$$y_{(T=100\ ^\circ\mathrm{C})} = y_{\max} - \frac{\alpha}{R} \ln\left(\frac{100\ ^\circ\mathrm{C} - T_\infty}{T_\mathrm{s} - T_\infty}\right) \tag{4.6}$$

where $y_{(T=100\ ^\circ\mathrm{C})}$ is the distance from the fuel surface to the 100 °C isotherm; or the minimum fuel layer thickness for boilover to occur. It should be noted, however, that this result is only applicable to the small-scale experiments reported in the current work and should not be extrapolated to the much larger diameters characteristic of fuel storage tanks.

Finally, from the temperature profile through the depth of the fuel, it is clear that a hot-zone does not form in either of the fuels tested here. The shape of the temperature profiles into the depth of the oil remains exponential throughout the steady burning period in the current experiments, and there is no evidence of any band of constant temperature fuel growing into the oil depth. For this reason, the present observations suggest that there is little likelihood of preferential formation and burning of lighter and heavier fractions,

during a heavy gas oil or a kerosene pool fire, at least for the small scale fires investigated here.

The establishment of a hot-zone during pool burning of liquids has been measured through various means, and distillation of the fuel is one key factor thought to indicate a propensity for boilover. This distillation process is typically characterized by fuel volatility that decreases over the course of the burning period, resulting in mass burning rate that decreases throughout the burning period. The linear mass versus time curve measured during long duration burning of the present heavy gas oil indicates that the mass loss rate remained approximately constant for the duration of the fire, rather than decreasing with time as would be expected if lighter ends burned off first. The experimental observations as noted suggest that the heavy gas oil studied here has a much lower propensity for boilover than crude oil or other multi-component petroleum products. Based on the observed behaviour, it is postulated that long duration burning of heavy gas oil pool fires will not result in the development, growth and propagation of a hot-zone, such as those that has been seen in boilover experiments with crude oil. The propensity for boilover of heavy gas oil in pools with a water sublayer and a further analysis of the temperature profiles is presented in Section 4.8. This section also investigates the burning characteristics of heavy gas oil in reservoirs in which there is a water sublayer and a discussion of boilover mechanisms.

A final characteristic of the heavy gas oil and kerosene fires under study here was the dependence of the flame height on pan diameter. A method of presenting the flame height as a function of pan diameter for the present experiments is shown in Figure 4.16 for the heavy gas oil experiments. For each image in this figure, a recording of the fire of a given diameter was separated into individual frames, and then one frame per second was extracted from the video for one minute of steady burning (for a total of 60 frames per pan diameter). These frames were blended into a single image by averaging the intensity of every pixel in each image. A clear flame shape is visible for the 0.19 and 0.26 m diameter pans since those experiments were conducted inside the burn structure under quiescent ambient conditions. Less well defined flame shapes are seen for the two larger pan sizes because these experiments were conducted outside and therefore the flame column was significantly impacted by the ambient winds; consequently the flame shape is smeared over a larger area and appears less intense. In the case of the 2.0 m diameter fire, the plume is clearly tilted sideways by the wind as well. Nonetheless, the figures are effective at showing the general shape and height of the flames for each fire diameter, and is effectual to compare the flame heights across different pan diameters.

From similar figures, the flame height for kerosene and heavy gas oil was estimated as the length of the high intensity flame area on the image, multiplied by a calibration

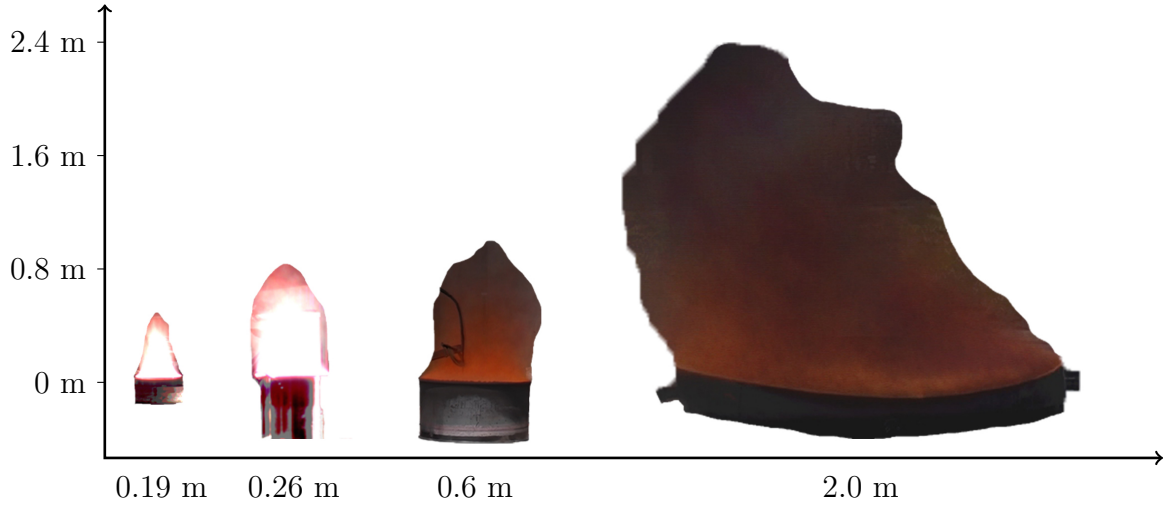

Figure 4.16: Time-averaged flame shape as a function of pan diameter for heavy gas oil.

constant to translate the measured length on each image to the actual length of the flame. While this method is less accurate for the larger fires due to ambient wind effects, it was found to be consistently more accurate than determining the flame height by measuring the flame length from arbitrary individual images from the video footage of the fire. The flame heights discussed in the following are therefore derived using the image averaging technique.

The height of the blurred region in each of the averaged flame position images was assumed to be the 50% intermittence flame height. This was verified by comparison to individual images of the flame to ensure that the flame was within the boundaries of the averaged flame region approximately 50% of the time. The measured values of the 50% flame height for each pan diameter are shown in Figure 4.17 for heavy gas oil and are plotted against data on the flame heights measured in solar oil pool fires as presented by Blinov and Khudyakov [38].

Values of flame height were also estimated using the flame height correlation by Heskestad [78] and shown in equation 2.7 as described in Section 2.1. This correlation was applied using both calculated and measured heat release rate data, shown plotted in Figure 4.17. The discrete points labelled 'eqn 1.7b (Measured HRR)' show the flame height calculated using the values of heat release rate measured during the heat release rate experiments (Section 4.2) at each of the experimental diameters. The same correlation, derived from the theoretical pool fire heat release rate model as equation 2.7, was used with values

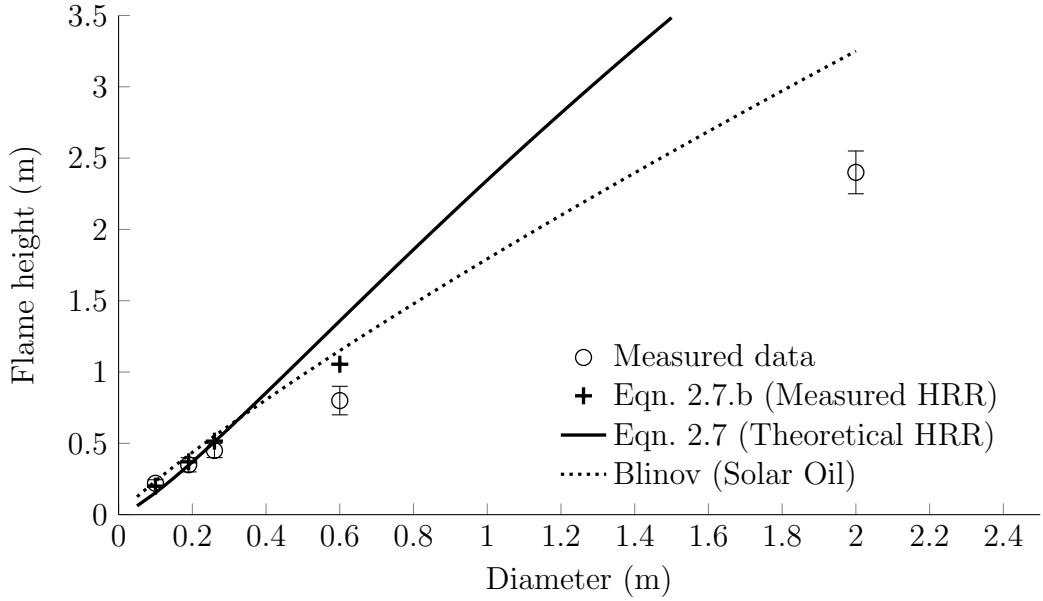

Figure 4.17: Measured flame height as a function of pan diameter for heavy gas oil compared with results from Blinov for solar oil [38], and using measured (equation 2.7) and theoretical (equation 2.7.b) values of heat release rate.

of $k\beta$ and $\dot{m}_\infty$ for heavy fuel oil taken from literature, and is shown as the curve labelled 'eqn 1.7b (Theoretical HRR)'.

It can be seen that the flame height correlation based on measured values of fire heat release rate produced a reasonably accurate estimate of the measured flame heights for each experimental fire diameter. Similarly, the flame heights reported by Blinov and Khudyakov [38] for solar oil fires are reasonably close to the present values given that solar oil is lighter than the present heavy gas oil. The fuel regression rate of this solar oil was greater than that of the heavy gas oil, therefore the heat release rate would be expected to be higher and consequently the flame heights longer than those measured here.

There is a large difference between the experimentally measured flame heights and those predicted for the 0.6 m diameter fire, with predicted value being considerably higher than the measurements. This difference can be partially explained by the clear flame tilt seen in Figure 4.16, as well as the other errors in measured flame height that would be caused by the effects of wind on flame structure. Heskestead's equation [78] with the heat release rate curve estimating using the parameters for heavy fuel oil predicts flame heights that are significantly larger than the experimental results. This is consistent with, and could

be a direct result of, the higher heat release rates seen in Figure 4.4 for heavy fuel oil, as again, the higher heat release rate causes a larger flame length.

The pool fire behaviour of the heavy gas oil was found to be consistent with the correlations and experimental observations presented for other heavy hydrocarbon fuels. The fuel regression rate was found to follow the behaviour as first documented by Blinov and Khudyakov [38], as well as the empirical calculation methods proposed by Burgess [59]. All of the experimental measurements derived from the fuel regression rate, namely the heat release rate, and flame height follow the expected trends as well. Finally, the heavy gas oil was found to not form a hot-zone, and the temperature profile into the depth of the fuel was found to be well represented by correlations for conduction dominated heat transfer into single component – or homogeneous – fuels.

4.5.4 Fire Decay and Extinction

The burning of the heavy gas oil showed three distinct burning phases, including the initial flame spread and steady burning periods discussed above. The final burning phase was characterized by a decay in fire intensity and the eventual extinction of the fire as the fuel was consumed. The processes driving these phenomena are discussed in this section.

Through the steady burning period of the fire, the fuel layer gradually decreased in depth, until the fuel layer became thin enough that heat transfer through the pan bottom began to play a role in the behaviour of the fire. At the same time, the freeboard height in the pan increased, thus increasing the area of pan walls exposed to the flames from the fire. At this time, the pan acted as a significant heat sink, reducing the energy from the flame that was available to vaporize the fuel. This was marked by a decrease in both the mass loss rate and the heat release rate of the fire, thereby further decreasing the energy available to form fuel vapour at the surface. It can be seen from Figure 4.15 described previously that the layer of oil beneath the fuel surface at a temperature above the initial fuel temperature was approximately 4 cm thick. The time at which the measured fuel regression rate began to significantly decrease corresponded well to the time at which the fuel layer decreased to less than 4 cm in depth, thus supporting the notion that the onset of fire decay relates to a combination of the effects of freeboard height and the increased heat loss through the bottom of the pan.

4.6 Effects of Emulsification of Water in the Fuel

A significant characteristic of the burning behaviour of, and a source of potential error in the data from, the heavy gas oil fires was driven by the effects of water emulsification in the fuel. Water is introduced into the heavy gas oil during the extraction and upgrading process. While much of this water is separated from the oil due to the difference in densities between the oil and water, a volume does remain emulsified within the oil. This fraction cannot be easily separated from the oil, and therefore remains well distributed and suspended in small pockets throughout the oil. As the fire was established over the surface of the fuel, then, the water in these suspended pockets became superheated, and quickly vapourised, forming pockets of steam. Due to the rapid expansion from water to steam, the vapourisation process manifested as a series of micro-explosions in the early stages of fire development (as noted in Section 4.5.2). This phenomenon is not unique to heavy gas oil, and has been noted for other heavy fuels and water-in-oil emulsifications [27]. The fuel ejections that occurred during fires established on undried heavy gas oil had a significant effect on many of the measured parameters; therefore, the key characteristics of this burning behaviour and its effect on other important fire parameters are discussed in more detail in this section.

Figure 4.18a shows an image of the overall fire behaviour, including oil ejections out of the test pan, during the initial burning period of a 0.3 m diameter heavy gas oil pool fire, where smoke trails and burning oil can be seen exiting the pan. The 'micro-explosions' shown in the Figure were characterized by an audible crackling noise, along with the expulsion of still-burning volumes of oil from the pool. As the vapourisation of water pockets occurred beneath the surface of the oil, the expansion of the steam imparted an upward momentum that projected the oil into the air, with consequent expulsion of oil from the pan. Figure 4.18b shows an image of the area covered by oil that was ejected from the pan during a brief 5 minute trial experiment conducted in a 0.06 m diameter pan. In this case, the maximum distance travelled by a pocket of ejected oil was 1.1 m, and over 1/3 of the fuel layer was ejected from the test pan.

With the undried oil, two distinct burning periods were observed. First there was a period of crackling and violent fuel ejections, lasting for 5 to 10 minutes after ignition of the fuel. During this period, the ejections progressively died down and the fire underwent a transition to a period of steady burning with infrequent crackling and fuel ejections. As the micro-explosions only occurred during the initial burning period, and gradually ceased as the fuel progressively heated, a likely explanation for the process is discussed below.

After ignition and during the time period over which the fuel ejections occurred, the recorded temperatures through the depth of the fuel were characterized by a sharp thermal

(a) Ejections during fire.

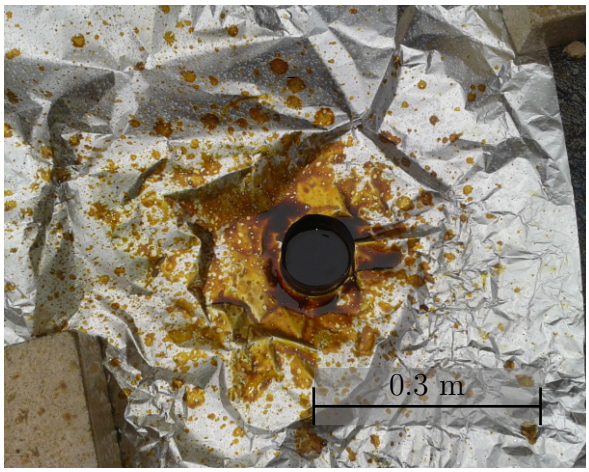

(b) Area covered by ejected fuel

Figure 4.18: Fuel ejections caused by emulsified water in heavy gas oil

gradient between the fuel surface and the bulk oil. This gradient began as a step change in temperature at the surface (0 min on Figure 4.13) and gradually progressed over time to a distribution with temperatures of 460 °C at the fuel surface to 40 °C at the first thermocouple, 2 cm below the surface (8.3 min on Figure 4.13)). The period of fuel ejection persisted for the duration of time taken for the typical exponential temperature decay (for example, the constant profile shown in Figure 4.15) to develop beneath the surface of the fuel.

From the measured temperatures during the present experiments, it was determined that the micro-explosions and fuel ejections occur only when there is a large temperature difference between the fuel surrounding the emulsified water pockets and the water itself. This explanation for the micro-explosion phenomenon has also been proposed for similar phenomena observed during the burning in other oils, specifically in situations where there are water droplets emulsified in fuels with high viscosity and mean boiling temperature much higher than that of water [27] as would be the case with heavy gas oil fires. In this work, the micro-explosion intensity has also been correlated to the temperature difference between the fuel and water, where a high temperature differential caused increased intensity of the ejections.

It is well understood that heating the heavy gas oil aids in the downward migration of emulsified water within the oil; therefore, development of the thermal gradient below

the surface of the oil likely acted to reduce the frequency and severity of the fuel ejections through two mechanisms. Firstly, the fuel was progressively heated at a given depth below the fuel surface, lowering the viscosity of the fuel, and allowing water to migrate more efficiently towards the bottom of the pan. Secondly, the formation of the aforementioned temperature profile allowed any remaining water trapped in the fuel layer to heat gradually as the fuel surface regressed towards the water pockets, which would allow the steam to form with less violence, and slowly escape through the surface.

Regardless of the mechanism driving the micro-explosions, the ejections of fuel during the initial burning period caused a significant increase in several characteristic features of the burning behaviour of the heavy gas oil fires under study. The remainder of this section discusses some of the changes measured during this initial burning period, and in experiments with undried heavy gas oil.

The periodic ejection of oil particles from the pan resulted in a fundamental error in the recorded mass loss rate, and thus fuel regression rate measurements during this period of burning. As shown in Figure 4.18, a significant volume of oil was ejected from the pan during the ejection phase. This loss of fuel from the pan is directly measured as a mass loss and therefore led to an overestimate of the fuel consumption, or fuel regression rate. This contributed to a difference of over 10% in measured mass loss rate between dried and undried oil tested at the same initial temperature and pan diameter. This is consistent with experiments by Wu, where a slight increase in regression rate was found for fuels containing emulsified water concentrations from 0% up to 10% volume per volume [70]. These experiments also showed a decrease in regression rate for water concentrations greater than 10%, perhaps due to the high heat capacity of the water; however, this range of water concentration was not of interest in the present work. It is unclear how the fuel ejections might have affected measured values of fuel regression rate for the larger diameter fires, because the circumference of a pan decreases relative to the area of the pan with increased diameter, and therefore relatively less fuel might be ejected from the pan. It is also hypothesized that higher lip heights would decrease the impacts of emulsified water on the fuel regression rate measurements; however, this was not tested in the present work.

The fuel ejections also caused an increase in the measured heat release rate that was independent of that seen as a result of the artificially increased values of measured fuel regression rate discussed above. Since the ejections of oil continued to burn once ejected from the pan (for example in Figure 4.18a), the ejections caused an increase in the effective flame surface area and thus measured heat release rate. It is also possible that some fraction of the ejected oil was sent directly into the flame or the hot fire plume. There it would be efficiently vapourised, which might lead to an increase in the rate at which the fuel is consumed, therefore increasing the heat release rate of the fire. This is consistent

with experiments by Ho [90], who measured increased values of heat release rate during 'spattering' of oil fires, albeit in this case the spattering was induced by application of a water suppression spray. The ejections in the work of Ho were caused by high velocity water droplets hitting the heated fuel surface, and caused a 300% increase in heat release rate, as measured for both mineral and cooking oils [90].

A significant increase in the rate of flame spread was also measured for the undried heavy oil tested in this work. The force of the fuel ejections driven by vaporisation of the emulsified water were found to enhance the sub-surface mixing of the liquid fuel ahead of the flame front. The flaming fuel also projected ahead of the flame front and, though it cannot be proven, their interaction with the cooler unburned fuel is hypothesized to have enhanced the pre-heating of the fuel ahead of the flame front – much like fire brands – with a consequent increase of the flame spread. The combined effect of the fuel ejections resulted in a flame propagation rate approximately 2.2 times greater in undried oil than in the dry oil experiments.

Figure 4.19 shows a comparison of the experimentally measured values of fuel density, fuel regression rate, heat release rate, flame spread rate and flame height for the dried heavy gas oil in comparison to those measured in the undried oil. Interestingly, the most significant increase in measured values were found for the flame spread rate over the undried oil.

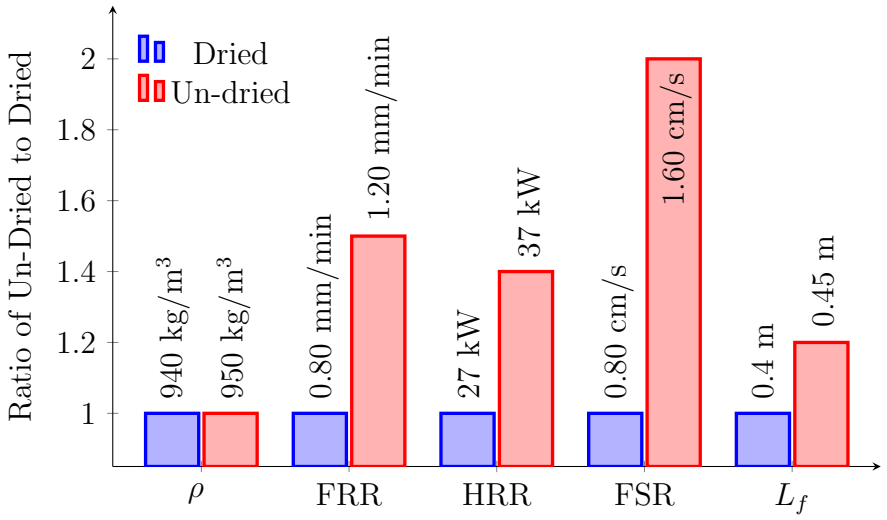

Figure 4.19: Effect of water emulsification in heavy gas oil on density and measured FRR, HRR, FSR, and flame length; as measured during 0.26 m pool experiment.

As mentioned above, the effects of the water emulsification in the oil were intensified in the small scale experiments relative to those in larger diameter pans due to the scale of the test pans. It is believed that the emulsified water pockets, though they may be of varying size, are somewhat consistently distributed throughout the oil, and therefore the explosive force of the various pockets is expected to be relatively independent of pan size. It was found in the present experiments that the distance travelled by the ejected particles was relatively constant, regardless of the pan diameter, supporting that idea that the strength of the micro-explosions was not affected by pan diameter. For this reason, while presenting a significant source of error in the present small-scale experiments, the behaviour of real fires may not be reflected by the measurements made using undried oil.

4.7 Effects of Fuel Weathering

Throughout the course of the present experimental series, it was also found that the heavy gas oil weathered with time. This weathering was characterized by an increase in the density of the oil, such that after a period of eight months, the density of the bulk oil had increased sufficiently that it no longer floated on water. Figure 4.26 shows an example of weathered oil sinking into the water layer during a boilover experiment. Weathering of the heavy gas oil is not unexpected, as most heavier fuels contain a combination of various hydrocarbons, from heavy, complex chains to light fractions. The lower vapour pressure of the lighter ends generally allows them to vapourise from the bulk fuel over time, even at ambient temperature [115, 145].

Weathering of the heavy gas oil was only noticed after the oil had been stored over the winter months, and therefore continuous monitoring of the effect of weathering on fire properties was not conducted. However, the global effects of a given period of weathering is provided. The heavy gas oil in this weathering study was shipped from Alberta in July of 2013, and the weathering experiments were conducted in June of 2014, therefore representing a one year weathering period. During that time, the oil was stored in a ventilated, closed top drum outdoors, and therefore was exposed to ambient temperatures throughout the summer and winter seasons.

Figure 4.20 shows a comparison of the measurements of fuel density, fuel regression rate, heat release rate, flame height and boilover intensity for fresh heavy gas oil, and that of one year weathered heavy gas oil. Consistent with the increase in density, it appears that the lighter, more volatile, fractions of the fuel were vapourised during weathering, and as a result, the heat release rate and fuel regression rate were seen to decrease substantially.

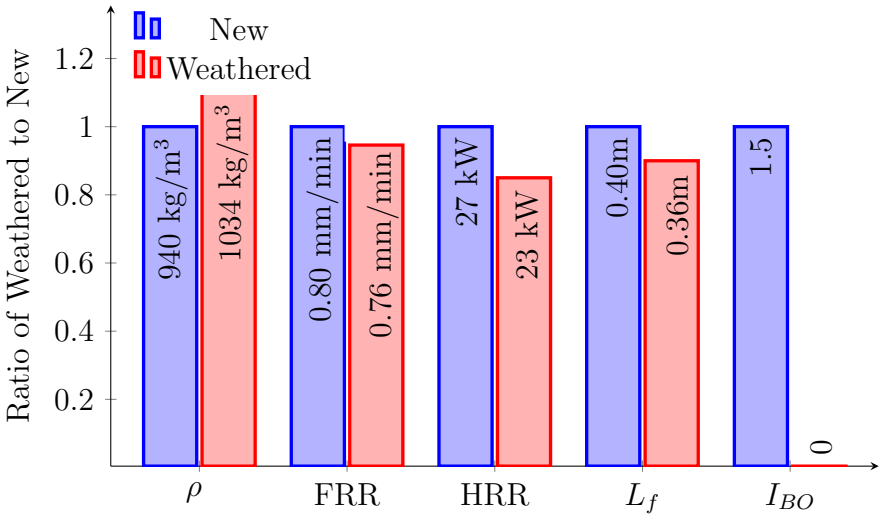

Figure 4.20: Effect of heavy gas oil weathering on FRR, HRR, flame length, and boilover intensity; as measured during 0.26 m pool experiment.

Since recognition of the effects of fuel weathering occurred late in this research, there has not been sufficient time to conduct a full experimental investigation of the weathering effects on burning behaviour of the heavy gas oil. Nonetheless, the increase in fuel density and decrease in fuel heat release rate between weathered and non-weathered samples of the heavy gas oil do indicate that the relative volatility of heavy gas oil decreases with weathering time. This is supported by experiments by Wu and Torero [70], who found a 32% decrease in regression rate from non-weathered light crude oil to the same oil after 80 hours of weathering. As many of the lighter hydrocarbon chains are likely to have vapourised during weathering, it can be concluded that the heat of combustion, and flame spread rate likely also decreased over the weathering period.

In apparent contradiction to the above explanations of the effects of weathering in the present experiments, is the more general observations that the fuel regression rate, heat release rate, and fuel temperature did not vary over the course of long duration burning periods previously discussed. This indicates that the fuel composition did not change during these experiments, and would suggest that the light hydrocarbons did not vapourise preferentially, such as would be required for a fuel to weather. It is possible, then, that weathering of the heavy gas oil under investigation in this work is a result of the fuel chemically breaking down over long periods of time. In experiments by Torero et al. [84], Wu et al. [115], and Garo et al. [145] the effects of weathering on the measured characteristics of the fire occurred immediately, with a measurable effect determined within

a weathering period of 2 to 5 days in heated and unheated conditions. In the present experiments, conversely, no effects of weathering were determined over a period of a month or more, and the weathering effects were only found to occur over the period of over eight months. The weathering of heavy gas oil is hypothesized, therefore, to be a much slower chemical process than has normally been reported in the literature. As such, the heavy gas oil is likely comprised of a complex mixture of hydrocarbons that are not easily separated, and is one further piece of evidence to support that the oil burns as a homogeneous mixture.

4.8 Boilover

A large number of experiments were conducted to investigate the general burning behaviour of heavy gas oil and kerosene using the instrumented pan burner, as were documented in the previous sections. An additional hazard in the case of long duration burning of oil in storage tanks is that of boilover, which was therefore investigated in this study. Boilover results when the heated fuel layer interacts with a water sublayer beneath the fuel, and is characterized by a rapid ejection of burning fuel from the tank during a fire. A full description of the boilover phenomenon and the proposed mechanisms for its occurrence is provided in Section 2.2. Experiments were conducted to investigate boilover propensity of heavy gas oil and kerosene fires using the instrumented pan burner, with the fuel layer floating on top of a water sublayer. In the boilover experiments, the linear, one dimensional rake shown in Figure 3.2a was installed to measure temperatures through the depth of the oil during the burning period. The experiments were conducted following the procedure described for the instrumented pan burner in Section 3.2. Due to the possibility of flame spread beyond the test pan, the load cell was not used for the boilover experiments, so the fuel regression rate was measured only from thermocouple and infrared video data.

It was indicated in Section 4.5.3 that the heavy gas oil did not form a hot-zone during the steady burning period with a thick fuel layer and without a water sublayer. In these experiments, the temperature profile through the depth of the fuel remained constant through the duration of each burn, and the 100 °C isotherm was consistently located approximately 2 cm below the fuel surface. From these observations it was hypothesized that a thick layer boilover was not likely to happen, and that a thin layer boilover was possible when the fuel layer decreased to a depth of less than 2 cm. With this in mind, experiments were performed to determine the propensity for boilover of heavy gas oil contained in deep walled pans containing a water sublayer.

The probability of boilover for each fuel was estimated from equation 2.9 as proposed by Mickaelis [23] using the quoted material properties for the kerosene and heavy gas

oil. This criterion results in a value of 0.6 for kerosene, and 2.8 for heavy gas oil. This high value, greater than 0.6, calculated for heavy gas oil confirms that the fuel does have material properties which exceed the expected minimum requirements to lead to boilover. Conversely, by this estimation, a thick layer of kerosene burning suspended on a water sublayer would not be expected to result in boilover. On this basis, boilover in heavy gas oil pools is not unexpected as it exceeds the threshold criterion above, the fuel is highly viscous, and there was a clear 100 °C isotherm that formed beneath the fuel surface. It remains then to examine in more detail the possibility and physical processes of boilover in the heavy gas oil fires.

In general, the heavy gas oil fires established over deep pools of fuel with a water sublayer exhibited five distinct burning phases. Figure 4.21 shows a selection of images demonstrating the overall fire behaviour in each of the phases. After ignition, the pool fire exhibited a period of fuel ejections (Figure 4.21a) which was followed by a phase of steady burning much the same as was seen in the initial burning phases for the fires with no water sublayer, as discussed in Section 4 (Figure 4.21b). At some time later, a second phase of fuel ejections occurred (Figure 4.21c), ending in a violent overflow of fuel from the test pan (Figure 4.21d and 4.21e), consistent with the classical definition of boilover. Finally, following the pan overflow, the flame decayed and eventually extinguished (Figure 4.21f). These distinct burning phases are described in more detail in this chapter.

Immediately following ignition, the fire was characterized by audible crackling sounds, ejections of small droplets of oil, and increased fire intensity. This is consistent with the ejection phenomenon previously noted and described in Section 4.6. This initial phase continued for approximately five to ten minutes, following which the frequency of the ejections decreased as the exponential temperature profile was established into the depth of the oil in the pan. As in the discussion for heavy gas oil fires with no water sublayer, it is hypothesized that the gradual heating of the oil facilitated downward migration of emulsified water leading to the gradual decline in oil ejections from the fire. This initial period was then followed by a phase of steady burning.

The duration of the steady burning period depended on the initial fuel depth and the fuel regression rate, as the steady burning time was extended for increased initial fuel depth. The burning behaviour of the heavy gas oil during the steady burning period of the boilover experiments was very similar to that of a typical pool fire and also closely resembled that observed during steady burning of the fire without a water sublayer, described in Section 4. It is believed that the thick layer of fuel insulated the heated surface layer of the oil against any heat losses to the water sublayer during this steady burning period. This is further supported by the fact that the fuel regression rate and flame height during this period were consistent with previous measurements – as detailed in Section 4.5 – as well as with

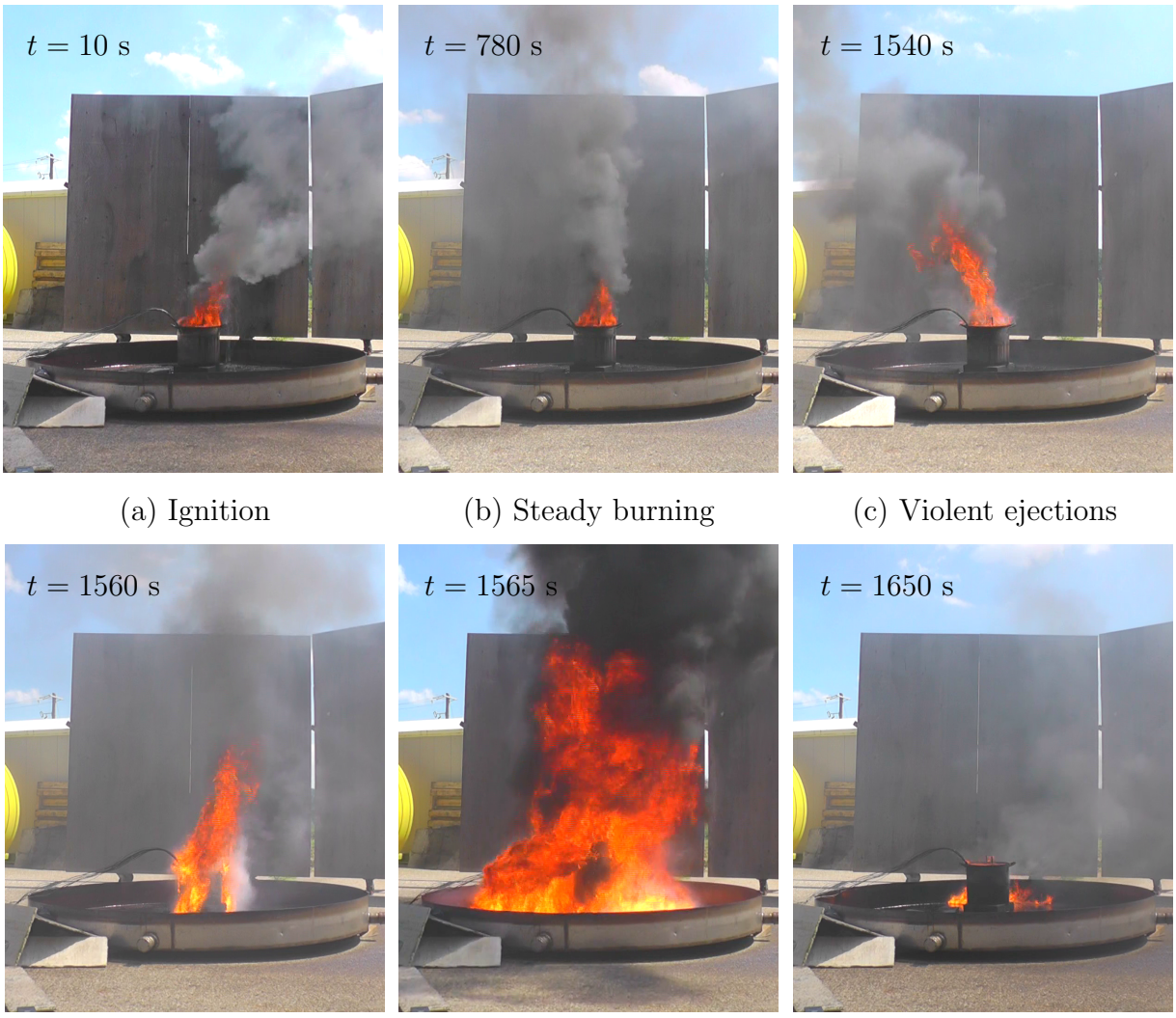

(a) Ignition (b) Steady burning (c) Violent ejections

(d) Boilover initiation (e) Fire spread (f) Flameout

Figure 4.21: Visualisation of boilover event at different time periods during 0.26 m diameter heavy gas oil pool fire experiment with water sublayer.

the various correlations proposed in literature [22, 38, 78]. This is consistent with expected behaviour, as there is less than 4 cm of heated fuel below the fuel surface during this period and therefore no heat losses to the water layer should occur until the fuel layer decreases to this level.

The end of the steady burning phase was marked by a second period of fuel ejections, similar in behaviour to the initial burning phase. In contrast to the waning of the ejections towards the end of the initial phase, however, the violence of the ejections during this stage was seen to increase over time, and within 15 to 60 seconds after the start of the ejections, a period of rapid froth generation occurred. This froth was generated in sufficient volume to overflow the test pan walls, and therefore spread flaming oil beyond the pan walls, resulting in a greater area of fuel burning, and a large increase in flame height. This increase in fire intensity was consistent with reported observations of boilover as documented in literature [27, 28, 92–94], and in historical events [2, 33, 34].

The froth layer that formed during boilover in these experiments was consistent in appearance to the froth layer that formed during the suppression spray experiments described in Section 4.4, supporting the observation that the formation of froth was a result of heated oil mixing with water and creating steam. Figure 4.22 shows a selection of images during and after boilover in a 0.6 m heavy gas oil boilover experiment. Figure 4.22a shows an image of the froth being formed in sufficient quantities to overflow the test pan during the boilover period, and Figure 4.22b shows the froth layer after boilover. Clear from Figure 4.22b is that there are significant pockets of steam vapour throughout the froth layer, such that the froth no longer resembles the original oil.

The boilover phenomenon observed here resembles a traditional boilover in terms of its consequences, in particular due to the increased fire intensity and flame spread beyond the test pan. The overall characteristics are more akin to a 'frothover', however, such as might be seen when water from a suppression spray mixes at the surface with heated oil and creates a steam and oil froth mixture that overflows a burning pan. In the present case, the overflow of hot heavy oil from the pan is caused by direct interaction of heated oil with the water at or near the water sublayer and therefore 'boilover' is a more appropriate term to use in describing this phenomenon.

The overflow, or boilover, period in these experiments lasted for approximately 20 to 60 seconds in many of the experiments, and was followed by a second and third boilover in some cases. Most often, the continued generation of steam from the water layer eventually impregnated the froth layer with water sufficient that the froth layer was no longer combustible. The layer of froth, as had been observed in the suppression experiments, was sufficient to suffocate the flame on the pool surface, and aided in the extinguishment of

(a) During boilover.

(b) Post boilover.

Figure 4.22: Evidence of steam-impregnated froth in test pan during and after boilover in heavy gas oil pool fire experiment in 0.6 m test pan with water sublayer.

the fire. In some cases, however, enough burning oil had pooled around the base of the pan that flames from the containment pan actually re-ignited the fuel in the pan. In this situation, the fire continued until either a second boilover occurred, or all of the fuel had been consumed.

To compare to the heavy gas oil boilover experiments documented above, experiments were also conducted to investigate the behaviour and propensity for boilover of fires in which a layer of kerosene was floated on a water sublayer. These experiments were conducted in the 0.26 m pan, using a thick layer of kerosene with the linear one-dimensional thermocouple rake shown in Figure 3.2a. Preliminary experiments documented in Chapter 4 indicated that kerosene has a boiling temperature of 240 °C and that the temperature profile into the depth of the fuel is such that the 100 °C isotherm was located approximately 1 cm beneath the fuel surface in 0.26 m pools; both of which indicate that thin-layer boilover is possible. Finally, in previously reported work, kerosene has been shown to exhibit a low-intensity thin layer boilover [98], characterized by slight splashing of the fuel layer and a minor increase in fire intensity.

Similar to observations for the heavy gas oil fires, the presence of the water sublayer was found to not affect the regression rate of the fuel during the boilover experiments using kerosene as fuel. Again the thick layer of fuel above the water most likely insulated the surface of the fuel from any differing heat transfer characteristics of the fuel-water interface. Further evidence of this was that the burning characteristics during the steady burning

period of fires in which there was a water sublayer did not differ from those measured during the same period in experiments without the water sublayer; the fuel regression rate and flame height were again well represented by correlations proposed for the steady burning period.

As the fuel layer decreased in depth and approached the level of the water sublayer, a brief period of slightly increased fuel burning rate ensued and slight splashing of the water layer was observed. No fuel was ejected from the pan, and there was a negligible increase in flame height. The phenomenon was synonymous with the thin-layer boilover such as that reported in [98], where only a thin layer of fuel remained when the water sublayer began to vaporise [146]. Temperature measurements during the kerosene boilover experiments indicate, as expected, no evidence of a hot-zone within the fuel, but instead that the temperature profile decayed exponentially from the surface, similar to thermal profile into the depth of the fuel discussed above for the case of the kerosene fire no water sublayer. Since the kerosene fire did not boil over, it is clear that anomalies in the experimental apparatus were not the cause for the phenomena described above for the heavy gas oil fires. Therefore, additional experiments were conducted to further explain the mechanisms of the froth formation and subsequent boilover in the heavy gas oil fires.

Further experiments were conducted to collect more detailed measurements of fuel regression rates and temperature distributions in the fuel during the heavy gas oil fires. A representative plot of the temperature history through the fuel depth for the 0.26 m diameter pan experiment is shown in Figure 4.23. It can be seen that the early portion of the temperature traces in this plot closely resemble the temperature traces shown in the temperature history plot for heavy gas oil without a water sublayer, as shown in Figure 4.9.

Despite the similarity to Figure 4.9, a significant difference in the temperature traces can be seen following approximately 25 minutes after ignition. At this point, the second period of fuel ejections, as shown in Figure 4.21c, was immediately followed by the generation of a sufficient volume of froth to overflow each of the test pans. This was marked by a change in recorded temperatures, evident in Figure 4.23 by the sudden drop in recorded temperatures. At this time, a temperature of approximately 120 °C was measured by all thermocouples as a layer of froth rapidly expanded vertically up along the thermocouple array, engulfing even those thermocouples that had previously been in the flame zone. The temperatures measured by the thermocouples are seen to be approximately that of steam, supporting the notion that the expanding froth layer is a homogeneous mixture of oil and steam. Closer examination of the video recordings of these experiments confirmed that the rapid change in temperatures corresponded with the time of initiation of boilover in the test pan. From these observations then, it was concluded that boilover of heavy gas oil in

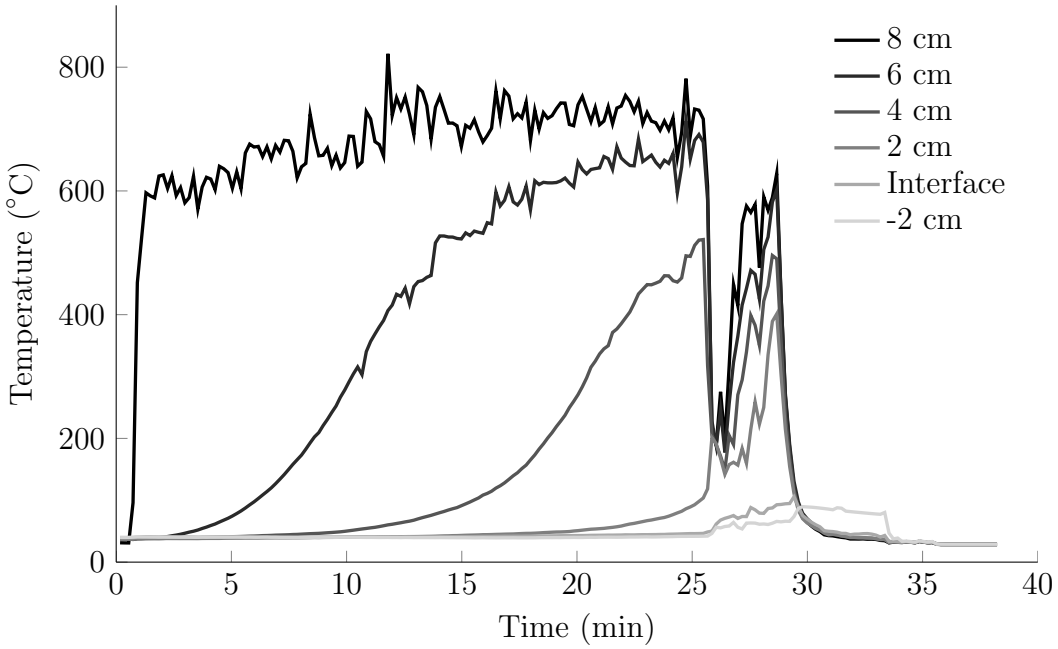

Figure 4.23: Characteristic temperature history at various depths in fuel, as measured in 0.26 m diameter heavy gas oil boilover experiment.

the present experiments was a result of rapid mixing of the heated oil with a small depth of the water layer.

Clear from Figure 4.22b is that the froth generated during boilover did differ substantially in properties relative to the original fuel. The froth had a much lower density than the original heavy gas oil, and contained pockets of air and water vapour. Due to expansion and mixing of the oil with steam, the froth occupied multiple times the original volume of oil, and therefore overflowed from the pan. As such, this mechanism of boilover differs from the traditional phenomenon of boilover, in which a rapid generation of steam due to sudden superheating of the water layer is thought to act as a piston which explosively ejects the thick fuel layer from the pan [28].

Measurements of temperature as a function of depth into the fuel, shown in Figure 4.24, further support the above description of the boilover in the present experiments. Similar to the heavy gas oil pool fire experiments conducted without a water sublayer, the measured temperatures were found to decay exponentially from the heated surface into the bulk of the oil, exhibiting a profile that remains constant over time and with no evidence of hot-zone formation throughout the initial period of burning. Contrary to the comparable

figure showing the temperature profile without a water sublayer (Figure 4.15), this figure does not show each temperature profile normalized to the initial fuel surface. Rather, each temperature trace progresses towards the bottom of the plot with the fuel surface regression, to show the combined effect of fuel regression and temperature development on the temperatures measured at the interface level – marked in red.

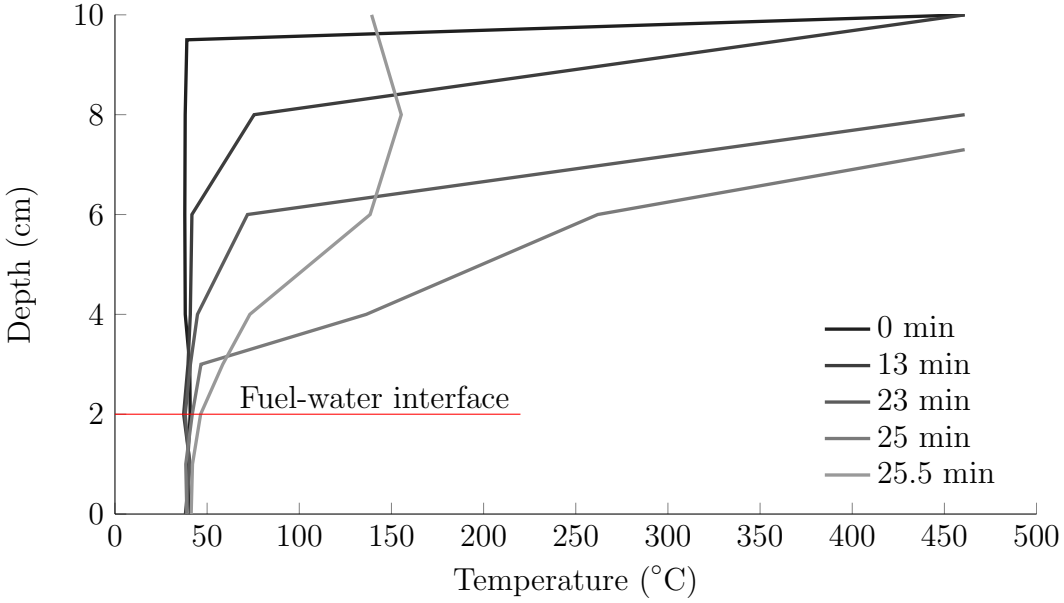

Figure 4.24: Temperature profile into depth of oil at various times as measured during 0.26 m diameter heavy gas oil boilover.

As discussed in Section 4.5 the 100 °C isotherm remained located at approximately 2 cm and the initial fuel temperature at about 4 cm below the surface of the fuel regardless of the initial fuel depth. The location of the isotherm was affected by the pan diameter; however, remained at approximately 2 cm from the fuel surface for the range of pan diameters considered during the boilover experiments. This plot also shows that the exponential temperature profile remains constant throughout the burning period, even with a water sublayer; therefore, a water sublayer is not a factor responsible for causing a hot-zone formation. In the experiment shown in Figure 4.24, boilover initiation occurred at a time of approximately 25.4 minutes, as verified by video footage and thermocouple data. It is clear from Figure 4.24 that the temperatures measured at the fuel-water interface did not reach a temperature of 100 °C at the time of boilover, as would be expected for water to be evaporated resulting in boilover. Furthermore, previously reported critical values of

Table 4.10: Measured parameters from boilover pool fire experiments with heavy gas oil and kerosene.

Fuel	d (m)	h_{i} (mm)	R (mm/min)	t_{bo} (min)	h_{bo} (mm)
	0.19	80	0.63	79 ± 16	30 ± 10
Heavy Gas Oil	0.26	80	1.1	36 ± 18	40 ± 20
	0.6	200	1.6	88 ± 25	60 ± 40
Kerosene	0.26	60	1.3	46	0

interface temperature for boilover have been measured to be 120 °C or greater in crude oils [95], but never below the boiling temperature of water. The boilover in heavy gas oil was therefore studied in further detail to better understand the mechanisms of heat transfer from the heated fuel layer into the water layer.

Several parameters were measured before and after each boilover experiment in order to better define the burning characteristics of the heavy gas oil when floated on a water sublayer. For this, the initial fuel depth, h_{i}, the fuel regression rate, R, and fuel thickness at boilover, h_{BO}, were measured based on the infrared camera recordings, and the time from ignition to the start of boilover, t_{BO} was derived from video recordings. A summary of the experimental conditions and measured properties from experiments in which the initial conditions were held relatively constant are shown in Table 4.10.

Of note from this table, is that the time to boilover, t_{BO}, is not consistent for any of the experiments, and varies widely between multiple experiments conducted with a similar initial fuel layer thickness. A plot of the time to boilover as a function of initial fuel thickness for experiments conducted on 0.19, 0.26, and 0.6 m fires is shown in Figure 4.25. It appears that there is a wide band of values and large variability in the measured times to boilover for a given initial fuel depth, with little dependence of time to boilover on the initial fuel thickness or pan diameter, though there is limited comparative experimental data for some pan diameters. This differs from what would be expected based on both models for the time to boilover, where for thick layer boilover it is a function only of the hot-zone growth rate, and independent of pan diameter – as shown in Figure 2.6a, and for thin layer boilover, where it is a function of only pan diameter – shown in Figure 2.6b. As there is a good consistency in the measured regression rates of the fires at each pan diameter, and no hot-zone was found to form, it was expected that a linear relation between time to boilover and initial fuel depth would be found.

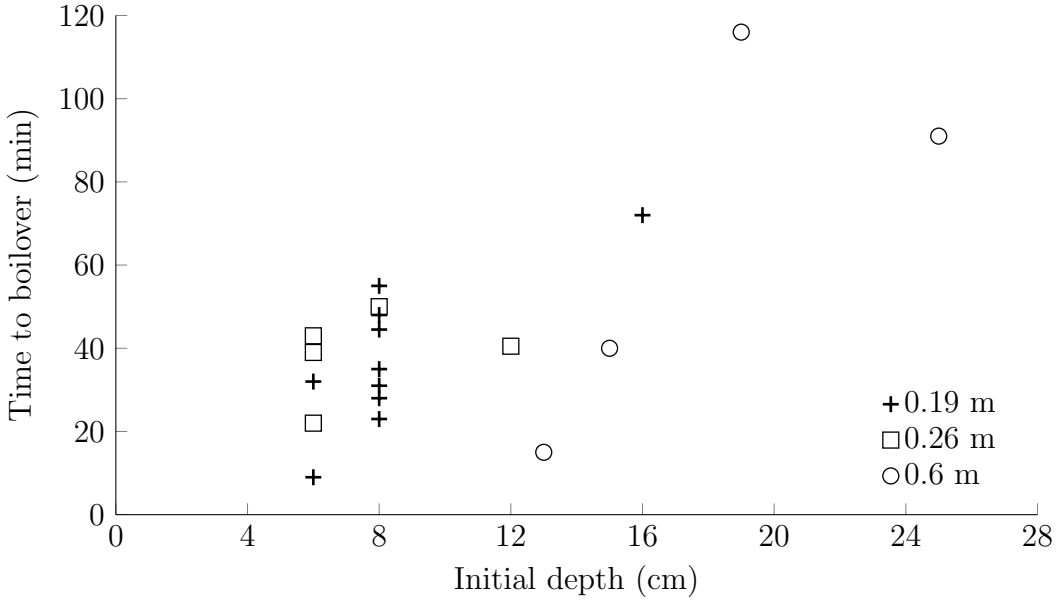

Figure 4.25: Effect of initial fuel depth on the time to boilover as measured for each of the experimental pan diameters.

Furthermore, Table 4.10 shows that the depth of fuel above the water layer at the time of boilover also varies significantly, from 2 to 10 cm across all of the test pans. Since it is clear from Figure 4.24 that the 100 °C isotherm remains at approximately 2 cm beneath the fuel surface, which is also consistent with the behaviour noted in Section 4.5.3, the occurrence of boilover at a fuel thickness greater than 2 cm is unexpected and alludes to the fact that there may be a secondary path of heat transfer which causes the water layer to boil in these experiments. Identification of this path formed the focus of the investigations outlined below.

Based on the combined observations discussed above, it was concluded that the boilover experienced in heavy gas oil was not initiated in the traditional sense by sudden vaporization of water at the fuel-water interface resulting from the formation, growth and interaction of a hot-zone that formed in the bulk fuel. In addition, it was well established that heat transfer through the pan walls was not a driver for heat transfer into the fuel layer that could lead to boilover. Finally, no correlation was found between the time to boilover and either the initial fuel thickness or fire diameter. To further elucidate the mechanisms at play in the present experiments, therefore, additional tests were conducted with the intent to visualize the interactions taking place at the oil-water interface during boilover.

A series of experiments were conducted on heavy gas oil fires in the 0.19 m diameter Pyrex glass pan with a screen installed around the pan lip to ensure that any ejected oil did not cover the walls of the pan and obstruct the view of the interface. One video camera was focused on the pan walls to record the behaviour of the fuel-water interface, while a second camera recorded the overall fire behaviour from a distance. A 8 cm deep layer of fuel was added to the pan over a 2 cm deep water layer to ensure that the camera recorded a clear interface between the two liquids.

Figure 4.26 shows a selection of images extracted from the two video recordings. In this series of images, a visible distortion of the interface layer occurs at a time of 21 minutes past ignition, while the fuel layer is still approximately 4 cm deep (Figure 4.26b). Shortly afterwards, projections of oil into the water layer were observed, along with violent disruptions of the previously well marked fuel surface and fuel-water interface (Figure 4.26d). Less than 30 seconds from the first signs of changes in the fuel layer, a violent boilover occurred (Figures 4.26e and 4.26f). Of note from these images is the oil sinking into the water sublayer on the left side of the pan, most obvious in Figure 4.26a. This did not affect the present results but is an example of the effect of weathering of the oil, as discussed in Section 4.7, where the density of the fuel increased as a result of evaporation of lighter hydrocarbons from the bulk material. It should also be noted that the experiment in which the images in Figure 4.26 were taken was the last boilover experiment in this series, and the weathering of the oil therefore had less affect in the earlier experiments.

Further examination of the video images indicated that each ejection of fuel from the top of the pan caused a downward projection of oil toward the water layer. This is as expected based on the conservation of momentum, where the force to eject the fuel out of pan is counteracted by an equal force within the fluid. Further analysis of the videos established that the locations where the fuel ejections exited the fuel surface corresponded to the locations of the fuel projections into the water layer. As the oil continued to burn, the depth of the oil layer decreased sufficiently for these downward projections of oil to enter into, and interact with, the water sublayer. Since the downward projected oil is heated, its density is lower than that of the water so it returns to the oil layer, encouraging mixing of water into the heated oil above the water sublayer. It is hypothesized that the introduction of this additional water into the heated oil layer causes further fuel ejections, thus creating a chain reaction of increasingly violent ejections of oil from the fire and therefore additional mixing of hot oil and water in the region of the fuel-water interface. At a critical point, sufficient heated oil was mixed with water from the sublayer such that pockets of the water evaporated and steam was created, which in turn readily mixed with the oil. This steam and heated oil mixture was found to form the low density, large volume of froth discussed above, causing the overflow of the pan. As is shown in Figure 4.15,

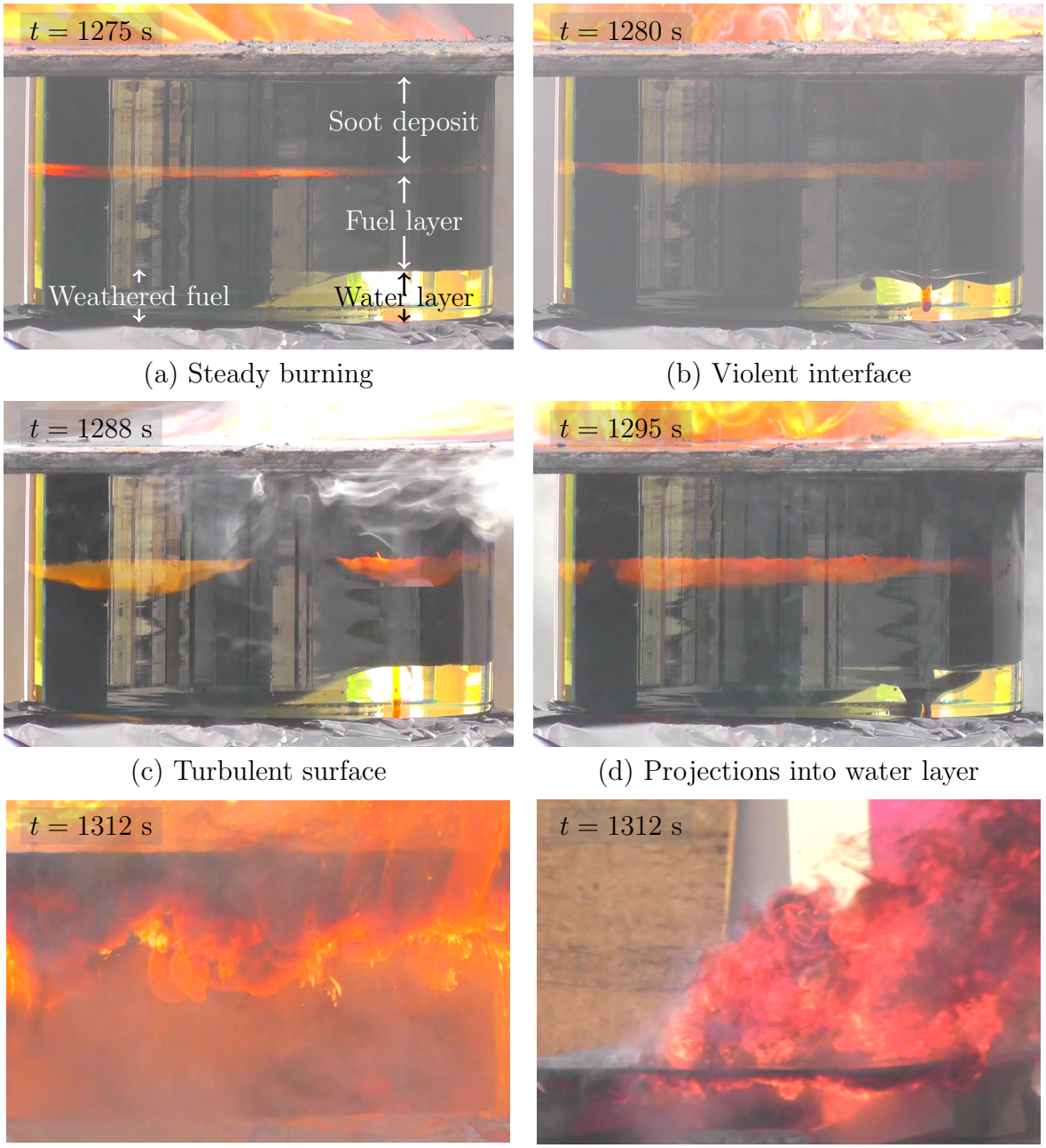

(a) Steady burning

(b) Violent interface

(c) Turbulent surface

(d) Projections into water layer

(e) Peak boilover

(f) Peak boilover

Figure 4.26: Visualisation of fuel-water interface at different times throughout heavy gas oil boilover in 0.19 m glass pan.

the temperature of the froth was approximately 88 to 110 °C, similar to what would be expected for the temperature of steam. This also helps to explain how the boilover process was initiated prior to the fuel-water interface reaching a temperature of 100 to 120 °C, as expected for boilover to occur.

Although the above experiments were conducted with a fairly deep water sublayer to aid in visualization of the process, additional experiments were also conducted with a thin water sublayer of approximately 5 mm depth. In these tests, the period of crackling fuel ejections was prolonged by several minutes, suggesting that very thin water layers increase the time to boilover. It is hypothesized that the bottom of the pan limited the travel of the oil projections, and they could not travel as far into the water layer. In this situation, it appears that less water was mixed into the bulk oil with each fuel projection and, as a result, more oil projections were required to initiate the formation of froth, thereby increasing the length of the period of fuel ejections. Furthermore, while boilover generally did occur shortly after the first visible oil projection into the water layer, multiple oil projections into the layer were actually necessary for the final initiation of entire boilover process. Therefore, no clear relation was found between the initial fuel depth and time to boilover; however, a reasonably consistent fuel depth was measured at the initiation of boilover in each test, of 6 ± 2 cm.

The aforementioned observations could indicate that there was a nearly consistent explosive force generated from the micro-explosions, suggesting that there is a critical minimum fuel thickness for boilover in the heavy gas oil. Across the diameters of fires studies here, at 0.19 to 0.6 m in diameter, this thickness was found to be 2 cm for very dry oil with few oil ejections, and up to 10 cm for undried oil experiencing frequent and violent ejections. However, the range of data for the various water concentrations and pan diameters is limited in these experiments results. As well, there was some variability in the experimental conditions, including wind and ambient temperatures, possibly introducing some error to the measurements. For these reasons, it is unknown how this value of critical fuel thickness for boilover will scale with pan diameter, and it is not expected to be consistent for diameters as large as those of real oil storage tanks.

After elucidation of the physical mechanisms that caused boilover in the heavy gas oil fires, it was also of interest to investigate the potential consequences of boilover in terms of other characteristics of the fire. While the ejection of fuel beyond the tank walls is of primary concern during boilover, the increase in flame radiation from the flame enlargement has resulted in severe injuries to first responders, as well as in secondary ignition of nearby objects. Figure 4.27 shows a graphic of the enlargement of the flame region during boilover in a 0.26 m diameter heavy gas oil fire experiment at various times, from the initiation of boilover, defined to be 0 s, to the start of pan overflow 4.0 s seconds later, where the

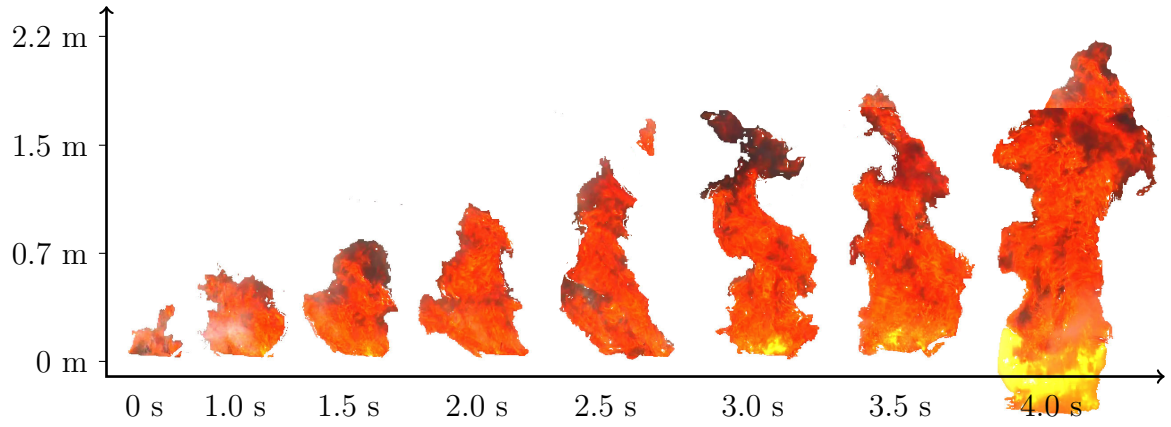

Figure 4.27: Flame enlargement at various times during boilover in 0.26 m diameter heavy gas oil boilover experiment, with pan overflow at 4.0 s.

fire begins to spread below the pan lip. Due to the ejections from the fuel layer and the turbulence at the fuel surface, it appears that fuel is splashed up into the flame column and consumed, resulting in an increase in the fuel consumption rate. As discussed in Section 4.5, the increased fuel consumption rate would result in an increased heat release rate and helps to explain the increased flame height.

Of note from Figure 4.27 is the rate at which the flame increases from its steady burning height at the initiation of boilover to the full height at the peak of boilover. The time from the initiation of the growth in flame height, which – in real fires – is often the first indication boilover, to the start of the pan overflow was approximately 4 seconds. During this time the flame length increased by approximately 2.5 times while the fire is still constrained to the test pan. However, as can be seen in Figure 4.21, once the frothing starts and oil spreads beyond the test pan, the relative diameter of the burning area increases, with an associated increase in flame length. The total radiative output of the flame during boilover should take account of the increase in footprint diameter, so this illustration provides a basis for a measurement of relative boilover intensity based on the observed increase in flame length.

Boilover intensity has been proposed as a parameter by which to represent the increase in mass loss rate, and thus increase in radiative output, of a fire during boilover. Unfortunately, measurements of mass loss rate are often not possible during boilover experiments, and even less likely during actual fires. Furthermore, when using instruments such as thermocouples or infrared cameras to measure regression rate during boilover, it is often impossible to distinguish the burning rate of the fuel from the reduction in mass due to

ejection of fuel from the pan during boilover. For these reasons, mass burning rate during boilover was not measured in the present work, but instead boilover intensity was linked to changes in measured flame height.

While mass loss rate during boilover is difficult to quantify, the mass burning rate is directly proportional to the heat release rate. The heat release rate is also proportional to the flame column height; therefore, it is expected that the growth in height of the flame column during boilover also represents a measure of the boilover intensity. A boilover resulting in more significant enlargement of the flame would therefore be considered to have a higher intensity than a boilover with only a small flame enlargement. A pan diameter normalized boilover flame growth relation is therefore proposed for the present study as

$$I_{\mathrm{BO,F}} = \frac{L_{\mathrm{f,BO}} - L_{\mathrm{f}}}{d} \tag{4.7}$$

where $L_{\mathrm{f,BO}}$ is the flame length at the peak of boilover, immediately prior to the overflow of the pan. This may not entirely represent the peak flame height reached during the boilover period, since overflow of fuel from the test pan causes an additional increase in the effective diameter, and thus flame height, of the fire. While this latter increase in flame size is certainly relevant to the boilover phenomena, the change in effective pool diameter was found to be dependent on the pan size, pan height, freeboard height at boilover, and material under the test pan; therefore, it does not represent a consistent and comparable change in flame characteristics during the process of boilover. The intensity of boilover was therefore thought to be best represented in the present experiments by the maximum flame height prior to overflow of the pan.

Figure 4.28a shows the normalized flame growth at boilover plotted against fire diameter. From this plot, it is clear that the flame height at boilover, and thus boilover intensity, grows with the diameter of the fire. At first look this appears counter to many recent findings, where a decrease in boilover intensity was found with increased pan diameter in several experiments [25,66,98]. However, all of these latter experiments were conducted on crude oil fires in which a hot-zone formed and led to boilover. These experiments were conducted on fires in which the fuel layer thickness was maintained at a constant value while the pan diameter was increased. As a result, the increased pan diameter leads to increased mass burning rate, and reduced fuel layer thickness at the time of boilover. Since for this mechanism of boilover there is a strong dependence of fuel layer thickness at boilover on the intensity of boilover [98], the boilover intensity reported in the literature therefore decreases with increased fire diameter. In contrast, in the present experiments, no hot-zone was formed, and there was a nearly constant fuel thickness at boilover, of 6 ± 2 cm, independent of fire diameter or initial thickness of the fuel layer. Therefore, in the present

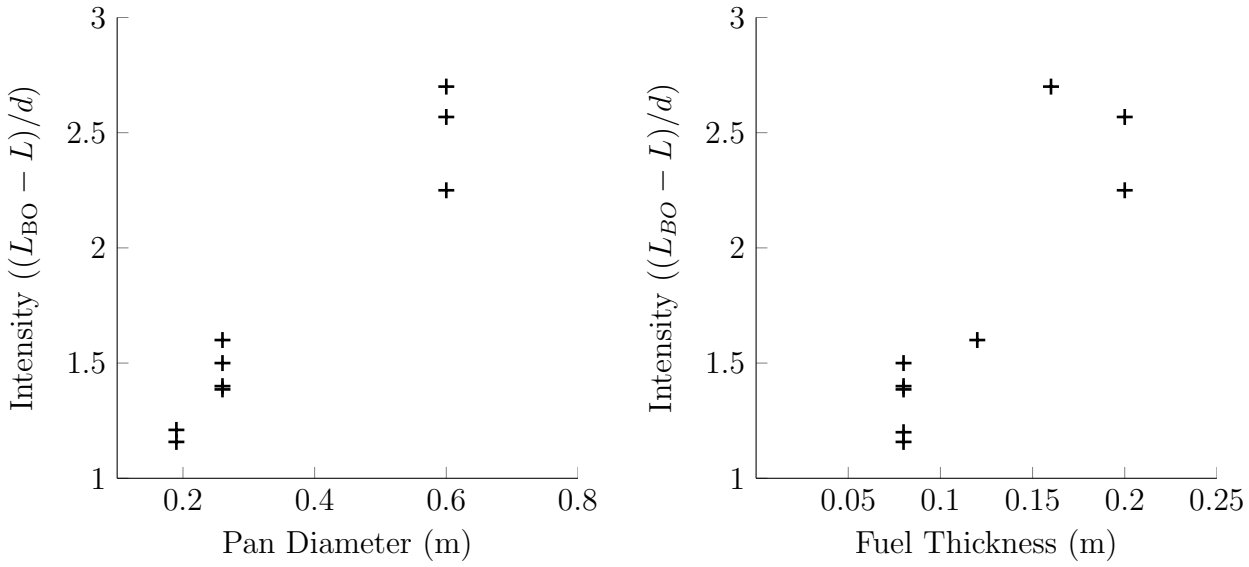

(a) Pan diameter.

(b) Initial fuel thickness.

Figure 4.28: Effect of pan diameter and initial fuel thickness on normalized flame length boilover intensity.

experiments, boilover was found to increase in intensity with increasing fire diameter, and it is believed that the larger surface area resulted in increased interactions between the fuel and water at the interface between the two layers. This resulted in an increase in the fuel consumption rate, thereby causing an increased heat release rate and flame height. Again, this conclusion is based from experiments at just three distinct pan diameters, and it is therefore unclear if the trend of increased intensity with larger diameters would be consistent at the large scale.

After boilover and extinction of the fire, the heavy gas oil and water froth mixture remaining in the test pan cooled back to ambient temperature, and the water was found to separate from the oil relatively quickly such that the remaining oil resembled the original heavy gas oil with no noticeable change in physical properties; including density, colour, and odour. This is again counter to observations made after boilover in crude oil, where the remaining fuel was found to be much denser than the original crude, and turned nearly solid once cooled [98]. The lack of change in fuel characteristics during boilover in the present heavy gas oil experiments provides yet another piece of evidence to support an

entirely different mechanism of boilover for this fuel as compared to the characteristic boilover associated with crude oil and other multicomponent fuels.

Given the mechanism of boilover observed in the present experiments, it was of interest to try to quantify the magnitude of the expansion ratio of the heavy gas oil when mixed with steam as one measure of the consequences of boilover. To examine this, a small amount of water was mixed into the oil and the mixture heated to 120 °C. Knowing the initial volume of the oil and the maximum volume of the froth that formed (i.e. when the froth was fully expanded), the expansion ratio was determined. This ratio was calculated to be approximately $1 : 1050 \pm 50$ for this experiment, which coincides well with the known expansion ratio of water to steam of 1 : 1700. It is expected that not all of the steam produced would be mixed with the oil, therefore it is sensible that the total volume expansion of the froth is less than that for steam alone. While this determination does not account for the volume of froth that would be burnt off during an actual boilover event, it does point to the extremely large expansion ratio of the froth, and supports the observations of froth overflow in the experiments. All of the above factors taken together, therefore, reinforce the fact that boilover, however caused, is a rapid and dangerous event. Furthermore, all tanks containing a water layer should be treated as having the capability to boilover, and first responders cannot wait for the first signs of boilover before retreating from the tank.

While the present experiments found no evidence of the formation of a hot-zone leading to boilover in the heavy gas oil, they clearly identified the risk of boilover when the fuel layer was sufficiently reduced. This phenomenon is more akin to the 'thin layer boilover', rather than the 'hot-zone' – or thick layer – boilover. This thin layer boilover in heavy gas oil; however, resembled the traditional thick layer boilover in appearance and severity, and resulted in fire spread beyond the test pan, as well as significant increase in fire size and intensity. For this reason, the consequences of, and emergency preparations for, boilover in heavy gas oil must not be confused with those of thin layer boilover. The expansion of the heavy gas oil when mixed with heated steam is sufficient to overflow large scale tanks, and should be regarded as a hazard in the case of a fire.

The boilover observed in the heavy gas oil was accelerated by the emulsified water in the oil that caused a chain reaction of fuel ejections and mixing of the water into the heated oil. As such, boilover occurred well before the 100 °C isotherm reached the water layer interface. Based on the present small scale experiments, it was found to happen in situations where the fuel layer might still be as thick as 10 cm. This result, while significant in the present small scale fires, is likely to have a less significant effect in actual fires. For example, in the present experiments, the fuel ejections accelerated the time to boilover by over 70% relative to the time it would have taken for the 100 °C isotherm to reach

the surface of the water sublayer for initial fuel depths of 8 cm in the 0.26 m pan. In comparison, assuming a similar fuel regression rate, this effect would have less than a 1% effect on the time to boilover in real tanks, often having a fuel thickness greater than 20 m.

Further, the consequence of the frothing boilover is especially significant in the small-scale experiments due to the relative volumes of water and oil in the pans, since the froth can expand up to 1100 times the volume of the original oil. However, even in the context of a large heavy gas oil storage tank where the relative volume of water may be much less, such an expansion ratio may still present a realistic hazard.

Chapter 5

Conclusions and Recommendations

This work presents the first systematic study and characterization of the fire properties of untreated heavy gas oil from the Canadian oil sands. As this fuel is often stored in large volume storage tanks, it is important to characterize some of the potential hazards related to this material in order to better prepare first responders in the case of a fire. The stated objectives were to characterize the burning behaviour of the fuel, and compare that burning behaviour to correlations presented in literature, as well to compare the burning behaviour to that of similar fuels. To achieve these objectives, the overall character of the fire was documented and measurements of fuel regression rate, heat release rate, and flame spread rate were performed. The combined data was used to characterize each stage in the fire development and the measured parameters were compared to calculated results from common predictive tools. Further, observations on the effects of water suppression and the propensity for boilover were made.

5.1 Conclusions

From the experimental measurements, the following conclusions have been developed:

Overall, untreated heavy gas oil is a heavy hydrocarbon, with material properties and burning behaviour similar to those of other heavy fuels documented in literature. The fuel regression rate, heat release rate, and flame spread rate of heavy gas oil are well represented by many of the present correlations, using input parameter values comparable to those listed for other heavy hydrocarbon fuels. The same parameters measured in kerosene fires agree largely with values and correlations presented in literature. This helps to confirm

the accuracy of the measurement techniques and improves confidence in the experimental measurements presented in this work.

The experimental measurements of fuel regression rate of heavy gas oil were well represented by the correlation presented by Burgess, with coefficients of $k\beta = 1.1$ m^{-1} and $R_\infty = 3.0$ mm/min. The heat release rate was also well represented by Burgess' correlation as multiplied by the effective heat of combustion. The theoretical heat of combustion of heavy gas oil was measured to be 43.5 MJ/kg. Finally, the rate of flame propagation of heavy gas oil was approximately 0.8 cm/s for the wind-neutral condition.

Similar to the heavy gas oil, the kerosene fuel used in these experiments was well represented by each of the correlations presented in literature. The regression rate for the present kerosene was found to fit to a coefficients of $k\beta = 1.7$ m^{-1} and $R_\infty = 3.7$ mm/min. The measured heat of combustion of this kerosene was 45.8 MJ/kg, and the wind-neutral rate of flame propagation was measured to be approximately 9.3 cm/s.

There is no evidence of the formation or propagation of a heated band of high temperature material – or hot-zone – into the bulk fuel during long duration pool fire experiments in heavy gas oil. While the impact of pan diameter on this result is uncertain, hot-zones have been measured experimentally in other fuels at pan diameters within the range of the present experiments, which lends confidence to the above conclusion. The long duration burning behaviour of the heavy gas oil also supports this finding, where temperature distributions into the depth of the fuel exponentially decayed from the surface in constant fashion with time, there was no measured decrease in fuel regression rate, heat release rate, or boiling temperature over the course of the burning period. Together these findings help to support that heavy gas oil burns much like a single component fuel, and that a distillation process resulting in a hot-zone does not occur.

Water application to heavy gas oil fires resulted in the formation of a froth layer that assisted in suppressing the fire. The froth acted to lower the surface temperature of the fuel across the pool, and aided in suffocating the fire. The formation of froth greatly reduced the water requirements for control of the fire; however, the mode of application of water was also important. A water mist application was found not to penetrate the flame column, and was unable to suppress the fire. A suppression spray with a high water density across the entire surface of the fuel is therefore required for the water to pass through the flames and mix with the heated oil at the surface to form froth and control the fire.

The presence of emulsified water in heavy gas oil resulted in increased fire burning intensity and therefore potentially increased the hazard from the fire. The emulsified water was measured to cause an increase in the measured heat release rate, fuel regression rate, and flame spread rate. While significant at the scale of the present study, it is unclear

if these increases in fire characteristics will scale with fire area to the size of real storage tanks.

While the heavy gas oil did not lead to boilover in the traditional fashion in the present experiments, a thin layer boilover did occur in experiments with an artificially added water sublayer. The thin layer boilover resulted from mixing of water from the sublayer back up into the heated fuel layer, resulting in the generation of a froth that expanded in volume and overflowed the test pan. This resulted in a significant volume of oil being ejected from the pan and rapid fire spread, similar to what takes place in a more traditional form of boilover. The expansion ratio of the froth was found to be greater than $1100 : 1$, therefore only a small volume of water is thought to be required to result in a what could cascade to a catastrophic boilover event.

5.2 Recommendations

This study successfully measured several burning characteristics of heavy gas oil fires and a comparison to correlations provided in the literature was made. While the experiments conducted provide useful data to the analysis of fire hazards in heavy gas oil – as well as other heavy oils – some further work is recommended. These recommendations are listed as follows.

Due to the breadth of the experiments conducted, only a basic set of experiments were conducted for each subset of experiments. For this reason, a more detailed analysis of the burning behaviour should be completed to fully analyse the effect of some of the key parameters - for example initial fuel temperature – on the various measured parameters, including heat release rate, fuel regression rate, and rate of flame spread.

This study was performed in the interest of investigating the hazards of untreated heavy gas oil while stored in storage tanks, and therefore several experimental parameters were chosen for that purpose. In the present experiments, the sufficiently deep fuel layers were used to mimic the behaviour in fires over a semi-infinite depth of fuel, and all experiments were constrained to pans of set diameter. However, there is also a risk of pool fires of heavy gas oil as a result of spills or releases, and it is therefore recommended that future studies investigate the burning behaviour of heavy gas oil in all possible scenarios, including fires over unconstrained liquid fuel spills. Such experiments should include determination of maximum unconstrained release areas, flame spread rates over thin fuel layers, and total burning times for fires over spills of various depths.

Suppression of untreated heavy gas oil pool fires resulted in a layer of froth on the fuel surface, which acted to suffocate and subsequently suppress the fire. While this effect had a significant effect on the small-scale fires in the present study, it is recommended that further suppression experiments be conducted on large fires to determine if this effect is reproducible in real fires. This layer of froth negated the typical requirements for aqueous film forming foam, and greatly reduced the suppression water requirements.

Boilover remains a serious concern during storage of any oil, and further experiments should be conducted to investigate whether a hot-zone forms in fires over larger diameter pans. While hot-zones have been measured in small-scale experiments on other fuels, it is not possible to capture all of the physics of larger fire scenarios in these small scale experiments. Some of the limitations of the current documented experimental measurements are understood and efforts to conduct large scale tests are being made for some fuels. Similar experiments are recommended for the case of heavy gas oil fires. As well, this experimental study was focused on the thick layer boilover of heavy gas oil; however, the thin layer boilover can present a hazard in the case of spills on bodies of water. Further analysis is required on the effects of thin fuel layer burning suspended on water if the in-situ burning of heavy gas oil spills on bodies of water is to be considered.

Finally, it was found near the end of the experimental period that the heavy gas oil weathers with time, and that the burning behaviour changes with weathering period. It is therefore recommended that a full analysis of the effects of weathering on burning behaviour be conducted. While less important in the case of storage tank fires, the weathering of oil has been previously noted as a significant factor that should be considered in understanding oil spill fires, where the fuel is exposed to environmental conditions for periods of time.

References

[1] S. Vasanth, S. Tauseef, T Abbasi, Rangwala A., and S. Abbasi. Assessment of the effect of pool size on burning rates of multiple pool fires using CFD. *Journal of Loss Prevention in the Process Industries*, 30:86–94, 2014.

[2] H. Persson and A. Lonnermark. Tank fires: Review of fire incidents 1951-2003. Technical report, SP Report 2004:14; Swedish National Testing and Research Institute, 2004.

[3] Buckeye Fire Equipment. Storage tanks: large diameter tanks – over 250 ft (76 m) in diameter. [Online] Accessed 07/06/2014 from: `http://buckeyefire.com/pdfs/foampdfs/storage/250.pdf`, 2009.

[4] H. Khordagu and D. Al-Ajmi. Environmental impact of the Gulf War: An integrated preliminary assessment. *Environmental Management*, 17(4):557–562, 1993.

[5] G. Marlair, M. Simonson, and R. Gann. Environmental concerns of fires: Facts, figures, questions and new challenges for the future. In *International Interflam Conference, 10th Proceedings*, pages 325–337, London, England, 2004. Interscience Communications Ltd.

[6] H. Holemann. Environmental problems caused by fires and fire-fighting agents. In *Fire Safety Science - Proceedings of the Fourth International Symposium*, pages 61–77. International Association for Fire Safety Science, 1994.

[7] A. Luketa. Assessment of simulation predictions of hydrocarbon pool fire tests. Technical Report SAND2010-2511, Sandia National Laboratories, Albuquerque, NM, 2010.

[8] C. L. Beyler. *SFPE Handbook of Fire Protection Engineering*, volume 3, chapter 3-11: Fire Hazard Calculations for Large, Open Hydrocarbon Fires. Society of Fire Protection Engineers, 2002.

[9] M. Muñoz, E. Planas, F. Ferrero, and J. Casal. Predicting the emissive power of hydrocarbon pool fires. *Journal of Hazardous Materials*, 144(3):725–9, 2007.

[10] A. Hamins, T. Kashiwagi, and R. Burch. Characteristics of pool fire burning. In *Fire Resistance of Industrial Fluids, ASTM STP 1284, American Society for Testing and Materials*, pages 1–27, 1995.

[11] M. E. Schneider and L. A. Kent. Measurements of gas velocities and temperatures in a large open pool fire. Technical report, Sandia National Laboratories, Albuquerque, NM.

[12] K. B. Mcgrattan, H. R. Baum, and A. Hamins. Thermal radiation from large pool fires thermal radiation from large pool fires. Technical Report NISTIR 6546, Gaithersburg, MD, 2000.

[13] P. K. Raj. Large hydrocarbon fuel pool fires: physical characteristics and thermal emission variations with height. *Journal of Hazardous Materials*, 140(1-2):280–292, 2007.

[14] E. Planas-Cuchi, C. Joaquim, A. Lancia, and L. Bordignon. Protection of equipment engulfed in a pool fire. *Journal of Loss Prevention in the Process Industries*, 9(3):231–240, 1996.

[15] Z. Xiaomeng, J. Qin, and L. Guangxuan. Effects of water-mist addition on kerosene pool fire. *Chinese Science Bulletin*, 53(20):3240–3246, 2008.

[16] A. Bouhafid, J. P. Vantelon, P. Joulain, and A. C. Fernandez-Pello. On the flame structure at the base of a pool fire. *Twenty-Second Symposium (International) on Combustion*, pages 1291–1298, 1988.

[17] S. Gollahalli and H. F. Sullivan. Liquid pool fires (A review). Technical Report 23, University of Waterloo, 1973.

[18] A. Nakakuki. Heat transfer in small scale pool fires. *Combustion and Flame*, 96(3):311–324, 1994.

[19] C. Qian, G. Tashtoush, A. Ito, and K. Saito. Structure of large scale pool fires. In *International Conference on Fire Research and Engineering*, 1995.

[20] Society of Fire Protection Engineers. *SFPE Handbook of Fire Protection Engineering*. National Fire Protection Association, third edition, 2002.

[21] D. Drysdale. *An Introduction to Fire Dynamics*. Wiley, Chichester, second edition, 1999.

[22] V. Babrauskas. Estimating large pool fire burning rates. *Fire Technology*, 19(4):251–261, 1983.

[23] D. Laboureur. *Experimental characterization and modeling of hazards: BLEVE and Boilover*. PhD. Thesis, Ecole Polytechnique De Bruxelles, 2012.

[24] N. L. Brogaard, M. X. Sø rensen, J. Fritt-Rasmussen, S. R. Ali, and G. Jomaas. A new experimental rig for oil burning on water results for crude and pure oils. In *Fire Safety Science – Draft of the Eleventh International Symposium*, pages 1–14, 2014, [Draft] Available at: `http://www.iafss.org/publications/fss/11/212/view`.

[25] F. Ferrero, M. Muñoz, B. Kozanoglu, J. Casal, and J. Arnaldos. Experimental study of thin-layer boilover in large-scale pool fires. *Journal of Hazardous Materials*, 137(3):1293–1302, 2006.

[26] J. S. Hua, W. C. Fan, and G. X. Liao. Study and prediction of boilover in liquid pool fires with a water sublayer using micro-explosion noise phenomena. *Fire Safety Journal*, 30(3):269–291, 1998.

[27] W. C. Fan, J. S. Hua, and G. X. Liao. Experimental study on the premonitory phenomena of boilover in liquid pool fires supported on water. *Journal of Loss Prevention in the Process Industries*, 8(4):221–227, 1995.

[28] P. Watkins. LASTFIRE boilover tests March 2010 - FOAMGLAS OBS trials. Technical Report P1032, May 2010, LASTFIRE, Aylesbury, UK, 2010.

[29] H. Koseki. Boilover and crude oil fire. *Journal of Applied Fire Science*, 3(3):243–272, 1993.

[30] F. Kozanoglu, B.and Ferrero, M. Muñoz, J. Arnaldos, and J. Casal. Velocity of convective currents in boilover. *Chemical Engineering Science*, 61(8):2550–2556, 2006.

[31] B. Kozanoglu, F. Ferrero, M. Muñoz, J. Arnaldos, and J. Casal. Thermal analysis of thin layer boilover. *Heat and Mass Transfer*, 44(12):1549–1555, 2008.

[32] K. Hasegawa. Experimental study on the mechanism of hot zone formation in open-tank fires. In *Fire Safety Science - Proceedings of the Second International Symposium*, pages 221–230. International Association for Fire Safety Science, 2003.

[33] Center for Chemical Process Safety. *Emergency Response: Tacoa Power Station Boil Over, Venezuela, December 19, 1982*, chapter 12. John Wiley & Sons, 2010.

[34] S. Mannan, editor. *Lee's Loss Prevention in the Process Industries*. Appendix 1. Butterworth-Heinemann, 2004.

[35] Canadian Oil Sands Limited. Canadian Oil Sands: Invested in our energy future, 2014.

[36] [Redacted]. Material safety data sheet for: Untreated heavy gas oil. Material Safety Data Sheet, 2006.

[37] H. Koseki. Large scale pool fires: Results of recent experiments. In *FIRE SAFETY SCIENCE-PROCEEDINGS OF THE SIXTH NTERNATIONAL SYMPOSIUM*, pages 115–132. International Association for Fire Safety Science.

[38] V. I. Blinov and G. N. Khudyakov. Diffusion burning of liquids. Technical Report 296762, US Army Engineer Research and Development Laboaratories, Fort Belvoir, VA, 1961.

[39] N. N. Bakhman and B. N. Kondrikovt. Burning of liquid fuels : effect of burner diameter on burning rate and measurements of quenching diameter. *Fuel*, 55(3):243–249, 1976.

[40] H. Koseki and G. W. Mulholland. The effect of diameter on the burning of crude oil pool fires. *Fire Technology*, 27(1), 1991.

[41] D. T. Gottuk and D. A. White. *SFPE Handbook of Fire Protection Engineering*, volume 3, chapter 2-15: Liquid Fuel Fires. Society of Fire Protection Engineers, 2002.

[42] B. Chen, S. X. Lu, C. H. Li, Q. S. Kang, and V. Lecoustre. Initial fuel temperature effects on burning rate of pool fire. *Journal of hazardous materials*, 188(1-3):369–74, 2010.

[43] R. J. Murad, J. Lamendola, H. Isoda, and M. Summerfield. A study of some factors influencing the ignition of a liquid fuel pool. *Combustion and Flame*, 15(3):289–298, 1970.

[44] H. D. Ross. Ignition of and flame spread over laboratory-scale pools of pure liquid fuels. *Progress in Energy and Combustion Science*, 20(1):17–63, 1994.

[45] D. White, C. L. Beyler, C. Fulper, and J. Leonard. Flame spread on aviation fuels. *Fire Safety Journal*, 28(1):1–31, 1997.

[46] J. Guo, S. Lu, M. Li, and C. Wang. Flame spread over aviation kerosene with an obstacle in liquid phase. *Journal of Thermal Science*, 20(6):543–547, 2011.

[47] M. Li, S. Lu, J. Guo, R. Chen, and K. L. Tsui. Initial fuel temperature effects on flame spread over aviation kerosene in low- and high-altitude environments. *Fire Technology*, Published online, 2014.

[48] J. B. Zhou, G. Q. Chen, P. M. Li, B. Chen, C. J. Wang, and S. X. Lu. Analysis of flame spread over aviation kerosene. *Chinese Science Bulletin*, 55(17):1822–1827, 2010.

[49] C. Di Blasi, S. Crescitelli, and G. Russo. Model of oscillatory phenomena of flame spread along the surface of liquid fuels. *Computer Methods in Applied Mechanics and Engineering*, 90(1-3):643–657, 1991.

[50] K. Takahashi, Y. Kodaira, Y. Kudo, A. Ito, and K. Saito. Effect of oxygen on flame spread over liquids. *Proceedings of the Combustion Institute*, 31(2):2625–2631, 2007.

[51] J. Guo, S. Lu, and C. Wang. Study on the subsurface flow induced by flame spread over aviation kerosene. *Journal of Thermal Analysis and Calorimetry*, 116(1):455–460, 2013.

[52] H. Ross and F. Miller. Understanding flame spread across alcohol pools. In *Fire Safety Science – Proceedings of the Sixth International Symposium*, pages 77–94. International Association for Fire Safety Science, 2000.

[53] K. Takahashi, A. Ito, Y. Kudo, T. Konishi, and K. Saito. Scaling and instability analyses on flame spread over liquids. *Proceedings of the Combustion Institute*, 30(2):2271–2277, 2005.

[54] R. Mackinven, J. G. Hansel, and I. Glassman. Flame spreading across liquid fuel at sub-flash point temperatures: Measurements and techniques. Technical Report AMS Department Report #926, July 1970, Princeton University, 1970.

[55] K Akita. Some problems of flame spread along a liquid surface. In *14th Symposium (International) on Combustion*, pages 1075–1081, Pittsburgh, PA, 1973. Combustion Institute.

[56] I. Glassman and J. Hansel. Some thoughts and experiments on liquid fuel spreading, steady burning, and ignitability in quiescent atmospheres. *Fire Research Abstracts and Reviews*, 10(3):297–322, 1948.

[57] H. D. Ross and F. J. Miller. Flame spread across liquid pools with very low-speed opposed or concurrent airflow. *Symposium (International) on Combustion*, 27(2):2723–2729, 1998.

[58] H. H. Hall. Oil tank fire boilover. *Mechanical Engineering*, 47(7):540, 1925.

[59] D. Burgess, A. Strasser, and J. Grumer. Diffusive burning of liquid fuels in open trays. *Fire Research Abstracts and Reviews*, 3(3):91–106, 1961.

[60] J. A. Fay. Model of large pool fires. *Journal of hazardous materials*, 136(2):219–32, 2006.

[61] F. Ferrero, M. Muñoz, and J. Arnaldos. Effects of thin-layer boilover on flame geometry and dynamics in large hydrocarbon pool fires. *Fuel Processing Technology*, 88(3):227–235, 2007.

[62] H. Koseki. Combustion properties of large liquid pool fires. *Fire Technology*, 25(3):241 – 255, 1989.

[63] J. M. Chatris, J. Quintela, J. Folch, E. Planas, J. Arnaldos, and J. Casal. Experimental study of burning rate in hydrocarbon pool fires. *Combustion and Flame*, 126(1-2):1373–1383, 2001.

[64] J. Grumer, A. Strasser, T. A. Kubala, and Burgess D. S. Uncontrolled diffusive burning of some new liquid propellants. *Fire Research Abstracts and Reviews*, 3:107–124, 1961.

[65] Y. Iwata, H. Koseki, M. L. Janssens, and T. Takahashi. Combustion characteristics of crude oils. *Fire and Materials*, 7(1):1–7, 2001.

[66] H. Koseki, G. W. Mulholland, and J. Tadahisa. Study on combustion property of crude oil – a joint study between NIST/CFR and FRI, eleventh joint panel meeting of the ujnr panel on fire research and safety, NISTIR 4449, 96–104, springfield, va, 1990.

[67] B. Z. Dlugogorski and M. Wilson. Effect of ullage on properties of small-scale pool fires. *Developments in Chemical Engineering and Mineral Processing*, 8(1-2):149–166, 2000.

[68] J. P. Garo and J. P. Vantelon. Boilover burning of oil spilled on water. *Twenty-Fifth Symposium (International) on Combustion*, pages 1481–1488, 1994.

[69] M. Benfer. *Spill and Burning Behavior of Flammable Liquids*. MASc. Thesis, University of Maryland, College Park, MD, 2010.

[70] N. Wu and J. Torero. Enhanced burning of difficult to ignite/burn fuels including heavy oils. Technical Report NIST-GCR-98-750, National Institute of Standards and Technology, Gaithersburg, MD, 1998.

[71] C. L. Mealy, M. E. Benfer, and T. Gottuk. Fire dynamics and forensic analysis of liquid fuel fires. Technical Report 238704, US Department of Justice - National Institute of Justice, Washington, 2012.

[72] E. Randsalu. *Measurement of Fuel Regression Rate in a Jet-A Fuelled Fire In Crosswind*. MASc. Thesis, University of Waterloo, Waterloo, ON, 2005.

[73] B. Chen, S. X. Lu, C. H. Li, Q. S. Kang, and V. Lecoustre. Initial fuel temperature effects on burning rate of pool fire. *Journal of Hazardous Materials*, 188(1-3):369–74, 2010.

[74] C. Best. *Measurement of Fuel Regression Rate of a Pool Fire in Crosswind With and Without a Large Downwind Blocking Object*. MASc. Thesis, University of Waterloo, Waterloo, ON, 2010.

[75] C. Lam. *Thermal Characterization of a Pool Fire in Crosswind With and Without a Large Downwind Blocking Object*. PhD. Thesis, University of Waterloo, Waterloo, ON, 2009.

[76] B. McCaffrey. Purely buoyant diffusion flames: Some experimental results. Technical report, National Bureau of Standards, Washington, DC, 1979.

[77] E. E. Zukoski, B. M. Cetegen, and T. Kubota. Visible structure of buoyant diffusion flames. In *Twentieth Symposium (International) on Combustion*, pages 361–366, Pittsburgh, 1984. The Combustion Institute.

[78] G. Heskestad. Peak gas velocities. In *Eighteenth Symposium (International) on Combustion*, volume 2, Pittsburgh, 1981. The Combustion Institute.

[79] D Stroup, G Taylor, and G Hausman. Chapter 3. estimating burning characteristics of liquid pool fire, heat release rate, burning duration, and flame height. In *Fire*

Dynamics Tools (FDTs) Quantitative Fire Hazard Analysis Methods for the U.S. Nuclear Regulatory Commission Fire Protection Inspection Program, pages 1–21. 2013.

[80] A. Nakakuki. Heat transfer in pool fires at a certain small lip height. *Combustion and Flame*, 131(3):259–272, 2002.

[81] A. Nakakuki. Heat transfer mechanisms in liquid pool fires. *Fire Safety Journal*, 23(4):339–363, 1994.

[82] Chih-Hung Lin, Yuh-Ming Ferng, Wen-Shieng Hsu, and Bau-Shei Pei. Investigations on the Characteristics of Radiative Heat Transfer in Liquid Pool Fires. *Fire Technology*, 46(2):321–345, 2008.

[83] A. Modak. The burning of large pool fires. *Fire Safety Journal*, 3(3):177–184, 1981.

[84] J. L. Torero, Stephen M. Olenick, J. P. Garo, and J. P. Vantelon. Determination of the burning characteristics of a slick of oil on water. *Spill Science & Technology Bulletin*, 8(4):379–390, 2003.

[85] K. A. Alnasser. Mathematical investigation of heat transfer in industrial crude oil tank during a fire. MASc. Thesis, Carleton University, Ottawa, CA, 2006.

[86] A. Nakakuki. Heat transfer in hot-zone-forming pool fires. *Combustion and Flame*, 109(3):353–369, 1997.

[87] H. Koseki, Y. Natsume, Y. Iwata, T. Takahashi, and T. Hirano. A study on large-scale boilover using crude oil containing emulsified water. *Fire Safety Journal*, 38(8):665–677, 2003.

[88] B. Persson, L.. Anders, and H. Persson. FOAMSPEX: Large scale foam application Modelling of foam spread and extinguishment. *Fire Technology*, 39(4):347–362, 2003.

[89] M. Gupta, A. Pasi, A. Ray, and S. R. Kale. An experimental study of the effects of water mist characteristics on pool fire suppression. *Experimental Thermal and Fluid Science*, 44:768–778, 2013.

[90] S. P. Ho. *Water Spray Suppression and Intensification of High Flash Point Hydrocarbon Pool Fires*. PhD. Thesis, Worchester Polytechnic Institute, Worcester, MA, 2003.

[91] L. Jianghong, L. Guangxuan, F. Weicheng, Y. Bin, and L. Xiyun. Study of liquid pool fire suppression with water mists by cone calorimeter. *Journal of Fire Sciences*, 20(6):465–477, 2002.

[92] B. Broeckmann and H. G. Schecker. Heat transfer mechanisms and boilover in burning oil-water systems. *Journal of Loss Prevention in the Process Industries*, 8(3):137–147, 1995.

[93] H. Koseki, Y. Natsume, Y. Iwata, T. Takahashi, and T. Hirano. Large-scale boilover experiments using crude oil. *Fire Safety Journal*, 41(7):529–535, 2006.

[94] L. Guangxuan, W. Huilin, L. Hongchang, C. Miaomou, L. Yonshen, H. Jinsong, Z. Wei, D. Yangxiao, and F. Weicheng. Experimental study of boilover phenomena in oil fires. In *Fire Safety Science - Proceedings of the Fourth International Symposium*, pages 422–433. International Association for Fire Safety Science.

[95] J P Garo, J P Vantelon, and A. C. Fernandez-Pello. Effect of the fuel boiling point on the boilover burning of liquid fuels spilled on water. *Twenty-Sixth Symposium (International) on Combustion*, pages 1461–1467, 1996.

[96] J. P. Garo, J. P. Vantelon, and C. Fernande-Pello. Effect of the fuel boiling point on the boilover burning of liquid fuels spilled on water. *Symposium (International) on Combustion*, 26(1):1461–1467, 1996.

[97] I. M. Shaluf and S. A. Abdullah. Floating roof storage tank boilover. *Journal of Loss Prevention in the Process Industries*, 24(1):1–7, 2011.

[98] H. Koseki, M. Kokkala, and G. Mulholland. Experimental study of boilover in crude oil fires. In *Fire Safety Science – Proceedings of the Third International Symposium*, pages 865–874. International Association for Fire Safety Science, 1991.

[99] K Hasegawa. Experimental study on the mechanism of hot zone formation in open-tank fire. In *Proceedings of the 2nd International Symposium on Fire Safety Science*, pages 221–230. International Association For Fire Safety Science, 1988.

[100] J. P. Garo, H. Koseki, J. P. Vantelon, and C. Fernandez-Pello. Combustion of liquid fuels floating on water. *Thermal Science*, 11(2):119–140, 2007.

[101] J. H. Burgoyne and L. L. Katan. Fires in open tanks of petroleum products: Some fundamental aspects. *Journal of the Institute of Petroleum*, 33:158, 1947.

[102] M. G. Zabetakis and D. S. Burgess. Research on the hazards associated with the production and handling of liquid hydrogen. Technical Report Report: BM-RI-5707., Bureau of Mines, Washington, DC, 1961.

[103] A. L. Brown and T. K. Blanchat. A validation quality heat flux dataset for large pool fires. In *Proceedings of the ASME Summer Heat Transfer Conference*, volume 2003, pages 71–78. ASME International, 2003.

[104] S. E. Petty. Combustion of crude oil on water. *Fire Safety Journal*, 5:123–134, 1983.

[105] B. D. Ditch, J. L. de Ris, T. K. Blanchat, M. Chaos, R. G. Bill, and S. B. Dorofeev. Pool fires An empirical correlation. *Combustion and Flame*, 160(12):2964–2974, 2013.

[106] C. Huggett. Estimation of rate of heat release by means of oxygen consumption measurements. *Fire and Materials*, 4(2):61–65, 1980.

[107] Fire Testing Technology. User's Guide for the Cone Calorimeter. Technical report, Fire Testing Technology Limited, West Sussex, UK, 2001.

[108] V. Babrauskas. Development of the cone calorimeter-a bench-scale heat release rate apparatus based on oxygen consumption. *Fire and Materials*, 8(2):81–95, 1984.

[109] ASTM International. ASTM E 1354: Standard test method for heat and visible smoke release rates for materials and products using an oxygen consumption calorimeter, 2013.

[110] International Standards Organisation. *ISO 5660-1:2002: Reaction-to-fire tests – Heat release smoke production and mass loss rate – Part 1: Heat release rate (cone calorimeter method)*. ISO, Geneva, 2002.

[111] National Fire Protection Association. *NFPA 271: Standard Method of Test for Heat and Visible Smoke Release Rates for Materials and Products using an Oxygen Consumption Calorimeter*. NFPA, Qunicy, MA, 2009.

[112] Standards Council of Canada. *CAN/ULC-S135-98: Standard Method of Test for Determination of Degrees of Combustibility of Building Materials Using an Oxygen Consumption Calorimeter (Cone Calorimeter)*. Standards Council of Canada, Ottawa, ON, 1998.

[113] F. Hshieh and H. D. Beeson. Note: Measuring the effective heats of combustion of transformer-insulating fluids using a controlled-atmosphere Cone Calorimeter. *Fire and Materials*, 26(1):47–49, 2002.

[114] J. Martinka, T. Chrebet, and K. Balog. An assessment of petrol fire risk by oxygen consumption calorimetry. *Journal of Thermal Analysis and Calorimetry*, 117(1):325–332, 2014.

[115] N. Wu, G. Kolb, and J. L. Torero. The effect of weathering on the flammability of a slick of crude oil on a water bed. *Combustion Science and Technology*, 161(1):269–308, 2000.

[116] S. K. Elam, R.A. Altenkirch, K. Saito, and M. Arai. Cone heater ignition tests of liquid fuels. *Fire Safety Journal*, 16(1):65–84, 1990.

[117] H. Pretrel, W. Le Saux, and L. Audouin. Determination of the heat release rate of large scale hydrocarbon pool fires in ventilated compartments. *Fire Safety Journal*, 62:192–205, 2013.

[118] W. K. Chow and S. S. Han. Estimation of heat release rate for gasoline pool fires. *International Journal on Engineering Performance-Based Fire Codes*, 9(2):59–64, 2007.

[119] B. Dlugogorski, J. Mawhinney, and V. Huu Duc. The measurement of heat release rates by oxygen consumption calorimetry in fires under suppression. *Fire Safety Science*, 4:877–888, 1994.

[120] J. U. Ezinwa, L. D. Robson, M. R. Obach, D. A. Torvi, and E. J. Weckman. Evaluating models for predicting full-scale fire behaviour of polyurethane foam using cone calorimeter data. *Fire Technology*, 50(3):693–719, 2011.

[121] J Soderbom, P. Van Hees, and P. Meirsschaert. Influence of ignition sources on heat release rate in the furniture calorimeter. *Fire and Materials*, 20(2):61–67, 1996.

[122] C. L. Beyler. *SFPE Handbook of Fire Protection Engineering*, volume 3, chapter 3-2: Calorimetry. Society of Fire Protection Engineers, 2002.

[123] H. Koseki, Y. Iwata, Y. Natsume, T. Takuhashi, and T. Hirano. Tomakomai large scale crude oil fire experiments. *Fire Technology*, 36(I):24–38, 2000.

[124] D. Evans, D. Madrzykowski, and G. Haynes. Flame heights and heat release rates of 1991 Kuwait Oil Field fires. *Fire Safety Science*, (4):1279 – 1289, 1994.

[125] F. Ferrero, M. Muñoz, and J. Arnaldos. Thin-layer boilover in diesel-oil fires: Determining the increase of thermal hazards and safety distances. *Journal of Hazardous Materials*, 140(1-2):361–8, 2007.

[126] M. Munoz, J. Arnaldos, J. Casal, and E. Planas. Analysis of the geometric and radiative characteristics of hydrocarbon pool fires. *Combustion and Flame*, 139(3):263–277, 2004.

[127] P. M. Mulherin and E. J. Weckman. Burning behaviour of untreated Heavy Gas Oil from the Canadian oil sands. In *Proceedings of the Combustion Institute - Canadian Section*, number Spring 2014, pages 328–333, Windsor, 2014.

[128] Recochem Inc. Material safety data sheet for: Kerosene. CAS # 64742-88-7. Material Safety Data Sheet, 2011.

[129] OMEGA Engineering Inc. Thermocouples. [Online] Accessed 01/07/2014 from: `http://www.omega.ca/guides/thermocouples.html`, 2014.

[130] FLIR Sytems Inc. FLIR T650sc Datasheet. [Online] Accessed 02/05/2014 from: `http://www.flir.com/WorkArea/linkit.aspx?LinkIdentifier=id&ItemID=59802&libID=85399`, 2014.

[131] ASTM International. *ASTM D 240-09: Standard Test Method for Heat of Combustion of Liquid Hydrocarbon Fuels by Bomb Calorimeter*. ASTM International, West Conshohocken, PA, 2009.

[132] Fire Testing Technology. Cone Calorimeter. [Online] Accessed 02/05/2014 from: `http://www.fire-testing.com/cone-calorimeter-dual`, 2013.

[133] National Fire Protection Association. *NFPA 15: Standard for Water Spray Fixed Systems for Fire Protection*. National Fire Protection Association, Quincy, MA, 2012.

[134] I. Staffell. The energy and fuel data sheet, W1P1 - Revision 1, [online] available at: `http://www.claverton-energy.com/wp-content/uploads/2012/08/the_energy_and_fuel_data_sheet.pdf`, 2011.

[135] American Bureau of Shipping. Marine fuel oil properties and characteristics and their impact on diesel engine, in ABS notes on heavy fuel oil. Technical report, Houston, TX, 1984.

[136] A. Buchanan. *Structural Design For Fire Safety*. Wiley, West Sussex, 2002.

[137] N. Wu, M. Baker, G. Kolb, and J. L. Torero. Ignition, flame spread and mass burning characteristics of liquid fuels on a water bed. *Spill Science & Technology Bulletin*, 3(4):209–212, 1997.

[138] J. Guo, S. X. Lu, J. B. Zhou, M. H. Li, and C. J. Wang. Experimental study of flame spread over oil floating on water. *Chinese Science Bulletin*, 57(9):1083–1087, 2012.

[139] CHEMGUARD Specialty Chemicals & Equipment. Fixed or semi-fixed foam fire protection systems for storage tanks. [Online] Accessed 07/09/2013 from: `http://www.chemguard.com/pdf/design-manuals/D10D03192.pdf`, 2013.

[140] A. Vali, D. S. Nobes, and L. W. Kostiuk. Effects of wall material on energy transport of laboratory-scale methanol pool fire. In *Proceedings of the Combustion Institute - Canadian Section*, number 780, pages 316–321, Windsor, ON, 2014.

[141] G. Heskestad. Similarity relations for the initial convective flow generated by fire: FM Report 72-WA/HT-17. Technical report, Factory Mutual Research Corporation, Norwood, MA, 1972.

[142] E. Planas-Cuchi and J. Casal. Flame temperature distribution in a pool-fire. *Journal of Hazardous Materials*, 62(3):231–241, 1998.

[143] The Engineering ToolBox. Thermal conductivity of some common materials and gases. [Online] Accessed 03/01/2014 from: `http://www.engineeringtoolbox.com/thermal-conductivity-d_429.html`, 2014.

[144] The Engineering ToolBox. Liquids and fluids - specific heats. [Online] Accessed 03/01/2014 from: `http://www.engineeringtoolbox.com/specific-heat-fluids-d_151.html`, 2014.

[145] J. P. Garo, J. P. Vantelon, J. M. Souil, and C. Breillat. Burning of weathering and emulsified oil spills. *Experimental Thermal and Fluid Science*, 28(7):753–761, 2004.

[146] J. P. Garo, P. Gillard, J. Vantelon, and A. Fernandez-Pello. On the thin layer boilover. *Fire Safety Science*, 6:579–590, 2000.